Flinders University

Australian Government
Department of Defence
Defence Science and Technology Group

Analysis of the Nitrate Ester Explosives- Xylitol Pentanitrate and Erythritol Tetranitrate

Kelly-Anne S. Stark

BSc (Forensic and Analytical Science) (Honours)

Thesis Submitted to Flinders University
for the degree of

Doctor of Philosophy

College of Science and Engineering
November 2022

Contents

Declaration

I certify that this thesis does not incorporate without acknowledgment any material previously submitted for a degree or diploma in any university and the research within will not be submitted for any other future degree or diploma without the permission of Flinders University; and to the best of my knowledge and belief, does not contain any material previously published or written by another person except where due reference is made in the text.

Kelly-Anne S. Stark

7th November 2022

Acknowledgments

When asked at the end of high school what I wanted to do with my life, I looked back on experiences of myself and the people I knew for my answer. I had always assumed I would end up at university and after multiple knee injuries from netball, I saw the importance that medical imaging has. I set out to start my university life in a medical imaging degree, however, ended up in nuclear medicine. Although this wasn't my first choice, I persevered for 1.5 years before deciding it wasn't for me. During a six month gap, I decided I should return to my strengths from high school which were mathematics and chemistry, which led me to choose the forensic science degree at Flinders University. From the first day I knew I had made the right decision, however, I always said I would never go on to do honours let alone a PhD! I wanted to finish my Bachelor degree and join the workforce as soon as possible, yet here I am. While completing my PhD, I have bought a house, been married, adopted a cat and a dog, and had a baby. These experiences have helped make me the person that I am today, and I would like to thank the people who have helped me along this journey.

To my supervisors, Paul, Claire, and Mark for giving me the support and encouragement I needed to make it to the end. Their input and guidance throughout the past 4 years has been phenomenal. To have three supervisors who are all very approachable, knowledgeable, and understanding has been wonderful and without you all, I do not think I would have made it to this point. I think we have all wondered whether I would ever finish my PhD, and this document is a testament to the support you have all given me.

To DST Group for providing the funds for my project and providing the samples I needed to complete my PhD.

To the Australian Government for the Australian Government Research Training Program Scholarship

To Mel for always being there for me. Who would have thought that two girls playing netball together would lead to 15 years of friendship? You have stood by me all these years and I am blessed to have you in my life.

To Jay-Jay, we may not have gotten off on the right foot, but you are now one of my closest friends. You have lent me your ear and your shoulder to cry on and I will always be grateful for that. I hope we will be friends for life and that I can offer you the support and friendship that you have given me over the past few years.

To my D&D group, Jennie, Tim, Amanda, Tristan, and Sam, for allowing me to immerse myself into another world and eating my weight in carrot sticks and cheese.

To Maria and Kym for being such wonderful people and accepting me into your family. I couldn't ask for better people to have raised my wonderful husband.

To my brother for being the person I look to for acknowledgment that I have chosen the right people to be in my life (you have more street smarts than I do!) and for giving me a niece and nephew who are such bright lights in my life.

To my mum and dad for raising, teaching, and supporting me in all my decisions (I know it wasn't always easy). I believe you both did an amazing job and as much as you don't believe me, I wouldn't change any part of my life with you both. I wouldn't be the person I am today without you.

To Nathaniel for coming on this journey with me. It hasn't always been easy, but I think over the past 5 years we have managed to make a good life for ourselves. You have supported me throughout this challenging part of my life, and I can't wait to start the next chapter with you.

To my daughter, Madeline, you have made this journey more difficult, but also more joyful and I wouldn't change that for anything. I hope you know that I will always be there for you I hope I will always be someone you can be proud of.

Summary

Nitrate ester explosives, such as nitroglycerin (NG) and pentaerythritol tetranitrate (PETN), have been used by Defence for decades. Recently, there has been an increased interest in the nitrate esters erythritol tetranitrate (ETN) and xylitol pentanitrate (XPN) by terrorists, amateur experimentalists, and the defence industry. Despite this interest, XPN was not well characterised in the academic literature.

Crystalline XPN was prepared by slow evaporation and subjected to single crystal x-ray diffraction to obtain a crystal structure. XPN crystalises in the centrosymmetric monoclinic space group $P2_1/n$. The density of XPN calculated from the crystal structure is 1.852 $g.cm^{-1}$ and the calculated heat of formation is -500.48 $kJ.mol^{-1}$. These values were entered into the computer program Cheetah 7.0 to determine the theoretical explosive performance of XPN. The calculated detonation pressure and velocity of detonation were determined to be 32.6 GPa and 8.780 $km.s^{-1}$, respectively, which are comparable to the theoretical performances of ETN, PETN and cyclotrimethylene trinitramine (RDX). Sensitiveness testing showed that XPN is a primary explosive that is significantly more sensitive to impact and friction than PETN.

Analytical characterisation data were also collected to provide forensic scientists, first responders and Defence with reference data for XPN. GC-MS, LC-MS, NMR, and vibrational spectroscopy data were obtained. Vibrational spectroscopy displayed characteristic vibrations that are expected for a nitrate ester, with XPN able to be differentiated from ETN. High field strength NMR was able to differentiate XPN from ETN, and benchtop NMR, while unable to resolve all peaks, was also able to differentiate XPN from ETN, PETN and NG. Using direct-MS, diagnostic chloride and nitrate adduct ions were measured for XPN and UPLC was successful in separating XPN from ETN, PETN and NG. Cold-EI GC-MS provided spectra that were unique to each nitrate ester explosive, however, the results were inconsistent due to the likely thermal degradation of the molecules. As such, UPLC is recommended for the identification of XPN over GC-MS, however, for in-field detection, Raman and IR spectroscopy are desirable.

The chemical degradation of rigorously purified ETN was investigated at 60, 80 and 100 °C. ETN was found to be stable at 60 °C for up to 28 days, whereas no ETN was detected at 28 days at 80 °C and no ETN was detected at 14 days at 100 °C. The presence of acid vapour increased the rate of degradation with no observable ETN at 14, 7 and 2 days at 60, 80 and 100 °C, respectively, whereas at 40 °C, ETN exposed to acid vapour was stable for the 28 day trial period. Stabilisation studies involving 0.2 % w/w of DPA or EC were conducted at 80 and 100 °C. There was no significant difference between the stabilised and unstabilised ETN samples at these temperatures.

List of figures

List of tables

List of abbreviations

Abbreviation	Definition
ANFF	Australian National Fabrication Facility
APCI	Atmospheric pressure chemical ionisation
APCI-MS	Atmospheric pressure chemical ionisation- mass spectrometry
ATR	attenuated total reflectance
BHT	Butylated hydroxytoluene
CAGR	Compound annual growth rate
CEEM	Centre of Expertise in Energetic Materials
CI	chemical ionisation
CJ	Chapman-Jouguet
CL20	Hexanitrohexaazaisowurtzitane
Cold-EI	cold electron-ionisation
DAD	Diode array detector
DART-MS	Direct analysis in real time- mass spectrometry
DBP	Double based propellant
DCM	Dichloromethane
DFT	density functional theory
diPHEN	Dipentaerythritol hexanitrate
DMF	dimethylformamide
DNAN	2,4-dinitroanisole
DNTN	1,4-dinitrato-2,3-bis(nitratomethylene) butane
DPA	Diphenylamine
DS	Degree of substitution
DSA	direct sample analysis
DSA-TOF-MS	direct sample analysis-time of flight-mass spectrometry
DSC	Differential scanning calorimetry
DST Group	Defence, Science and Technology Group
EC	Ethyl centralite
EdiN	Erythritol dinitrate
EGDN	ethylenegycol dinitrate
EI	Electron ionisation
EmonoN	Erythritol mononitrate
ESD	electrostatic discharge
ESI	Electrospray ionisation
ETN	Erythritol tetranitrate
EtriN	Erythritol trinitrate
FID	Flame ionisation detector
FWHM	full width at half maximum
GC	Gas chromatography
GC-MS	gas chromatography-mass spectrometry
GO	Graphene oxide
HDMS	high definition mass spectrometer
HMTD	Hexamethylene triperoxide
HMX	octahydro-1,3,5,7-tetranitro-1,3,5,7-tetrazocine

HPC	High performance computing
HPLC	High performance liquid chromatography
HQ	Hydroquinone
IED	Improvised explosive device
IR	Infrared spectroscopy
LC	liquid chromatography
LC-MS	Liquid chromatography-mass spectrometry
MHN	Mannitol hexanitrate
MS	Mass spectrometry
NC	Nitrocellulose
NG	nitroglycerin
NMR	Nuclear magnetic resonance spectroscopy
PETN	Pentaerythritol tetranitrate
PTFE	Polytetrafluoroethylene
PTFE-DBP	Polytetrafluoroethylene-double based propellant
RDX	cyclotrimethylenetrinitramine
SCXRD	single crystal X-ray diffraction
SEM	Scanning electron microscopy
SHN	Sorbitol hexanitrate
SMX	1,4-dinitrato-2,3-bis(nitratomethylene) butane
TATP	Triacetone triperoxide
TG	thermal gravimetric
TGA	Thermal gravimetric analysis
TKX-50	Dihydroxylammonium 5,5’-bistetrazole-1,1’-diolate
TLC	thin layer chromatography
TMS	Tetramethylsilane
TNAZ	1,3,3-trinitroazetidine
TNT	Trinitrotoluene
TOF	Time of flight
triPEON	Tripentaerythritol octanitrate
UPLC	ultra performance liquid chromatography
UV	Ultraviolet
VOD	Velocity of detonation
XPN	Xylitol pentanitrate
XteN	Xylitol tetranitrate

Publications

The following is a list of publications by this author included as a part of this thesis.

Stark, K. A. S.; Alvino, J. F.; Kirkbride, K. P.; Sumby, C. J.; Metha, G. F.; Lenehan, C. E.; Fitzgerald, M.; Wall, C.; Mitchell, M.; Prior, C., Crystal Structure, Sensitiveness and Theoretical Explosive Performance of Xylitol Pentanitrate (XPN). *Propellants Explos. Pyrotech.* **2019,** *44*, 541-549.

Stark, K. A. S.; Fitzgerald, M.; Lenehan, C. E.; Kirkbride, K. P., Analysis of Nitrate Ester Explosives Using Cold-EI GC-MS. In *50th International Annual Conference of ICT*, Karlsruhe, Germany, 2019

Stark, K.-A. S.; Gascooke, J. R.; Gibson, C. T.; Lenehan, C. E.; Bonnar, C.; Fitzgerald, M.; Kirkbride, K. P., Xylitol pentanitrate – Its characterization and analysis. *Forensic science international* **2020,** *316*, 110472-110472.

Chapter 1: Introduction

1.1 Explosives

An explosive can be classified as any substance capable of producing an explosion; that is, it is capable of a sudden release of energy [1-2]. An explosion can be classified as chemical, mechanical, thermal, electrical or nuclear, however, from a forensic perspective, chemical explosions are of most interest [1-2]. An explosive may be initiated using thermal, mechanical or electrostatic initiation sources [3]. Explosives do not require the presence of external oxygen to maintain an exothermic reaction [3]. Many explosives consist of at least two ingredients, an oxidiser (for example inorganic nitrates, perchlorates, etc.) and a fuel (for example carbohydrates, hydrocarbons etc.)- whereas molecular explosives are designed to include oxidising and reducing components within a single molecule [e.g. trinitrotoluene (TNT) and pentaerythritol tetranitrate (PETN)] [3-5].

Chemical explosives can be further broken down into primary, secondary and tertiary explosives [3]. Tertiary explosives, such as ammonium nitrate and ammonium perchlorate, are the least sensitive and are the hardest to detonate, whereas secondary explosives, such as PETN, are slightly more sensitive to external stimuli, although they typically require a primary explosive for initiation [1-3]. A primary explosive is very sensitive to stimuli, such as heat, impact, friction, and electrostatic discharge [1-3]. [1-3]. There is no worldwide accepted standard for when an explosive is considered primary, however, it is typically proposed that if it is more sensitive to impact and friction than the nitrate ester explosive PETN, then it can be considered a primary explosive [6]. Primary explosives are used in small quantities in military applications as part of an energetic train to initiate secondary explosives [6]. One of the most common and powerful primary explosives is lead azide, which is used in detonators for military applications; some other important primary explosives are mercury fulminate, silver azide, lead styphnate etc [1-3]. Due to the sensitivity, primary explosives are dangerous when used or made in large quantities. While some primary explosives are used for military applications, there are others that are used as improvised or 'homemade' explosives by terrorists and amateur experimenters, of which triacetone triperoxide (TATP) is one of the most commonly produced [5, 7-9].

One of the most important factors of an explosive material is its oxygen balance [3]. When an explosion takes place, a molecule will break down into its constituent atoms. If the explosion results in complete combustion it will form by-products such as water, carbon dioxide, sulfur dioxide and aluminium oxide, however, if incomplete combustion occurs, by-products such as hydrogen and carbon monoxide may form [2-3]. The products formed during the explosion are influenced by the amount of oxygen available during the reaction. To determine if a potential explosive material will

have enough oxygen present to result in complete combustion, the oxygen balance can be calculated using Equation 1 [1, 3]:

Equation 1: Oxygen balance

$$\Omega = \frac{\left[d - (2a) - \left(\frac{b}{2}\right)\right] \times 1600}{M}$$

Where M is the molecular weight of the molecule and a, b and d are from the number of carbon, hydrogen and oxygen atoms respectively ($C_aH_bN_cO_d$) [1, 3]. An example of an explosive that contains enough oxygen in the molecule to result in complete combustion is nitroglycerin (NG) ($C_3H_5N_3O_9$) which has an oxygen balance of +3.50 weight % (as shown in the example calculation below) [1-3]. An example of an explosive with incomplete combustion is TNT which has an oxygen balance of -74.0 weight % [1-3].

$$\Omega = \frac{\left[d - (2a) - \left(\frac{b}{2}\right)\right] \times 1600}{M}$$

Where M= (3*12)+(5*1)+(3*14)+(9*16)

M= 227

$$\Omega = \frac{\left[9 - (2 \times 3) - \left(\frac{5}{2}\right)\right] \times 1600}{227}$$

$$\Omega = \frac{[0.5] \times 1600}{227}$$

$$\Omega = \frac{800}{227}$$

$$\Omega = +3.50\ \%\ weight$$

Other parameters that define an explosive's properties are the velocity of detonation (VOD), detonation pressure and density. The VOD is the rate at which the detonation wave propagates through an explosive (expressed in $m.s^{-1}$) and the detonation pressure is the pressure (MPa) in the detonation reaction zone as it progresses alone the charge, and the density (ρ) is the mass per unit volume of a substance [2, 7]. The detonation pressure and VOD increase as the density of the explosive increases, with these values being used to determine the efficiency of the explosive material [1-2]. Explosive performance may be measured experimentally, or determined theoretically using a thermochemical code such as Cheetah [3].

Sensitiveness refers to the susceptibility of an explosive to ignite when exposed to external stimuli, such as friction, impact and electrostatic discharge [3]. Friction testing can be conducted using a BAM friction apparatus (Figure 1) in which a small amount of material is placed upon a ceramic plate [3]. The ceramic plate is then dragged under a weighted ceramic peg with the force of the peg being

modified by adding different weights to the load arm [3]. A positive result is typically determined by a small explosion or a popping sound and the friction level reported is the force at which a negative result occurs six times (with the previous weight resulting in at least one positive result) [3].

Figure 1: BAM friction apparatus.

Sensitivity to impact is typically determined by the drop hammer method [3]. This method is performed by dropping a known weight from fixed heights onto a small (approx. 10mg) sample of explosive material contained in a hammer anvil apparatus (Figure 2) [1, 3]. The Bruceton Staircase technique can be used to determine the median drop height which gives a 50% probability of ignition [1]. This value can then be used to determine the figure of insensitiveness (F of I) using Equation 2, where the standard material is cyclotrimethylenetrinitramine (RDX) which has an F of I of 80 [1]. The lower the value of F of I, the more sensitive the material is to impact [1].

Figure 2: Small hammer anvil apparatus.

Equation 2: Figure of insensitiveness

$$F\ of\ I = \frac{median\ drop\ height\ of\ sample}{median\ drop\ height\ of\ standard} \times F\ of\ I\ of\ standard$$

Electrostatic discharge is one of the most frequent and least characterised cause of accidental explosions [3]. The sensitiveness to electrostatic discharge is determined using a test apparatus (Figure 3) which applies varying spark energies (e.g. 4.5, 0.45 and 0.045 J) to a material and observing if ignition occurs [3]. Data obtained from this test may indicate if the static built up in a person's clothing is enough to cause initiation of the material [3].

Figure 3: Electrostatic discharge apparatus purpose built by the Defence Science and Technology Group.

1.2 Nitrate ester explosives

Nitrate esters are a class of organic compounds which are essentially esters of nitric acid [10]. They are generally formed through the nitration of alcohols by using either the mixed acid (sulfuric and nitric acid) method (Figure 4) or acetyl nitrate (fuming nitric acid in the presence of acetic anhydride and acetic acid) (Figure 5) [10-12].

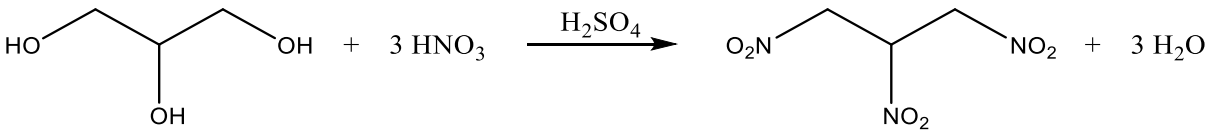

Figure 4: Formation of nitroglycerin (NG) using the mixed acid method.

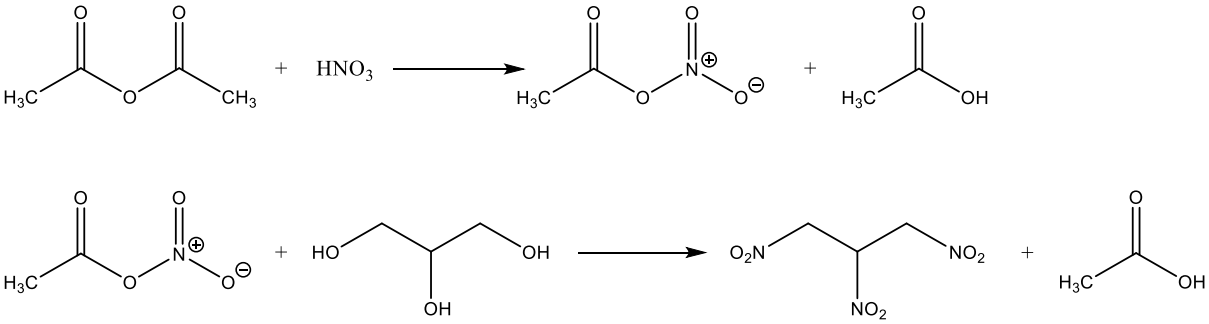

Figure 5: Formation of NG using the acetyl nitrate method.

As many compounds in this class have high oxygen content, favourable combustion characteristics and high reactivity, nitrocellulose, NG and PETN are usually found in commercial and military applications [10-11, 13]. NC, NG and PETN are some of the most common nitrate ester explosives and are often used as high explosives or in propellants [10-11, 14]. Nitrate esters undergo degradation over time with the potential for autocatalytic decomposition to occur [10-11, 13-19].

Black powder was one of the first man-made explosives (discovered in approximately 700 AD), also called gunpowder because of its later main use [20]. It was used as a pyrotechnic and propellant up until the 19th century. It was soon replaced for limited applications with NG, discovered by Professor Ascanio Sobrero and developed by the Nobel family, in the form of dynamite, a mixture of NG and an absorbent [20]. NG is the nitric acid ester of glycerol which is prepared by mixing highly concentrated glycerol with nitric and sulphuric acids [2]. Alfred Nobel soon developed a new gun powder which was a mixture of NG and NC which was given the name of a double based propellant (DBP), ballistite [20].

NC was first discovered around the same time as NG; however, its preparation was refined over decades by many workers. In 1845 it was used for mineral blasting and experimentally in guns where it was demonstrated to be better than Black powder because it was smokeless, smokeless propellants are advantageous as smoke shows the location of the shooter. However, over two decades, there were many accidental explosions due to the instability of NC [20]. It wasn't until 1868 that a stable product was developed in the form of dry compressed highly nitrated guncotton. In 1884, NC propellant used in smokeless shotguns was prepared, which later became known as a single-based propellant in order to differentiate it from ballistite [20]. Many modifications were made to propellants over the years and in the 1930s triple based propellants containing nitroguanidine were developed [2, 20].

1.3 Nitrocellulose

NC is a polymer with a cellulose backbone formed by the nitration of cellulose in an exothermic esterification (Figure 6). Nitration is generally achieved using a mix of nitric acid and sulfuric acid in a molar ratio range of 1:1 to 1:3 [21]. The level of nitration obtained in the NC polymer is responsible for the physical and chemical properties of the NC and hence its use. NC with a level of nitration below 12% is generally used for films and paints etc. while NC with a high nitration level (>12%) is generally used for energetic materials [21-25]. The highest level of nitration theoretically is 14.14%, however, practically a level of nitration above 13.5% is not feasible [21-24]. The level of nitration can also be reported as the degree of substitution (DS) (Equation 3) which indicates the number of hydroxyl groups exchanged for nitrate groups [21, 24-25]. This value is linked to the physical properties of NC

such as viscosity and solubility- as the DS increases the solubility decreases and the viscosity increases [21, 23-24, 26].

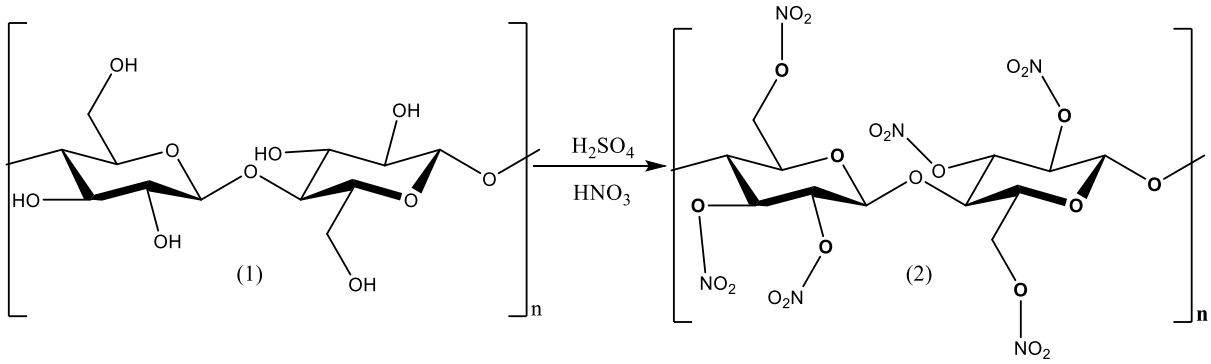

Figure 6: Nitration of cellulose (1) to form NC (2) [21, 27]

Equation 3: Degree of substitution equation for NC [21, 25]

$$DS = \frac{3.6 \times nitrogen\ content\ (\%)}{31.13 - nitrogen\ content\ (\%)}$$

NC undergoes primary decomposition in which thermolysis results in NO_2 loss from the NC chain and may also result in chain scission [22, 27-31]. The NO_2 may then act as an oxidiser and cause secondary reactions to occur [27, 31]. The secondary decomposition reactions occur faster than the primary reactions and causes autocatalytic decomposition. The overall process for NC decomposition can be seen in Figure 7 [22]. Initially, thermolysis results in the loss of the NO_2 to produce a free radical that is itself highly reactive [22, 32]. The free radical causes a carbon-carbon bond scission in the NC chain which produces an aldehyde and another radical which undergoes further decomposition to produce another aldehyde and an NO_2 radical [22].

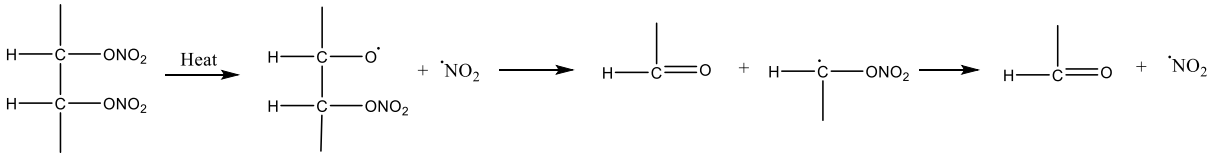

Figure 7: The decomposition of NC through thermolysis [22].

Decomposition of NC can cause the propellant to become unstable, creating the potential for self-ignition [31, 33-34]. As the decomposition of NC results in the elimination of NO_2 from the NC chain and chain scission, the nitrogen content will decrease and so will the molecular weight [22, 31, 33-34].

Both can influence the way in which the propellant will function. Due to the decrease in molecular weight, the chemical and physical properties of the propellant, such as tensile strength, morphology, and glass transition temperature change [30-31, 33]. The propellant grain may become more finely powdered, leading to an increase in surface area and burn rate [26, 35].

1.3.1 Stabilisation of NC

To avoid autocatalytic decomposition, stabilisers, such as diphenylamine (DPA) (Figure 8 (1)), ethyl centralite (EC) (Figure 8 (2)) and Akardite, are added to the propellant to react with any nitrogen dioxide formed [28, 36]. Nitric oxides react with stabilisers to form various nitroso and nitroaromatic compounds, which themselves can act as stabilisers until the aromatic moieties can no longer be nitrated. While decomposition of NC will still occur, autocatalytic decomposition will be avoided until such a time when the stabiliser content is eliminated. Once the stabiliser content is diminished, the autocatalytic process will begin. Therefore, as both the stabiliser and NC are important factors in propellant degradation, it is necessary to quantify the amount of stabiliser remaining and the amount of decomposition of NC to determine whether the propellant is both safe and will still function effectively. To monitor the decomposition of NC, the remaining stabiliser concentration is typically quantified via high performance liquid chromatography (HPLC), however, other methods such as gas chromatography-mass spectrometry (GC-MS), infrared spectroscopy (IR), Raman spectroscopy etc. have also been investigated [29, 37-46].

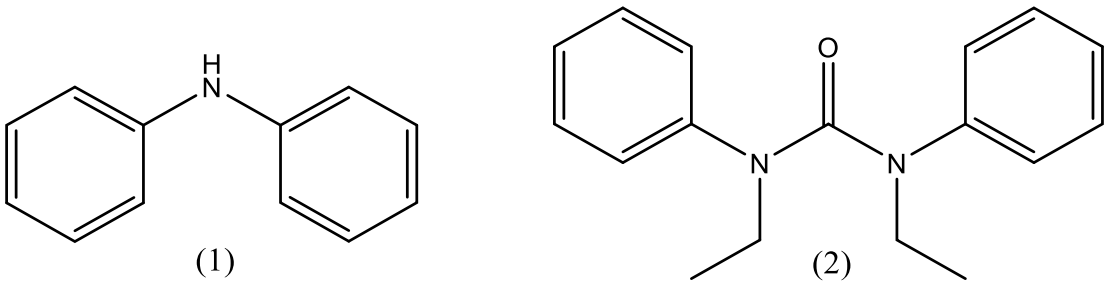

Figure 8: Structures of diphenylamine (1) and ethyl centralite (2).

1.4 Nitroglycerin

NG (Figure 9) can be produced in the same manner as other nitrate esters, with the precursor of NG, glycerol, being nitrated with mixed acids [10]. It has been reported to be either a pale yellow or colourless liquid which emits a sweet smell when heated to 50 °C and is said to taste bittersweet and spicy [10, 14]. As with many nitrate ester explosives, NG is also prone to thermal decomposition, like that of NC, where in a sealed vessel, NG will produce NO_x that can cause autocatalysis and hence accelerate decomposition [47-48]. This decomposition has potential to cause the NG to explode.

Although it has high sensitivity and is prone to thermal decomposition, NG is generally used in double and triple based propellants or mixed with gelatinizing agents for use in dynamite [10, 47-50].

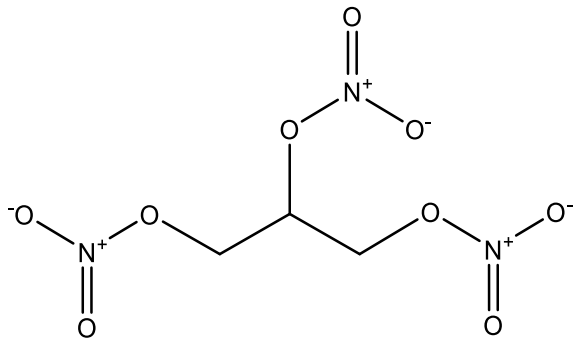

Figure 9: Structure of NG

1.4.1 Stabilisation of NG

Although NG is used in double and triple based propellants, there is little information on the effects of stabilisers on NG as much of the focus is on the stabilization of NC. One article investigated the effects of common stabilisers such as DPA, EC and Akardite II and phenolic compounds on the thermal stability of NG [48]. The results of the study suggest that DPA delays the exothermic peak of NG from 4.6 h for neat NG to 13.8 h for NG with 6 wt.% DPA [48]. However, there was a small exothermic peak that occurred before the main heat release (Figure 10) which doesn't occur for neat NG [48]. The authors suggest that this heat release is due to reactions between DPA and NG, as the amount of heat released was dependant on the amount of DPA used (32, 100 and 152 J per gram of NG for 2, 4 and 6 wt.% DPA respectively) [48]. It is possible that this effect accounts for a previous study which suggested DPA has little stabilising effect on DBPs [29, 48]. The results of the study suggest that Akardite II was the best stabiliser to use for NG, while phenolic compounds, such as butylated hydroxytoluene (BHT) had a similar effect as 2-NO-DPA and hydroquinone (HQ) destabilised NG [48].

Figure 10 has been removed due to Copyright restrictions.

Figure 10: A thermodiagram of NG with DPA. A small exothermic peak is observed before the main peak for NG with DPA which is dependent on the amount of DPA used. These data were taken from Kutoh et al. (2010) [48].

The stability of NG can also be affected by water and residual acid; hence it should be washed with sodium carbonate to achieve a neutral or alkaline material for safe storage. Although the thermal stability affects the safe storage life of a propellant, the mechanical properties also has an effect [51]. NG is known to migrate and evaporate from propellant formulations, which leads to a change in the mechanical properties of a propellant. A study by Sun et al. (2018), showed that over a 3 day period, the concentration of NG in a propellant reduced by 25.6%. Over this same time period, it was determined that the tensile strength of the propellant increased by 130% when tested at 50 °C and the elongation decreased by 51% when tested at -40 °C [51]. The migration of NG can be inhibited by the addition of polymers, such as polyurethane and epoxy resin, to a DBP formulation, however NG evaporation has been less studied [51].

The study by Sun et al. (2018) also investigated the possibility of adding polytetrafluoroethylene (PTFE) to a propellant mixture to enhance the mechanical properties [51]. It was observed that the addition of PTFE limited the diffusion and evaporation of NG due to the crystallinity and as such the mass loss of NG was reduced and the mechanical properties were significantly improved [51]. The elongation of polytetrafluoroethylene-double based propellants (PTFE-DBP) was increased by 115% from 6.34% to 13.6% at -40°C compared to neat DBP, while the tensile strength was increased from 3.28 MPa for neat DBP to 5.62 MPa for PTFE-DBP [51]. Over an ageing period of 3 days, the PTFE-DBP had a mass

loss of 14.0%, compared to 25.6% for near DBP. Although the mass loss could still lead to a decline in mechanical properties, it was observed that at 50°C, the tensile strength of PTFE-DBP remained constant, whereas the neat DBP tensile strength increased significantly [51]. When aged for 3 days at -40°C, the elongation of the PTFE-DBP decreased by 16.2% compared to 51% for neat DBP. However, although additives can improve some characteristics of NG, such as a reduction in mass loss, they can also lead to a reduction in the chemical stability, hence, a compromise needs to be made between these factors.

1.5 PETN

PETN is a nitrate ester explosive, symmetrical in structure, first produced in 1891 and is typically a white crystalline solid [52]. It is used widely for military applications such as detonators, detonation cord and in demolition devices [2-3, 53]. Like NG, it also has a long history of being used as angina medication [52]. As it is a secondary explosive, a detonator is often required for initiation [52]. PETN has a lower toxicity than NG, has a detonation pressure and velocity that is slightly lower than RDX but higher than TNT [52-53]. However, it is inferior to ammonium nitrate and is likely to be replaced in future by explosives such as RDX, octahydro-1,3,5,7-tetranitro-1,3,5,7-tetrazocine (HMX), hexanitrohexaazaisowurtzitane (CL20) or dihydroxylammonium 5,5-bistetrazole-1,1-diolate (TKX-50) [1, 52].

1.5.1 Stabilisation of PETN

PETN is considered the most chemically stable and least reactive of the nitrate ester group [16, 54]. While it undergoes thermal decomposition, which occurs in a similar manner to NC decomposition where homolytic cleavage of the O-NO_2 bond occurs, it is relatively thermally stable [16, 54]. The temperature difference between the melting point and the decomposition temperature onset is small and hence neat PETN melt cast explosives aren't possible [10, 18]. To address this issue, PETN is generally combined with other explosives, such as TNT and NG, to form castable mixtures or is desensitised with phlegmatizers such as paraffin wax [10, 18]. By mixing two explosives, it is possible to change the properties of each, for example, adding TNT increases the thermal stability of PETN [18].

Further to thermal decomposition, PETN is prone to coarsening or sublimation; over a long time period, this can change the performance and properties of PETN [55-56]. Studies have been conducted to determine whether the homologues, dipentaerythritol hexanitrate (diPHEN) and tripentaerythritol octanitrate (triPEON), can control this ageing process [55-56]. It was determined that they have a small impact on the ageing process and can change chemical properties of PETN. For example, it was determined that the addition of these homologues reduced the vapour pressure of PETN, while the heat of sublimation was not affected [56]. Doping PETN with 1000 ppm of diPHEN led to ~20%

decrease in mass loss rate compared to neat PETN and up to a 35% decrease for 5000 ppm and 10000 ppm concentrations [55]. When using triPEON at 1000 ppm a decrease in mass loss rate of ~35% was observed, while higher concentrations actually yielded less of a change [55]. These results indicate that a PETN crystal can only accommodate a maximum level of homolog impurities (5000 ppm for diPHEN and 1000 ppm for triPEON) [55].

Another study by Zhang and Weeks (2015) investigated the effect that graphene oxide (GO) had on the stability of PETN [57]. GO is a 2D material commonly used in material sciences, which due to its large surface area has been known to alter the properties of materials with which it is mixed [57]. In the study by Zhang and Weeks [57], GO was added to PETN in order to form GO doped PETN composites (GO-PETN) with concentrations of GO ranging from 0.25 to 5% [57]. Scanning electron microscopy (SEM) was used to assess the morphology of GO-doped PETN. It was found that the PETN microcrystals in the composites were similar in size to neat PETN despite being coated with GO (Figure 10) [57].

To assess the effect that GO had on the thermal stability and sublimation rate of PETN, differential scanning calorimetry (DSC) and thermal gravimetric analysis (TGA) were conducted [57]. DSC analysis showed that the activation energy for thermal decomposition increased as the concentration of GO increased, indicating that GO doping increases thermal stability of PETN (Figure 12Figure 11). TGA analysis indicated that the rate for sublimation of PETN decreased with increasing GO concentration, however, the activation energy for sublimation decreased. The vapour pressure was also lower in GO-PETN than in neat PETN. From the results of this study, further investigation into increasing thermal stability of other nitrate esters should be considered.

There have been several studies which focused on the sublimation rate of PETN doped with Zn, Ca, Fe, Na and porphyrins [58-61]. These studies have indicated that porphyrins decrease the sublimation rate [58], while Zn has mixed results with one indication that it increases the sublimation rate [60] and others suggesting it decreases the rate depending on concentration of the Zn [59, 61].

Figure 11 has been removed due to Copyright restrictions.

Figure 11: SEM images of neat PETN and various GO-PETN composites. A) neat PETN; B) 0.25 %; C) and D) 0.5 %; E) 1 %; F) 2.5 %; G) 5 % GO-PETN composites; H) GO powders. These data were taken from Zhang and Weeks (2015) [57]

Figure 12 has been removed due to Copyright restrictions.

Figure 12: Plot of the activation energies obtained via DSC analysis for thermal decomposition of pure PETN and 0.25-5% GO doped PETN. These data were taken from Zhang and Weeks (2015) [57].

1.6 Improvised explosives

An improvised explosive device (IED) is classified as a 'homemade' bomb/explosive or a destructive device which is used to cause serious harm [9, 62]. Improvised or home-made explosives used in homemade devices that are designed to cause injury or death range from small pipe bombs to devices capable of causing mass damage and loss of life [8-9]. They are used by terrorists and are typically made by combining an oxidiser and a fuel such as a chlorate and a carbohydrate; however, some contain the oxidiser and fuel in the molecular structure, such as NG [5, 8]. Improvised explosives can range from home-made production of explosives commonly used by the military, such as NG, to non-military explosives, for example triacetone triperoxide (TATP) and hexamethylene triperoxide diamine (HMTD), which have simple synthetic procedures and readily accessible precursors [7, 9].

Improvised explosives have long been a public safety concern and have been found in clandestine laboratories and in post blast residues [7]. They are usually produced by individuals working from a recipe that can be easily found online, in the form of books, forums, articles etc., using kitchen equipment instead of laboratory grade equipment [7-9]. However, these recipes are often inaccurate,

incomplete and dangerous to follow [8]. As some improvised explosives are highly sensitive to impact and friction, such as TATP, dealing with these is one of the most dangerous assignments first responders and bomb technicians can face [7]. In 2007, IEDs were responsible for 60% of military fatalities by insurgents in Iraq and 25% in Afghanistan [9]. By 2009, this figure had doubled in Afghanistan [9]. Due to the sensitivity of these explosives, many individuals have been killed or injured in the preparation process [8].

There have been 28,729 recorded incidents of explosive violence between October 2010 and September 2020, resulting in over 350,000 casualties [62]. Of these incidents, it is reported that approximately 48% of the explosive weapon casualties were the result of IEDs. Between October 2010 and September 2020, there were 136,669 civilians killed or injured by IEDs [62].

There have been many famous terrorist attacks using IEDs, such as the Russel street bombing in Melbourne (1986), the NCA bombing in Adelaide (1994), the Shoe bomber in London (2001), the Bali bombings (2002) and the underwear bomber (2009) [5, 8, 63-67]. Many different explosives were used in these incidents such as TATP and PETN in the shoe bomber incident, oxidizer/fuel mixtures, TNT, RDX and PETN in the Bali bombings and gelignite and detonators were stolen from a mine for use in the Russel street bombing [5, 8, 63-64, 66-67].

As these explosives are dangerous to prepare and use, individuals are continuously looking for new materials to manufacture, with nitrate ester explosives becoming more popular, particularly erythritol tetranitrate (ETN).

In November 2010, California authorities found up to 9 pounds of explosives at a residential address, including hexamethylene triperoxide (HMTD), PETN and ETN [68]. In 2014, a former UW-Madison student was found in possession of ETN which he claims he was using to make a homemade rocket [69]. He also had plans to use ETN to create a heavy armour piercing round that he would make available to law enforcement. He claims he had made the ETN a few months prior and had previously made another 3 or 4 batches [69].

In 2018, a man who owned a chemical and solvent company had his home raided [70]. Authorities found methamphetamine, 10 firearms and four explosive devices, of which the man admitted the largest device contained ETN [70]. Also in 2018, a UK binman was found with a large number of bombs after an explosion occurred [71-72]. The IEDs found at the premises were reported to contain black powder, flash powder and ETN [71-72]. The man was sentenced to 3 years and four months in prison and there was no obvious suggestion of terrorist motives. Instead it was deemed that he had a committed interest in explosives [71-72].

In 2018, a Japanese 16 year old boy was found to have refined and sold uranium [73]. He was also accused of manufacturing ETN and has been labelled a 'chemistry geek' rather than having an interest in terrorism [73]. Another man in Northern Ireland faced 3 charges of terrorism that occurred between 2011 and 2016 [74-75]. It was said that he was manufacturing explosive substances, including ETN and pipe bombs, and possessed a document containing information which could be used by a person preparing an act of terrorism [74-75].

1.6.1 Erythritol tetranitrate

ETN (Figure 13) is a solid crystalline nitrate ester that was first discovered in 1849 [76]. It has a similar molecular structure to NG (Figure 9), being a longer chain analogue of NG, and similar in physical and explosive properties to PETN (Figure 14). While ETN was one of the first nitrate esters discovered, its precursor, erythritol (Figure 15), was expensive to manufacture and not widely available [15]. In the past, erythritol was extracted from seaweed, but a new manufacturing method using microbial techniques is now available [15, 77]. This new method reduces the cost of production of erythritol and since then its availability has increased dramatically due to its popularity as a sugar alternative [77]. ETN can be formed through various processes, the two main processes being the mixed acid and acetyl nitrate methods [12, 78]. However, amateur experimenters are always looking for other preparation methods due to the availability of the reagents, especially concentrated nitric acid. As such, a method of preparation likely to be used involves combining ammonium nitrate, sulfuric acid (which produces nitric acid *in situ*) and erythritol [79]. Due to the availability of erythritol to the public, the ease of production and its explosive properties, there has been an increase in the use of ETN as an improvised explosive.

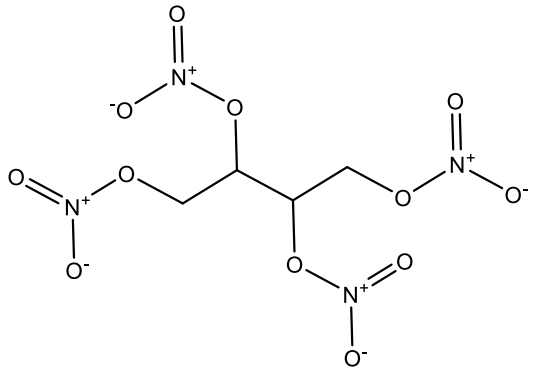

Figure 13: Structure of ETN

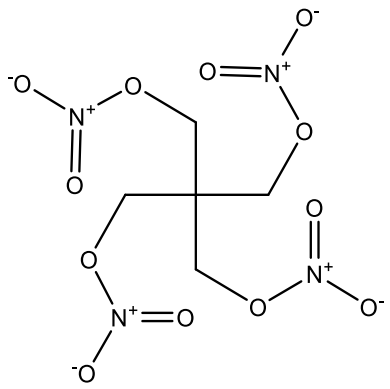

Figure 14: Structure of PETN

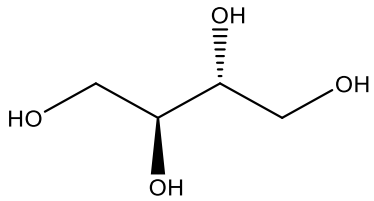

Figure 15: Structure of erythritol

As there has been an increase in the use of ETN as an improvised explosive in recent years, there has been research into its detection and explosive properties [12, 17, 78, 80-86]. These studies have determined the experimental vapour pressure, 3.19×10^{-3} Pa, compared the friction and impact sensitivity of ETN to PETN and investigated thermal decomposition [12, 17, 84, 87]. There have also been investigations into detection of ETN and its decomposition products [15, 17, 88]. Liquid chromatography-mass spectrometry (LC-MS), direct mass spectrometry (such as direct analysis in real time-mass spectrometry (DART-MS)), IR, Raman spectroscopy and GC-MS are some of the analytical techniques which have been investigated for ETN detection [12, 82, 84]. A study by Oxley et al in 2012, shows that ETN, PETN and 1,4-dinitrato-2,3-dinitro-2,3- bis(nitratomethylene) butane (DNTN or SMX) (Figure 16) were able to be separated using GC-MS [12]. However, the mass spectrum for ETN gave ions of 30, 46 and 76 m/z which are typical ions for various nitrate esters, the chromatographic peak for PETN did not reflect its concentration and the DNTN was a very broad peak. While Oxley et al. do not comment on why the GC-MS of PETN and DNTN were unsuccessful, it is possible PETN was undergoing degradation on column resulting in peak areas lower than expected. Oxley et al. make no mention of by-product peaks nor do they provide a chromatogram for PETN [12]. It is possible that the optimal gas chromatography (GC) conditions used for ETN were not acceptable for DNTN, hence

it gave a broad peak. Again, a chromatogram was not provided and there was no mention as to whether other GC conditions were investigated for DNTN [12].

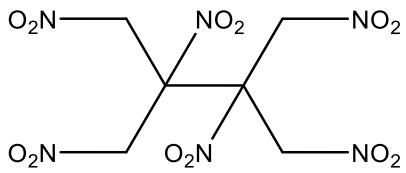

Figure 16: Structure of DNTN.

1.6.2 Thermal decomposition of ETN

Computational and experimental studies into the thermal decomposition of ETN have become more frequent in recent years. Through these studies, information about the decomposition pathway and the decomposition products of ETN has developed. In 2017, Oxley et al., identified three main decomposition products using high resolution LC-MS. These were erythritol trinitrate (EtriN), erythritol dinitrate (EdiN) and erythritol mononitrate (EmonoN) (Figure 17; A, B and C respectively) [17]. Initial decomposition pathways, such as O-NO_2 bond breakage, like that of NC (Figure 7) and exothermic release of HONO, were considered. Activation energies of each pathway were determined and O-NO_2 bond cleavage (121.3 kJ.mol^{-1}) was found to be approximately 37 kJmol^{-1} lower than release of HONO (158.3 kJ.mol^{-1}) indicating that O-NO_2 bond cleavage is the energetically favoured pathway [17].

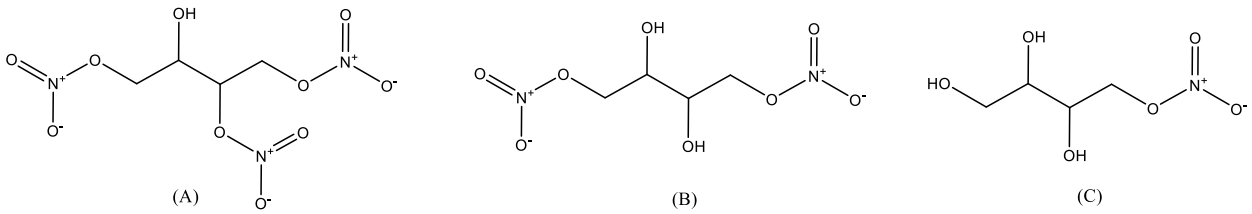

Figure 17: Structure of A) erythritol trinitrate (EtriN), B) erythritol dinitrate (EdiN) and C) erythritol mononitrate (EmonoN) [12, 89].

Another study investigated thermal stability of ETN in various environments such as extreme heat (47 °C) and cold temperatures (-4 °C), as well as elevated humidity (90 % relative humidity) [84]. Results of this study indicated that elevated temperatures and increased humidity result in an increase in the decomposition rate of ETN, with less than 5 % remaining after 7 days under extreme heat and 0 % remaining after approximately 4 days under increase humidity (Figure 18) [84]. In cold environments, ETN was found to be the most stable, with approximately 76 % remaining after 42 days. The results of this study indicated that there may be additional decomposition pathways occurring in ultraviolet (UV), increased humidity and ozone-rich environments [84]. Although this study has shown decomposition of ETN within 7 days, it was conducted on the nanogram scale; hence it is unclear if

the same rate of decomposition occurs with larger quantities of the explosive. There is little information on the effect residual acid or acid vapour would have on the decomposition rate and whether it is possible for the explosive to be stabilised to reduce the rate of decomposition.

Figure 18 has been removed due to Copyright restrictions.

Figure 18: Stability curves for ETN for seven environmental conditions; A) room temperature, -4 °C, 30 °C and 47 °C; B) under ozone, 90 % relative humidity and UV. These data were taken from Sisco et al. (2017) [84].

As ETN has a low melting point (61 °C) [12, 15, 90], and has a high temperature at which it undergoes violent decomposition (~200 °C) [12, 15, 90], it is thought that ETN could be used in melt cast explosives [91-92]. There are many properties that are needed for successful melt casting, such as a low vapour pressure, significant separation between the melting point and the temperature at which decomposition occurs, and there should be no cracking or shrinking upon cooling [91-92]. Most melt cast explosives do not generally meet all the requirements. Examples of melt cast explosives used by the military industry include TNT, 2,4-dinitroanisole (DNAN), 1,3,3-trinitroazetidine (TNAZ).

A study by Kunzel et al, 2017, reports on the sensitivity and performance of ETN in a crystalline form and in a melt cast form, the results of which indicate that there is no significant difference between the two in regard to the sensitivity towards impact and friction [90]. However, other studies investigating the sensitivity of ETN in its solid state and in molten form, show a large difference between the impact sensitivity (D_{H50} solid ETN 14.7 ± 3.4 cm and D_{H50} molten ETN 1.0 ± 0.6 cm) [93]. It is suggested that this is due to hot spots caused by bubble collapse and increase in density or shear forces in a liquid. Chemical analysis was conducted on the neat ETN and the molten ETN which had been allowed to resolidify with results suggesting there was no significant difference between the samples [93]. As a consequence, the authors suggest the difference in sensitivity between solid and molten ETN is due to the phase change rather than chemical effects [93]. In addition, the effect of impurities on the thermal stability of molten ETN was investigated. The results indicate that impurities

lead to a decrease in the thermal stability; samples that had not undergone sufficient purification began decomposition within 22 minutes at 90°C [93]. These samples had much lower activation energies (24.5 and 4.6 $kJ.mol^{-1}$) compared to samples that had been extensively purified (62.9 $kJ.mol^{-1}$) [93].

According to Oxley, Smith and Brown (2017) ETN is more powerful and more sensitive than TNT and was thought to have potential to replace TNT in melt case explosives [89]. However, they suggest that neat ETN may be too sensitive for melt casting and hence eutectic mixtures may be of use [89]. Some of the eutectic mixtures investigated were ETN-TNT, ETN-PETN, ETN-DNAN etc. and it was shown that ETN eutectic formulations show potential, however it is suggested that further testing should be conducted [89].

Another study investigated the thermal behaviour and kinetics of mixtures of ETN with PETN or RDX [15]. It was determined that mixing ETN with either PETN or RDX resulted in ETN being less sensitive to initiation. The ETN/RDX mixture resulted in decomposition of the RDX and ETN separately, however, the ETN decomposition occurred at a higher temperature than for neat ETN and that the autocatalytic decomposition of RDX was inhibited [15]. From these studies, there is potential for improvised melt cast ETN and melt cast mixtures of ETN to be encountered by police and other first responders, however the latter may be less likely due to the complexity of co-melt casting multiple explosives.

This research suggests that combining ETN with other explosives has potential to improve its characteristics, it could also reduce the effectiveness of ETN and the explosives it is combined with. Although there is significant research on melt cast ETN, there is little research on the effect of combining it with stabilisers such as DPA and EC. Therefore, there is a gap in literature regarding the stabilisation of ETN using conventional stabilisers that are successful for NC stabilisation.

1.6.3 Xylitol pentanitrate

Xylitol is another sugar substitute that can be converted into a short chain nitrate ester explosive through nitration of the alcohol functional groups. Like erythritol, xylitol is also widely available in supermarkets and is in high demand in the food industry. The market for xylitol is expected to exceed US$ 1148.6 million by 2023, with a compound annual growth rate (CAGR) of more than 5.7% during 2018-2023 [94]. The main drivers for the demand of xylitol are its use as a sugar alternative for diabetics (the metabolism is insulin independent), it has a similar sweetness to sugar but with 40% less calories and has been shown to reduce tooth decay compared to sucrose [94-97].

The method for the industrial production of xylitol used to rely on the conversion of D-xylose by chemical hydrogenation in the presence of a nickel catalyst at elevated temperatures and pressure [95, 97]. However, this method resulted in a recovery of 8-15% xylitol and the resultant product was

very expensive due to the extensive separation and purification procedures used [97]. As there was a high demand for xylitol, there was a requirement to find alternative preparation methods that are cheaper and less laborious. Currently xylitol is manufactured using a thermochemical pre-treatment of lignocellulosic biomasses which produces hemicellulosic hydrolysate, rich in xylose [96]. This is then further purified and reduced to form xylitol [96].

Xylitol pentanitrate (XPN) is produced through the nitration of xylitol using a similar method as that used to produce ETN [98-99]. Although it is reported by Wikipedia to be a liquid, it was first reported as a crystalline solid with a low melting point [98, 100-101]. As it typically forms a liquid rather than a crystalline solid, it hasn't found much use as a military explosive, however, as the raw material is so widely available, it is possible that it may become of interest to amateur experimenters and terrorists.

There has been little reference to XPN in literature, with 19 publications observed when conducting a structure search on the SciFinder database, one of which makes up a chapter of this thesis. A search of the term 'xylitol pentanitrate' on the SciFinder database also provides 19 publications, however there are some differences to the articles found. From the term search, another paper that makes up a chapter of this thesis is obtained, and one article is observed twice. From the publications found, only 7 present experimental data, with 2 being a part of this thesis [102-103] and 1 publication which presents computational IR data [104]. Of the 5 experimental data publications, 2 examine the thermal stability and decomposition of XPN among other nitrate esters [85, 105], two report the electrochemical properties [106-107] and one presents atmospheric pressure chemical ionisation-mass spectrometry (APCI-MS) data [99].

The two studies that investigate the thermal stability and decomposition of nitrate esters, did so by determining the activation energy, obtaining DSC and TGA data. The peak decomposition temperature and critical temperature (the lowest temperature at which the material can be heated without undergoing thermal decomposition) of 10 nitrate esters were determined [85, 105]. The first paper in the series gave a theoretical order of stability with XPN being the second least stable nitrate ester tested after mannitol hexanitrate (MHN) [85]. It was also stated that an increase in nitro groups results in a lower activation energy, hence there is less energy needed to break the O-NO_2 bond. For XPN, the activation energy was determined to be 140.1 kJ.mol^{-1} (with the mean activation energy of all nitrate esters tested being 145 kJ.mol^{-1}), the peak decomposition temperature was 184.4°C (with a heating rate of 10 °C.min^{-1}, a pressure of 0.1 MPa and a mass of 2-3 mg) and the critical temperature was calculated to be 169.3 °C [85]. The second paper, which reports the thermal stability and decomposition of nitrate esters, is a follow on paper from the first [105]. In this paper they found the mean activation energies of the 10 nitrate esters tested to be 152 kJmol^{-1}, while XPN has an activation energy of 140.1 kJ.mol^{-1}, which is in agreement with the first study [105]. The decomposition pathway

is again suggested to be through bond cleavage of the O-NO_2 bond with the theoretical bond dissociation energy being 152-161 kJ.mol^{-1}. The study suggests that as all the nitrate esters tested decomposed in liquid form, the crystal lattice of the molecule has no effect on decomposition and hence the decomposition rate is dependent on the chemical structure of the molecule [105]. Again, it is suggested that an increase in nitro groups results in a lower stability, hence XPN is less stable than ETN [105]. Both studies also report the VOD and density of XPN, however, the reported values are different in each study. The values for the VOD were found to be 7.10 km.s^{-1} and 8.61 km.s^{-1} and the values for the density were reported as 1.58 g.cm^{-3} and 1.72 g.cm^{-3} [85, 105]. The second paper also reported a heat of combustion of 2409.7 kJ.mol^{-1} for XPN [105].

There is one study that investigates the mass spectrum of XPN through APCI-MS, along with sorbitol hexanitrate (SHN) and MHN [99]. As is typical for nitrate esters, the APCI-MS was conducted in negative mode with the molecular mass of XPN not being observed. Although some fragments such as $[XPN+NO_3]^-$, $[NO_3]^-$ and various carbonate adduct ions were observed, dichloromethane (DCM) was added to improve sensitivity and selectivity for the detection of MHN, SHN and XPN [99]. The addition of chloride ions for nitrate ester analysis by mass spectrometry (MS) has been previously shown to improve the selectivity and sensitivity of other nitrate esters, such as ETN. It was reported that each nitrate ester followed a similar fragmentation pathway in the presence of DCM and produced chloride adducts, such as $[M+Cl]^-$, for XPN [99]. The ion at m/z 331.2 was either due to $[XPN+NO_2]^-$ or due to a lesser nitrated by-product $[XteN-H]^-$ (e.g. xylitol tetranitrate (XteN)); LC-MS was used to determine if the fragment occurred as a result of MS fragmentation or if there was a lesser nitrated by-product in the starting material [99]. It is shown in the supplementary information that this ion could be from either $[XPN+NO_2]^-$ or $[XteN-H]^-$ as there was a XteN impurity within the sample [99].

Although there has been reports of some explosive performance data of XPN, such as VOD, the values reported are inconsistent and hence there is a need for further investigation [85, 105]. Additionally, there is a lack of information reported on the crystal structure of XPN, along with chromatographic, Raman, nuclear magnetic resonance spectroscopy (NMR) and experimental IR data.

1.7 Methods of identification

1.7.1 Gas chromatography-mass spectrometry

GC is a technique which can separate complex mixtures. The system has either a packed column or a capillary column with the latter being more commonly used [108-111]. Capillary columns are hollow tubes of varying lengths (most commonly 30 m long) with the inner wall coated with a liquid stationary phase of varying thickness [108, 111]. While liquid chromatography (LC) uses a liquid mobile phase, GC uses a gas mobile phase [108, 111-112].

The sample is injected into the gas chromatograph which vaporises the sample. The gas is then transported through the column, which is where separation occurs, with compounds which have a higher affinity to the stationary phase eluting later than those with a lower affinity [108, 111-112]. As components elute from the column, they pass into a detector which elucidates a response which is plotted against time. The retention time of a compound can provide qualitative data, whereas the area or height of the peak produced can provide quantitative data. The retention time of a compound should remain constant so long as identical chromatographic conditions are used. For a compound to be analysed by GC, it must be thermally stable and volatile [108, 111-112].

The two most common detectors used for GC are the flame ionisation detector (FID) and a mass spectrometer [108, 112]. With an FID, the compound is mixed with hydrogen and a makeup gas before exiting the column through a jet tip. The jet tip has a high air flow surrounding it. As the hydrogen is combustible in air, the column effluent is burned, forming ions [108, 112]. These ions form a small current when a potential difference is applied. An FID has high sensitivity and a linear range for compounds containing carbon and this detector produces a response which is proportional to the number of carbon atoms in the molecule [108, 112].

An electron ionisation MS ionizes compounds by bombardment with a highly energetic electron beam (70 eV) [108, 112]. Depending upon the structure of the molecular ions thus produced they survive intact or undergo some extent of fragmentation into characteristic ions; the mixture of molecular ions and fragment ions are accelerated into the mass analysing device. There are many types of mass analysers which can be used such as a quadrupole, time of flight (TOF) or an ion trap [108, 112]. Many mass analysers (with the exception of TOF devices) only allow selected fragments with particular mass to charge ratios (m/z) to pass though at any one time to the detector (usually an electron multiplier) which is where a signal is produced [108, 112]. A mass spectrum, depicting the abundance of molecular ions and fragments, is produced by scanning the mass analyser to allow all ions to eventually be collected. A plot of total ion count vs time provides a total ion chromatogram whereas, a plot of a particular ion count vs provides a selected ion chromatogram. At each peak in the chromatogram the mass spectrum can be viewed.

GC-MS has been used to analyse nitrate esters and their decomposition products. While nitrate esters such as NG can be suitable for GC analysis, the temperatures of the GC can cause decomposition. Additionally, mass spectra of nitrate esters may be similar. A study by Oxley and colleagues [12] found that GC-MS of ETN and other nitrate esters contain the m/z peaks of 46 and 76, which are the only diagnostic peaks observed. This is problematic as GC-MS is unable to differentiate between various nitrate esters, using mass spectra only, hence standards are used to identify the chromatography peaks [12]. Oxley et al also suggest that ETN degrades in the chromatography column and injection

port of a GC-MS due to high temperatures. To address this problem, a column was cut from 30 m to 10 m in order to reduce the time ETN was subjected to high temperatures [12]. Additionally, the optimal injection port temperature was determined to be 100 °C, with decomposition observed when the inject port temperature was above 150 °C.

GC-MS has also been used for the analysis of NC based propellants [28, 113-114]. This is conducted by analysing the stabiliser and stabiliser derivatives in the propellant as it ages. Samples may undergo artificial ageing at high temperatures to simulate prolonged storage [28]. The concentration of stabiliser and the stabiliser derivatives can be monitored by [28-29, 38, 41, 113, 115]. It is thought that GC-MS could be used for ETN decomposition analysis to determine if ETN can be stabilised in a similar manner to NC. It should be noted that GC-MS is not the typical method for analysis of NC based propellants with DPA as a stabiliser. This is due to the main derivative of DPA, N-NO-DPA, thermally degrading back to DPA [28, 113-114].

1.7.2 Liquid chromatography-mass spectrometry

One of the most common techniques for nitrate ester analysis is LC or an LC with MS attached [12, 17, 84, 87, 116]. LC is a technique that separates compounds based on their polarity [108]. There are two main types of LC known as normal phase and reverse phase LC, with the latter being the most common. Normal phase LC has a polar stationary phase, such as amino or dimethylamino compounds, and a non-polar mobile phase, whereas reverse phase LC uses a non-polar stationary phase, such as C-18, and a polar mobile phase [108-109]. The time taken for a compound to elute from the stationary phase is called the retention time. This retention time is unique and is dependent on the interactions a compound has with the stationary phase; the more interactions, the longer it takes to elute [108-109].

Upon exiting the column, the molecules enter a detector where a physicochemical response gives rise to a chromatogram. One of the most common detectors used in HPLC is a diode array detector (DAD) which is a UV detector [108, 117-118]. A DAD is able to provide detection at either a single wavelength or multiple wavelengths and depending on the lamp used, it can emit radiation from 190-900 nm [108, 118]. The radiation passes through a flow cell and then a mechanically controlled slit. This is then passed through a grating which disperses the radiation into individual wavelengths [118]. An LC chromatogram plots the integrated light intensity over the wavelength range against the retention time [108, 117].

HPLC does not provide structural identification. However, when combined with MS, structural elucidation of the test species is possible [108]. There are two common ionisation methods used for LC-MS, namely electrospray ionisation (ESI) and atmospheric pressure chemical ionisation (APCI) [108-

109, 118]. Upon elution from the column, the molecules are passed into an ion source and converted to gas phase ions before entering the high vacuum of the MS. Like with GC-MS, a mass analyser is used to separate ions based on the m/z ratio, with the most common mass analysers being the quadrupole, TOF and ion trap [108]. The detector is then used to count the number of ions at each m/z value giving rise to a mass spectrum [108].

Electrospray ionisation is a soft ionisation technique [108]. This is because it applies little energy to the molecule and hence the ions formed typically remain intact [108, 118]. The solution is introduced into a capillary which has a high electric field at the end. This causes the solvent to become positively charged. Evaporation of the solvent occurs until the electrostatic repulsion is larger than the surface tension, where it reaches its Rayleigh limit and becomes unstable. This causes coulomb fission to occur which produces smaller, more stable droplets. This process continues until the droplets are of a certain radius and form gas phase ions which move into the mass spectrometer [108-109, 118-121]. This process can be enhanced with the addition of heat, collision induced dissociation, dry curtain gas etc [119]. These are then passed into a heated region causing the droplets to desolvate creating charged analyte ions which move into the mass spectrometer [108-109, 118]. As ions tend to remain intact, ESI-MS generally provides molecular or adduct ions e.g. $[M+H]^+$ or $[M+Na]^+$ [108, 118]. ESI can be operated in positive or negative mode, with the polarity being changed from positive to negative by changing the polarity of the potential imparted on the spray capillary [108-109]. In negative mode ESI-MS, ions such as $[M-H]^-$ and $[M+Cl]^-$ are produced [108].

In APCI-MS, a corona discharge is used to ionise the column eluent under ambient conditions [108-109, 118]. The column eluent is first sprayed into a heater jacket which causes the eluent to vaporise. Once vaporised, it is passed over a corona discharge needle [108-109, 118]. In APCI-MS, methanol can be included in the mobile phase to form $CH_3OH_2^+$ ions which can then be used for proton transfer to form positively charged ions [108]. Therefore, it is typically the bulk solvent which is ionised by the corona discharge and in turn collides with the eluent vapour molecules to initiate charge transfer [108-109].

ESI-MS can be used for a large range of compounds, including large proteins, whereas APCI-MS is limited to molecules under 2000 Da [108, 118]. ESI-MS and APCI-MS are considered complementary techniques, meaning when one fails, the other can often be used instead [109]. They can also both be used as direct injection-MS techniques, which involves injecting the analyte solution directly into the mass spectrometer without the use of a separation technique.

As discussed previously, LC-MS has been used to determine the decomposition products of ETN [12], whereas direct MS was used to monitor the loss of ETN under different environmental conditions over

time [84]. It has been found that nitrate esters can be difficult to identify using MS as they tend to form adducts with any impurities in the system and with decomposition products of the nitrate ester; Hence molecular ions aren't usually seen [116]. A study was conducted where additives such as ammonium nitrate, ammonium chloride, carbon tetrachloride etc., were added to the LC-MS system to promote chloride or nitrate adduction with the nitrate esters [116]. It was observed that ammonium nitrate and ammonium chloride were superior to other additives [116]. In the study by Oxley et al. (2012) which identified decomposition products of ETN, carbon tetrachloride was added to the mobile phase to form chlorine adducts [12], whereas Oxley et al. (2017) and Rapp-Wright et al. (2017) used ammonium chloride or ammonium acetate to produce adduct ions which were then probed using LCMS [17, 87]. Therefore, for analysis of ETN by LC-MS, method development will need to be conducted to determine which additive will provide suitable mass spectra and to determine the best mobile phase.

As mentioned previously, there is one article in the literature which reported the mass spectrum of XPN using APCI-MS [99]. As with other nitrate ester explosives, such as ETN, $[M\text{-}H]^-$ ions were not observed; with the addition of dichloromethane, chloride adducts were formed [99]. Although APCI-MS has been reported for XPN, ESI-MS is not observed in literature. This gap will be addressed using direct mass spectrometry techniques, which do not require chromatographic separation, such as direct-ESI-MS and a technique known as direct sample analysis-time of flight-mass spectrometry (DSA-TOF-MS) will also be used to obtain mass spectra of XPN and ETN.

1.7.3 Vibrational spectroscopy

Raman and IR spectroscopy are based on the interaction of electromagnetic radiation with molecules [122]. Electromagnetic radiation travels through a vacuum at the speed of light (c= 2.99 x 10^8 m.s^{-1}) and is related to wavelength (λ), the length of one complete wave cycle, and frequency (ν), the number of wave cycles that pass through a point in one second (Equation 4) [108, 117, 123-124]. The IR region of the electromagnetic spectrum corresponds to the vibrational energy level transitions within a molecule; the photons in this region do not have enough energy to cause electronic transitions [108].

Equation 4: The relationship between frequency (ν), wavelength (λ) and the speed of light (c)

$$\nu = \frac{c}{\lambda}$$

The way in which the energy is transferred differs between IR and Raman [122]. IR directly measures the vibrational energy level transitions as a result of IR radiation absorption [122]. Raman is a light scattering event where an incident photon of frequency higher than the infrared region loses energy to the molecular vibration of a molecule [122, 124]. The scattered photon has a reduced frequency

compared to the incident photons [122, 124]. IR and Raman spectroscopy are complementary techniques. They both provide information on the functional groups of a molecule as different functional groups will absorb IR radiation at specific wavelength which will induce different vibrational modes within a chemical bond [122-123].

For a molecule to be IR active, the absorbed radiation must cause a change in dipole moment; this occurs when two covalently bonded atoms differ in electronegativity [108, 122-124]. Therefore, homonuclear diatomic molecules, such as Cl_2, H_2 and N_2, are not IR active [108, 122-123]. For a molecular bond to be Raman active, there must be a change in polarizability of the molecule [122-124]. Bonds that are non-polar, such as N_2 and C=C, can undergo this change in polarisation and therefore produce intense peaks in Raman [122-124].

The spectra obtained from IR and Raman experiments depict a plot of the intensity of absorption (IR) or emission (Raman) as a function of wavenumber (IR) or wavenumber shift from the laser excitation frequency (Raman), with the wavenumber being inversely proportional to wavelength (Equation 5). The vibrational bands observed in the spectra are unique to functional groups and hence provide unique spectra for different molecules; IR and Raman are considered fingerprint techniques as no two molecular structures will produce the same spectrum [108, 122-123]. The spectra are able to provide information about the molecular structure and it is possible to identify unknown species by comparison to IR and Raman spectral databases [122].

Equation 5: The relationship between wavenumber ($\tilde{\nu}$) and wavelength (λ)

$$\tilde{\nu} = \frac{1}{\lambda}$$

Since the early 2000s, the use of Raman and IR for field testing of explosives has increased due to the development of portable instruments and the frequency of terrorist threats [125]. While GC-MS and LC-MS require some degree of sample preparation, Raman and IR can be conducted with very little, if any, sample preparation [126]. Due to the nature of the instruments, only mg quantities of an explosive are needed for analysis and a spectra can be acquired within a few minutes [126]. Raman and IR spectra have been well documented for the nitrate ester explosives, NG, PETN and ETN [36, 78, 81-82, 126-132]. However, as has been previously discussed, there is only one article found relating to IR of XPN [104]. This article provides computational data only, hence there is a lack of IR and Raman experimental data of XPN in literature. First responders and the forensic and military communities would find the addition of this information to be of high interest.

1.7.4 Nuclear Magnetic Resonance Spectroscopy

All atomic nuclei have a nuclear spin (I) which is dependent on the mass number and the atomic number of the nucleus [124, 133]. Nuclei that have an odd number of protons and/or an odd number of neutrons are spin active. This means their nuclei act as though they are rotating on the nuclear axis [124, 133]. For nuclei to be suitable for NMR, they cannot have a spin of 0, e.g. C^{12} and O^{16} have a spin of 0 and hence are not suitable for NMR [124, 133].

When a magnetic field (B_0) is applied to an atomic nuclei, the nuclear magnetic moment (μ)- the magnetic moment of the nucleus which arises from the spin of the protons and neutrons- orients itself within allowed orientations [124, 133]. A nucleus with a spin, I, will have possible allowed orientations given by $2I + 1$. The orientations are given by the value of the magnetic quantum number (m_1). m_1 has values of -I, -I+1, ….., I-1, I. For a nucleus with a spin of $\frac{3}{2}$, it will have 4 possible orientations, $I = (2 * (\frac{3}{2}) + 1)$, and therefore have m_1 values of $-\frac{3}{2}, -\frac{1}{2}, \frac{1}{2},$ and $\frac{3}{2}$ [124, 133]. The selection rule for NMR is $\Delta m_1 = \pm 1$, therefore m_1 can only change by one unit. The magnetic field causes the spin states to split into different energy levels. The difference in the energy between the two spin states is directly proportional to the magnetic field strength, given by Equation 6, where the difference is energy corresponds to the energy of radio waves [124, 133].

Equation 6: The energy difference between to spin states

$$\Delta E = \frac{h\gamma B_0}{2\pi}$$

In Equation 6, *h* is planks constant, γ is the gyromagnetic ratio and B_0 is the magnetic field strength.

Although it may seem like two spin nuclei would have the same energy difference when placed in the same magnetic field, this is not the case. The atoms and electrons surrounding the nuclei influence the local magnetic fields at the nuclei [124, 133]. A peak position, chemical shift (δ), in an NMR spectrum is reported in parts per million (ppm) and is reported relative to a reference material [124, 133]. For ^{1}H NMR, the reference material is typically tetramethylsilane (TMS). In a ^{1}H NMR spectrum, the protons which appear upfield (lower ppm) are in electron rich environment and are magnetically shielded (i.e., their local magnetic field strength is relatively low), whereas protons that appear downfield are in an electron poor environment and are deshielded (i.e, their local magnetic field strength is closer to the applied magnetic field strength) [124, 133]. For CH_4, the chemical shift is 1.0 ppm, however, if a hydrogen is replaced with electronegative atoms, the protons become deshielded, e.g. CH_3I= 2.2 ppm, CH_3Cl= 3.1 ppm [124]. Double and triple bonds in molecules also affect the shielding of a proton, with an alkene deshielding protons and an alkyne shielding them. Each chemical

shift in an NMR spectrum can be related to a number of hydrogens; if two protons have the same environment, they are chemically equivalent and will have the same shift in ^{1}H NMR [124, 133].

NMR provides important structural information by observing the interplay of different nuclei, such as ^{1}H and ^{13}C, contained in the molecule. Hence, NMR is useful in determining the structure of unknowns and determining sample purity. The NMR spectra for NG, PETN and ETN are well documented [17, 81, 134]. However, there is no literature containing NMR data for XPN. As NMR instrumentation has progressed, benchtop NMR has been developed with Bruker selling an 80 MHz NMR spectrophotometer that can fit inside a fume hood [135]. Although the benchtop NMR has a lower magnetic field strength, leading to lower resolution spectra, some laboratories may not have the space for an NMR with higher magnetic field; therefore, it would be beneficial to obtain spectra for the nitrate ester explosives using a benchtop NMR.

Chapter 2: Analysis of Nitrate Ester Explosives Using Cold-EI GC-MS

The research conducted in this chapter was peer-reviewed and published. This first appeared in:

Stark, K. A. S.; Fitzgerald, M.; Lenehan, C. E.; Kirkbride, K. P., Analysis of Nitrate Ester Explosives Using Cold-EI GC-MS. In *50th International Annual Conference of ICT*, Karlsruhe, Germany, 2019.

For the purposes of this publication, the approximate contribution of each author was Stark, K.A.S. 50%, Fitzgerald, M. 20%, Kirkbride, K.P. 20%, and Lenehan C.E. 10%

The full text of the publication has been incorporated in Chapter 3 below.

Please note- Minor formatting amendments have been performed to the presentation of the publication to keep it consistent with the presentation of the thesis, however text and data remain unchanged from the published version

2.1 Chapter Summary

XPN is a nitrate ester explosive that is gaining interest due to the increased availability of its precursor. A GC-MS method has been developed for this explosive. Electron ionisation (EI) GC-MS spectra of nitrate esters typically do not display a molecular ion; often only 46 and 76 m/z ions are detected. This makes it difficult to identify an unknown nitrate ester without the use of standards and retention time data. A cold-EI MS method has been developed that can distinguish between the nitrate esters NG, ETN, PETN and XPN. Differentiation was possible due to the presence of high m/z ions.

2.2 Introduction

XPN is a nitrate ester explosive that is rarely mentioned in the literature. It was first isolated as a crystalline product in 1960, however, literature discussing the substance dates back to the late stages of the 19th century [100]. One factor that could have contributed to the lack of interest in XPN as a military or improvised explosive was that xylitol, the precursor to XPN, was expensive to manufacture. However, due to new manufacturing methods, driven by the food industry, xylitol may now be produced cheaply and in bulk quantities by the reduction of xylose, which is derived from wood waste. [136]. Consequently, it is expected that there will be an increase in illegal and legitimate use of XPN analogous to what has occurred for ETN, a shorter chained homologue of XPN. As such, analytical methods for the identification and analysis of XPN are important, as are methods to distinguish this species from similarly structured and commonly produced nitrate esters, such as NG, PETN and ETN.

Nitrate ester explosives can be identified using a variety of chromatographic techniques, however they are prone to thermal degradation during GC [137]. In addition, when GC is combined with MS using conventional EI, the nitrate esters that survive chromatography typically do not display a molecular ion; mass spectra of nitrate ester explosives often only show ions at 46 and 76 m/z [137]. Although it is possible to identify an unknown as a nitrate ester due to the presence of the 46 and 76 ions, further identification is not possible without the use of standards and comparison of retention time data.

Cold electron ionisation (cold-EI) offers some potential for the GC-MS analysis of energetic materials, including nitrate esters. Here the eluent exiting the GC column is converted into a supersonic molecular beam or jet [138]. This is achieved by diluting the eluent in a flow of make-up gas (helium) and then forcing the mixture at high speed through a small nozzle into a vacuum and through a pinhole into the ion source. This causes analyte molecules to lose energy via vibrational and rotational cooling prior to entering the ion source, which in turn minimizes analyte fragmentation after ionization and, consequently, an increase in abundance of molecular and high m/z ions [138]. Another benefit of this technique is that ions are less likely to suffer collision with the hot interior surfaces of the ion source, which is another cause of ion fragmentation. Although a range of electron energies can be employed in conventional EI MS, an energy of 70 eV is commonly used. Commercially available cold-EI MS equipment allows a reduction in the electron ionisation energy to further enhance the abundance of molecular or high m/z ions, though this technique is not effective for all compounds [139-140].

Fialkov and Amirav have studied the use of cold-EI for analyses of NG and PETN. Although less fragmentation was observed compared to conventional EI-MS, they suggest that cold-EI is unable to provide molecular ion information [140]. As such, they used cluster chemical ionisation (cluster CI), which utilises a similar approach to cold-EI with the exception that methanol vapour is mixed with the make-up gas and GC column eluent [140]. This method was successful at obtaining molecular ions for NG and PETN, however it is an approach that is not yet commercially available. Although cold-EI mass spectrometry of nitrate ester explosives may not produce molecular ions, it has been shown to yield high m/z ions of relatively high abundance. The purpose of this article is to: 1) explore the use of cold-EI GC-MS for the analysis of XPN, and 2) determine if XPN may be distinguished from the more common nitrate ester explosives NG, ETN and PETN.

2.3 Experimental

2.3.1 Reagents

XPN and ETN were provided by the Defence, Science and Technology Group (DST Group, Australia), HPLC grade DCM was purchased from Sigma Aldrich (Sydney, Australia) and ETN, NG and PETN

(Accustandard brand) were purchased from Novachem (Melbourne, Australia) as 1 mg.mL^{-1} solutions in acetonitrile.

2.3.2 Gas chromatography of XPN

A PerkinElmer Clarus 680 gas chromatograph coupled with a PerkinElmer AxIon iQT MS/MS system equipped with a PerkinElmer cold-EI source was used for analysis with a J&W DB-5 column (0.25 mm internal diameter with a 0.25 µm film thickness) cut to 10 m in length. A CTC CombiPal autosampler was used with a 0.5 µL injection volume. NG, ETN, PETN and XPN were diluted with DCM to a working concentration of 0.1 mg.mL^{-1}

The optimal conditions for GC analysis of XPN were determined to be an injector temperature of 160°C, carrier gas flow rate of 1.5 mL.min^{-1}, oven program beginning at 40°C with a 20°C.min^{-1} ramp to 130°C, followed by a 5°C.min^{-1} ramp to 175°C and 20°C.min^{-1} ramp to 280°C. The make-up gas flow rate for the cold-EI accessory was 60 mL.min^{-1}, source temperature was 150°C and transfer line temperature was 200°C. The electron ionisation energy used was 70 eV with a mass range of 45-500 m/z.

2.4 Results and discussion

2.4.1 GC conditions

The gas chromatogram of XPN, measured using a 30 m column, did not produce a peak diagnostic of that species. This was expected, as it has been reported that the four carbon nitrate ester homologue, ETN, underwent thermal decomposition on a 30 m column [12]. Consequently, the experiments reported here made use of a column cut to 10 m and XPN was observed to elute at 9.6 minutes when a 160°C injection temperature was used with an oven program beginning at 40°C, with a hold for 1.5 minutes, and a temperature ramp of 15°C.min^{-1} to 280°C. The ion source was set at 200°C and the transfer line at 200°C. The carrier gas flow rate was 1.5 mL.min^{-1} and the cold-EI make-up gas flow rate was 60 mL.min^{-1}. While it was possible to detect XPN with these conditions, repeatability was poor. This may be attributed to the temperature at which XPN eluted (180°C) being above its decomposition temperature (140°C), reported using DSC [85, 141]. To minimize exposure of XPN to heat within the column the flow rate was increased to 4 mL.min^{-1}. Although the average linear velocity of the carrier gas was determined to be 74.2 cm.sec^{-1}, for a column of the dimensions used and He as carrier gas, the height equivalent to a theoretical plate is within 80 % of its maximum, which is consistent with adequate performance. The oven program and injector temperature were then varied to further optimise the signal intensity for the XPN peak. A lower oven temperature program rate (10°C.min^{-1}), isothermal runs (140°C and 160°C), a higher oven temperature program rate (20°C.min^{-1}) and a multi-

linear oven temperature program were trialled. Injection temperatures from 160°C to 220°C were also tested.

The current optimal GC conditions (used to acquire the chromatogram depicted in Figure 19) were: an injection temperature of 160°C; a multi-linear oven program (beginning at 40°C, ramping at 20°C.min^{-1} to 130°C, at 5°C.min^{-1} to 175°C, and at 20°C.min^{-1} to 280°C); an ion source temperature of 150°C; a transfer line temperature of 200°C and a make-up gas flow rate of 60 mL.min^{-1}. Under these conditions, which gave an elution temperature for XPN of 157°C, the retention time and mass spectrum of the target species were repeatable.

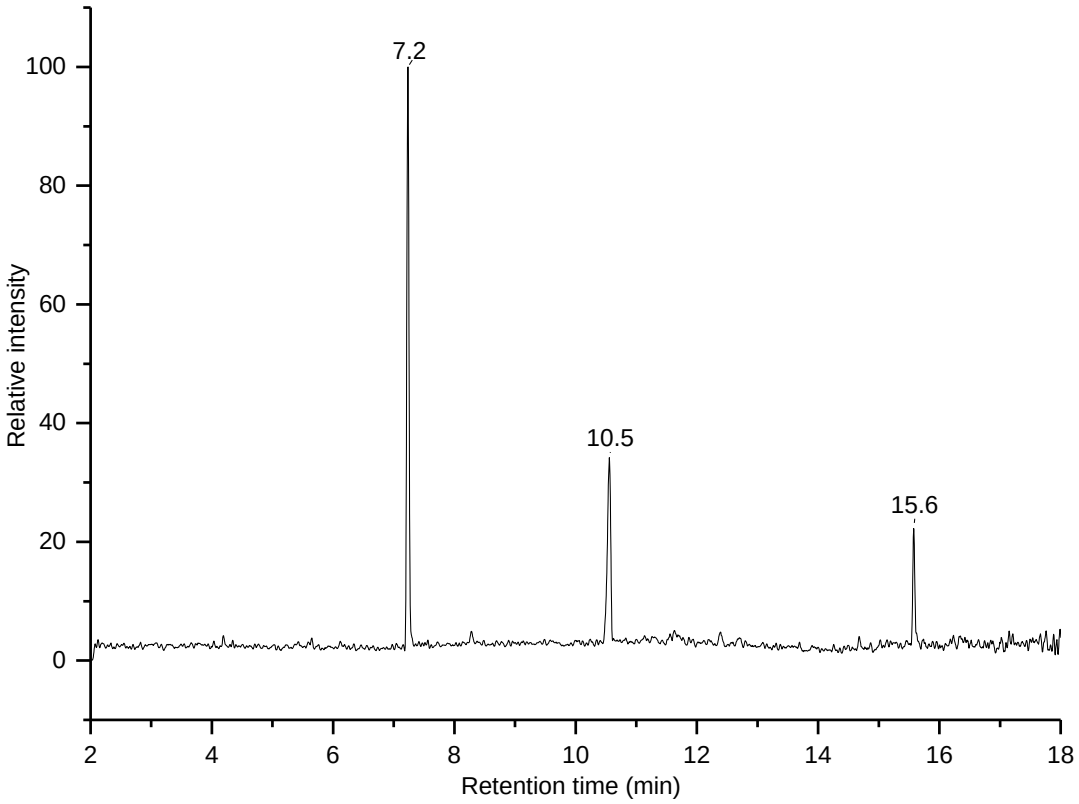

Figure 19: Gas chromatogram of XPN (10.5 min) and DPA (7.2 min) obtained using the optimal conditions. The peak at 15.6 minutes was tentatively identified as 4-nitro-DPA by comparison against a NIST library spectrum. The significance of the DPA and 4-nitro-DPA peaks are discussed later.

2.4.2 Cold-EI of nitrate ester explosives

The nitrate esters NG, PETN, ETN and XPN were examined using GC coupled with cold-EI MS to determine if these species could be differentiated. Each of the nitrate esters were subjected to GC using the optimised conditions for XPN with varying electron voltages (5 eV to 70 eV) and make-up gas flow rates (30 mL.min^{-1} to 90 mL.min^{-1}). As expected, a higher make-up gas flow rate resulted in an increased abundance of the higher mass ions with respect to the base peak (46 m/z for all nitrate

esters examined), however at low and high make-up gas flow rates, the total ion signal magnitude diminished for all analytes. Therefore, there is a trade-off between limits of detection and mass spectral selectivity, with a make-up gas flow rate of 60 mL.min^{-1} observed to achieve the best compromise. Reducing the electron ionization voltage from 70 eV has been shown to enhance the intensity of the molecular ion for some compounds [139], however for the nitrate esters examined in this study there was no significant difference. As a reduction in ionization voltage also results in a decrease in total ion abundance for each analyte, 70 eV was used for measuring all spectra reported herein.

Spectra for all nitrate esters studied displayed the typical 46 m/z $[NO_2]^+$ and 76 m/z $[CH_2ONO_2]^+$ ions. NG also gave a diagnostic ion at 151 m/z (Figure 20). PETN displayed an ion at 240 m/z (Figure 21) and ETN gave a 226 m/z ion and the ion at 151 m/z also observed for NG (Figure 22). XPN gave a similar spectrum to ETN (Figure 23), except for a large 193 m/z ion. Although molecular ions were not observed for any of the nitrate esters, it was found that each produced unique mass spectra that allowed differentiation between them.

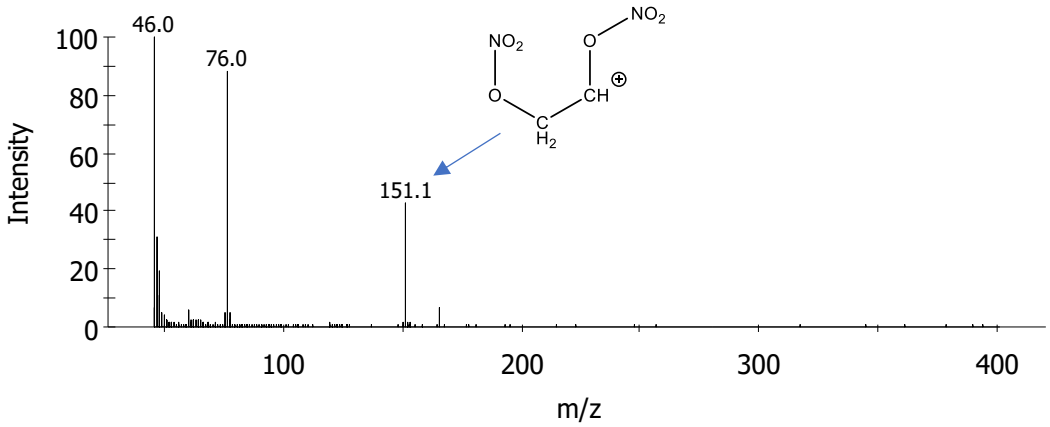

Figure 20: Mass spectrum of NG obtained with an electron ionisation energy of 70 eV and a makeup gas flow rate of 60 mL.min^{-1}.

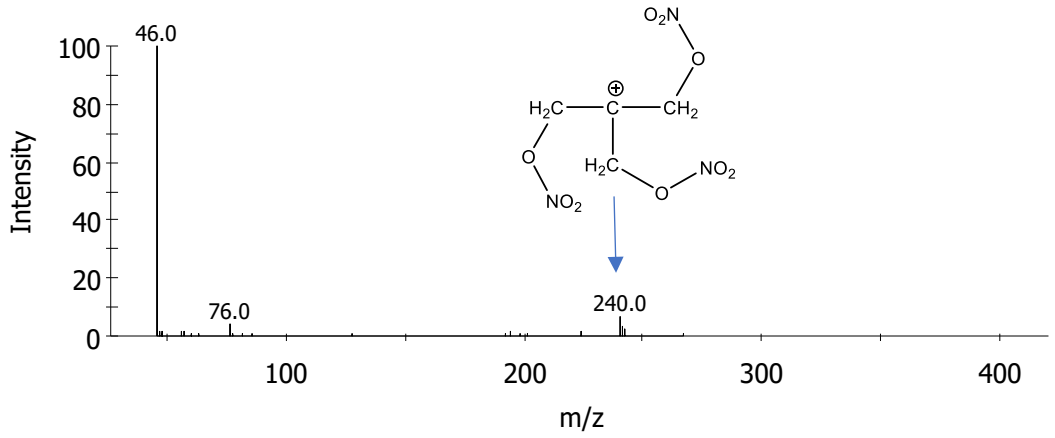

Figure 21: Mass spectrum of PETN obtained with an electron ionisation energy of 70 eV and a makeup gas flow rate of 60 mL.min^{-1}.

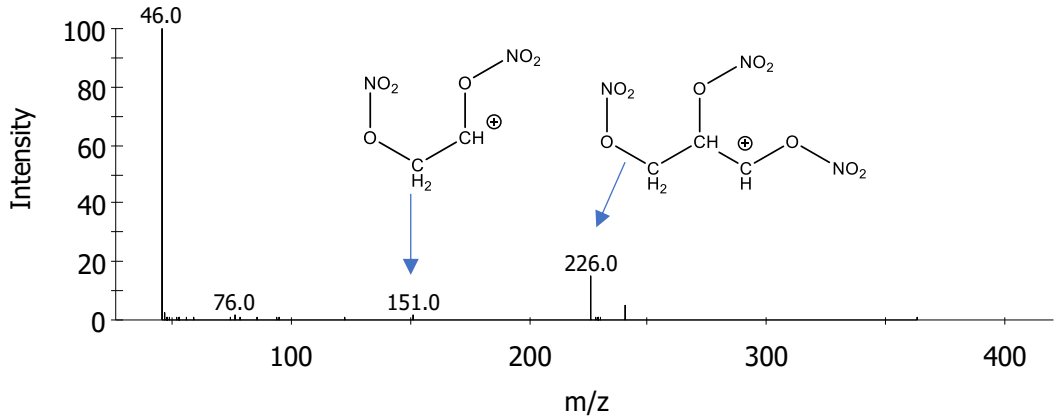

Figure 22: Mass spectrum of ETN obtained with an electron ionisation energy of 70 eV and a makeup gas flow rate of 60 mL.min^{-1}.

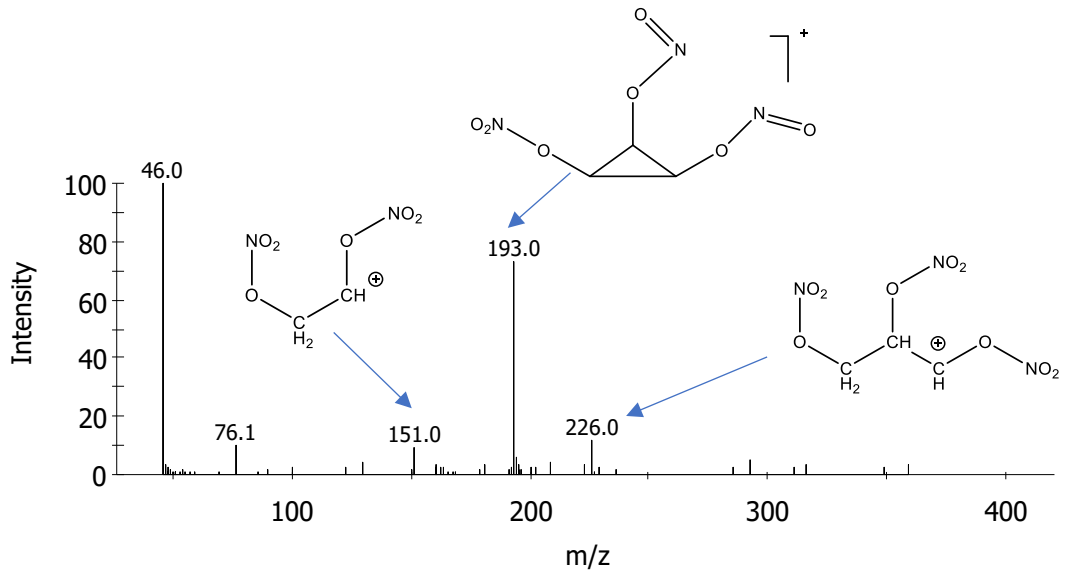

Figure 23: Mass spectrum of XPN obtained with an electron ionisation energy of 70 eV and a makeup gas flow rate of 60 mL.min^{-1}.

There is an ion at 151 m/z in the cold-EI mass spectrum of NG. This ion is also detected in low abundance in the mass spectrum of other nitrate esters, with the exception PETN, where it is absent. Structure (1) is tentatively assigned to this ion (Figure 24); this ion cannot be produced from PETN due to the absence of a methine carbon atom in the molecule. Presumably, for NG this ion arises *via* the homolytic cleavage of the terminal C-C bond resulting in loss of CH_2-ONO_2 radical. In the MS of ETN, which is the next higher homologue of NG, the corresponding next higher homologue of ion (1) at 226 m/z is observed (presumably structure 2, Figure 24) as well as ion (1) in lower abundance. Ion (1) from ETN could arise from loss of O_2NO-CH-CH_2-ONO_2 radical. As expected, XPN produced ions (1) and (2) as a result of analogous fragmentations.

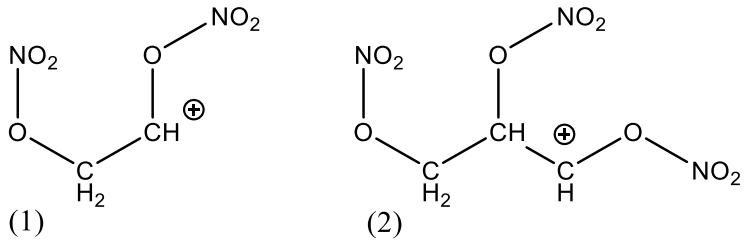

Figure 24: Postulated structures for the 151 and 226 m/z ions derived from nitro esters under cold-EI.

Surprisingly, XPN produced an ion at 193 m/z in high abundance. The mass of this ion suggests a formula $C_3H_3N_3O_7^+$, which is difficult to rationalize via simple fragmentations from XPN. The presence of 3 hydrogen atoms in the ion suggests two possible mechanisms: a) both CH_2-ONO_2 groups have been lost from XPN in addition to 2 oxygen atoms, or b) XPN loses O_2NO-CH-CH_2-ONO_2 as well as a

hydrogen atom and 2 oxygen atoms. The loss of 2 oxygen atoms suggests that a rearrangement takes place that produces a peroxy bond that further rearranges to extrude dioxygen in either mechanism a) or b) above. As the loss of $O_2NO\text{-}CH\text{-}CH_2\text{-}ONO_2$ radical from XPN would produce ion (2), which is also evident in the MS of ETN, then the spectrum of ETN may also be expected to feature a peak at 193 m/z if mechanism b) operates. As no peak is present, mechanism a) is proposed as the more likely.

A possible pathway is tentatively proposed for mechanism a), whereby the molecular ion of XPN (3) undergoes the loss of two $CH_2\text{-}ONO_2$ moieties as depicted in Figure 25 to produce ion (4) of 225 m/z, which in turn rearranges to produce the peroxy ion (5) that then undergoes what should be an entropically favourable extrusion of dioxygen to form ion (6) of 193 m/z. Although Figure 25 depicts the formation of (4) via a two-electron movement, it is possible that (4) could be produced via one-electron movement or a stepwise loss of two $CH_2\text{-}ONO_2$ radicals followed by cyclization.

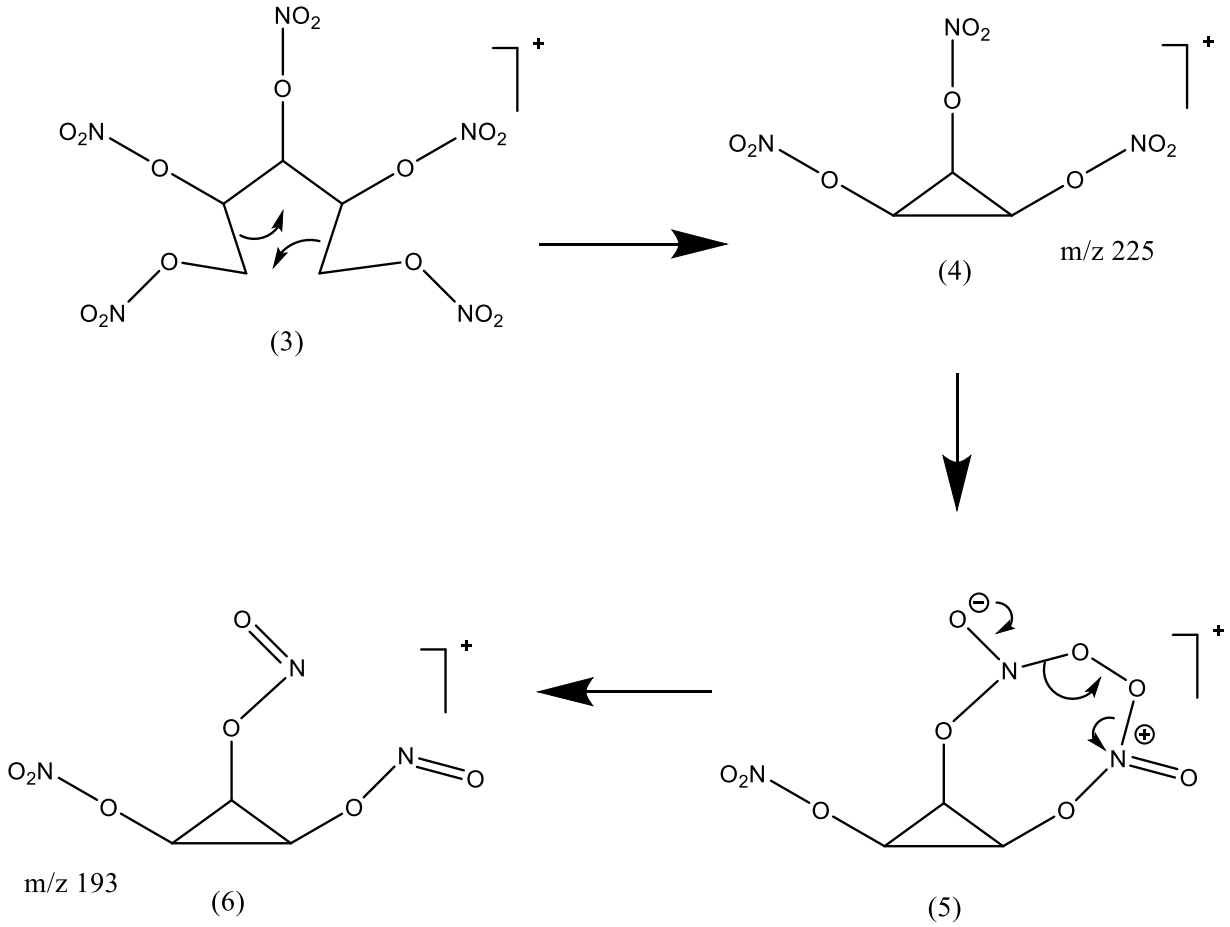

Figure 25: Postulated mechanism for the production of the 193 m/z ion from XPN under cold-EI.

While the GC-MS data displayed above were repeatable, consistency was difficult to achieve even under optimal conditions. On occasions it was not possible to detect any of the nitroesters, even though injection of a solution of a test substance (methyl heptadecanoate) indicated that the

instrument was functioning correctly. Analytical success required a clean and deactivated injection liner, but even the installation of a new liner on occasions did not instantly restore the expected nitroester signal. This may be attributed to some XPN decomposing in the injector end of the GC column and the products of decomposition thus arriving at the MS during the solvent delay period (2 minutes). To further explore this, DPA was co-injected with XPN. From these experiments a peak identified as a 4-nitro-DPA was detected as well as XPN (see Figure 19). The signal magnitude for 4-nitro-DPA appeared to be negatively correlated to the signal magnitude for XPN as GC operating conditions were varied. This suggests that decomposition of XPN takes place upon injection, presumably to yield nitrous acid that nitrates DPA before the compounds traverse the GC column where they otherwise usually would be separated.

2.5 Conclusions

A cold-EI GC-MS method has been developed that is suitable for the analysis of the nitrate ester XPN. As this nitrate ester is very thermally labile, it is necessary to reduce the time that the analyte is on the column. It was determined that a shorter column, higher flow rate and lower ramping temperatures increased the signal intensity of XPN. This chromatographic method is also applicable to NG, ETN and PETN and when used in conjunction with cold-EI MS, all the nitrate esters studied could be distinguished from one another by characteristic, high molecular weight ions. The XPN molecular ion appears to undergo a rearrangement that is not available to the other nitrate esters examined. This led to the formation of a 193 m/z ion, which has been tentatively assigned as 1-nitrato-2,3-dinitritocyclopropane.

While a measure of success was achieved in the analysis of low molecular weight nitroesters using GC-MS, the process is not simple and is prone to unpredictable failure, which potentially could lead to an unacceptably high type 2 error rate in an operational analytical laboratory.

Chapter 3: Characterisation of Xylitol Pentanitrate

The research conducted in this chapter were peer-reviewed and published. This first appeared in:

Stark, K.-A. S.; Gascooke, J. R.; Gibson, C. T.; Lenehan, C. E.; Bonnar, C.; Fitzgerald, M.; Kirkbride, K. P., Xylitol pentanitrate – Its characterization and analysis. *Forensic science international* **2020,** *316*, 110472-110472.

For the purposes of this publication, the approximate contribution of each author was Stark, K.A.S. 55%, Gascooke, J.R. 5%, Gibson, C.T. 5%, Bonnar, C. 5%, Kirkbride, K.P. 10%, Lenehan, C.E. 10%, Fitzgerald, M. 10%.

The full text of the publication has been incorporated in Chapter 3 below.

Please note- Minor formatting amendments have been performed to the presentation of the publication to keep it consistent with the presentation of the thesis, however text and data remain unchanged from the published version

3.1 Chapter Summary

Xylitol is a polyhydric alcohol that may be nitrated to form an explosive (XPN). Consequently, forensic and first response personnel may encounter XPN in post-blast residues or as a bulk material. Despite this, key analytical data for XPN that may be used in first response or forensic operations to aid its detection are not yet available in the literature. The present article provides infrared spectrometry, Raman spectrometry, NMR, chromatography, and mass spectrometry data to address this knowledge gap.

3.2 Introduction

Short-chain polyhydric alcohols are precursors for the commercial preparation of explosives such as ethyleneglycol dinitrate (EGDN), NG and PETN. The illegal manufacture of these and other non-commercial nitroesters, such as ETN, is of concern to authorities responsible for the investigation of criminal and terrorist activities [1].

Xylitol (structure 1, Figure 26) is one of three possible stereoisomers of pentane-1,2,3,4,5-pentol, and has the *2R*, *3r*, *4S* configuration. Due to the plane of symmetry in its structure, xylitol is achiral, similar to its related *2R*, *3s*, *4S* isomer ribitol, but unlike its other stereoisomer arabitol, which occurs as *2R*, *4R* and *2S*, *4S* enantiomers.

Xylitol may be nitrated to give XPN (structure 2, Figure 26) [2,3], a straight-chain homologue of EGDN, NG and ETN. XPN has been described as a plasticizer for double-base propellants [4] and although it is reported to be a liquid in the publicly-available source Wikipedia [5], it was first described in the scientific literature as a crystalline solid with a low melting point [98]. Recently, single crystal X-ray analysis of the nitrate ester of xylitol confirmed the pentanitrate, structure 2, in Figure 26 [7]. That work also reported a theoretical velocity of detonation for XPN of 8.780 $km.s^{-1}$, which is comparable to values reported for ETN and PETN, and marginally higher than the entirely computationally derived value of 8.610 $km.s^{-1}$ reported previously [8]. XPN exhibits higher friction and impact sensitiveness compared to ETN and PETN [7] and the work of Yan *et al*. [8] indicates that XPN has a lower critical temperature for thermal decomposition than ETN, which in turn has a lower critical temperature than PETN.

A survey of the open literature (CAS SciFinder Scholar structure search performed 16/11/2019) reveals only 19 publications referring to XPN. Of these publications, only six present experimental data related to its analysis. Of the six analytical publications, two examined its thermal stability and decomposition kinetics using thermal analysis [8, 10], one reported a crystal structure [7], two report electrochemical properties [11, 12], and one presented atmospheric pressure chemical ionisation (APCI) mass spectrometry data [3]. There are no reports of Raman, infrared or nuclear magnetic resonance data.

The purpose of this article is to address this knowledge gap by providing Raman, infrared, high and low field nuclear magnetic resonance and mass spectrometry data for XPN. These techniques are typical of those used by first responders and forensic analysts and the data presented will be useful references for forensic and counter-terrorism investigations.

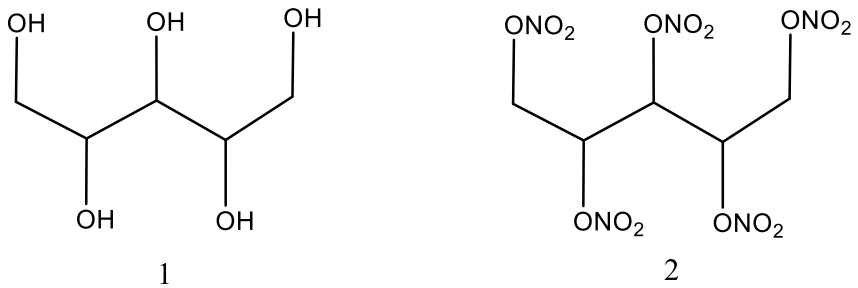

Figure 26: Structures of xylitol (1) and xylitol pentanitrate (2)

3.3 Experimental

3.3.1 Reagents

Xylitol, 98% sulfuric acid, acetic anhydride, toluene, and ethanol (Sigma-Aldrich, St Louis, USA) were used as received. Red fuming nitric acid (Sigma-Aldrich, St Louis, USA) was distilled before use. HPLC-grade methanol, d6-acetone, d3-chloroform, DCM, ammonium chloride, ammonium nitrate and 98% formic acid were purchased from Sigma-Aldrich (Sydney, Australia). Ammonium acetate was purchased from BDH Laboratory Supplies (Poole, England)

3.3.2 Synthetic Procedure

Caution: XPN is a sensitive primary explosive and as such should only be synthesised in minimal quantities by experienced and appropriately trained chemists, in purpose-built explosive laboratories.

XPN was synthesized using a literature procedure [2] then twice recrystallised from ethanol/water and shown to be free from lesser nitrated species by liquid chromatography.

3.3.3 Infrared spectrometry

IR spectra were collected using a Perkin Elmer Frontier FTIR spectrometer (Perkin Elmer, Waltham, MA, USA) operating over a spectral range of 600-4000 cm^{-1} at a resolution of 4 cm^{-1} and by co-adding 20 scans. Transmission spectrometry was carried out using a thin film of melted XPN whereas attenuated total reflectance (ATR) spectra were collected using solid XPN with the aid of a diamond ATR accessory (Perkin Elmer, Waltham, MA, USA).

Infrared microspectrometry performed on individual needles of XPN was carried out using a Nicolet Nexus 870 spectrometer attached to a Nicolet Continuum microscope equipped with a 15 x Cassegrain objective (NA 0.5) and a narrow band MCT detector (Thermo Fisher, Waltham, MA, USA). Data were acquired through a 20 x 100 µm diaphragm using 4 cm^{-1} resolution over the spectral range 4000-700 cm^{-1} and by co-adding 128 scans.

3.3.4 Raman spectrometry

Raman data were obtained using an XplorRA Horiba Scientific confocal Raman microscope (Horiba Scientific, Kyoto, Japan). Frequency calibration was achieved by assigning the signal from a silicon wafer to 520 cm^{-1}. Spectra were acquired using a 50X objective (numerical aperture 0.55) and an excitation wavelength of 532 nm. A 1200 grooves/mm grating was used to acquire the Raman spectra giving peak positions accurate to ~ ± 2 cm^{-1}. The typical integration times for the Raman spectra was 20 seconds for 6 accumulations at a power level of 1.2 mW. The sample was placed on a glass slide and Raman spectra were acquired at 5 separate positions on the sample surface.

3.3.5 Spectral data modelling

Quantum chemical calculations were performed using the Gaussian 09 suite of programs (Version 09, Revision B.01). Density functional theory (DFT) calculations were performed using the B3LYP functional with the 6-31G(d) basis set. Computed vibrational frequencies were scaled by a factor of 0.9613 [13]. IR and Raman spectra were simulated by convoluting the computed energy and intensities of the fundamental vibrations with a 10 cm^{-1} full width at half maximum (FWHM) Gaussian function. The more recent Minnesota M06-2X functional was trialled, but the intensities in the simulated infrared and Raman spectra were not consistent with that observed experimentally.

3.3.6 Nuclear Magnetic Resonance spectrometry

High field NMR spectra were recorded on a Bruker Avance III spectrometer (Bruker, Billerica, MA, USA) operating at 600 MHz for ^{1}H and 150.9 MHz for ^{13}C. $CDCl_3$ was used as the solvent and internal lock and chemical shift calibrant for ^{1}H and ^{13}C spectra (7.26 ppm and 77.36 ppm, respectively). For completeness, spectra were also measured using $(CD_3)_2CO$ as the solvent (see Supplementary Information). Chemical shifts are presented in ppm and coupling constants (J values) in Hz for all spectra. In the proton mode 16 scans were collected and in carbon mode 1024 scans were collected. Low field ^{1}H NMR data for XPN, ETN, PETN, and NG were collected using a Magritek Spinsolve benchtop NMR spectrometer operating at 60.96 MHz (Magritek, Aachen, Germany). Each explosive (10 mg) was dissolved in 1 mL of deuterated $CDCl_3$ or $(CD_3)_2CO$ (see Supplementary Information) and analysed for 10 minutes. Spectra were calibrated in accordance with the high-field experiments (above).

3.3.7 Direct mass spectrometry

3.3.7.1 Electrospray ionization mass spectrometry

Solutions of 100 $\mu g.mL^{-1}$ of XPN in methanol containing either 0.2 mM of ammonium nitrate or 0.2 mM ammonium chloride and 0.2 mM ammonium acetate were prepared. Negative ions generated using direct injection ESI were analysed using a Waters Synapt High Definition Mass Spectrometer (HDMS) (Waters, Milford, MA, USA). The solutions were injected into the HDMS using a syringe pump with a flow rate of 20 $\mu L.min^{-1}$.The desolvation temperature was 200°C, desolvation gas flow rate was 500 $L.h^{-1}$, the source temperature was 80°C and the capillary voltage was set to 3.5 kV. The acquisition rate was 1 $scan.sec^{-1}$ for 30 seconds with a mass scan range of 130 to 500 m/z. The measured mass was compared to the calculated accurate mass and discrepancies reported in ppm.

3.3.7.2 Direct sample analysis-time of flight mass spectrometry (DSA-ToF MS)

An AxION 2 Time of Flight (ToF) Mass Spectrometer, equipped with a "Direct Sample Analysis" (DSA) sample introduction system (Perkin Elmer, Waltham, MA, USA), was operated in negative ionisation mode with a heater temperature of 150°C and a corona current of 4 µA. The voltage used for the endplate was 200 V with a capillary entrance of 800 V and a capillary exit of -100 V. Spectra were acquired with an acquisition rate of 1 Hz.

An atmospheric pressure chemical ionisation (APCI) ToF Tuning mix (G1969-85010, Supelco/Agilent Technologies, Santa Clara, CA, USA), diluted 1:10 in milliQ water, was continuously nebulised into the nitrogen flow to enable accurate mass calibration (m/z 955.971923, 655.991085, 119.036320). XPN samples were dissolved in DCM to a concentration of 1 $\mu g.mL^{-1}$, of which 10 µL was pipetted onto sampling mesh (Perkin Elmer, Waltham, MA, USA) and allowed to dry. All samples were analysed in triplicate. No further reagents were added to promote adduct formation.

Spectra were analysed using the "ToF MS Driver" software (Perkin Elmer, Waltham, MA, USA, version 8.1) by averaging ~5 spectra/sample and calculating the accurate mass to $\pm$0.00005 amu. The measured mass was then compared to the calculated accurate mass for the relevant ions, with discrepancies reported in ppm.

3.3.8 Ultra-performance liquid chromatography-diode array detection

A Waters Aquity liquid chromatograph (Waters, Milford, MA, USA) was used with a Kinetex C18 ultra performance liquid chromatography (UPLC) column (2.6 µ, 50 x 2.10 mm, Phenomenex, Torrance, CA, USA). A gradient separation using 0.1 % aqueous formic acid solution (A) and methanol (B) was used. The mobile phase was 98 % A for 1 minute, ramping linearly to 100 % B at 14 minutes then back to 98 % A at 15.5 minutes where it was maintained until 20 minutes. A constant flow rate of 0.200 $\mu L.min^{-1}$ was maintained with a column temperature of 30°C and absorbance detection between 210 and 400 nm using a Waters photodiode array detector equipped with a deuterium UV-lamp (Waters, Milford, MA, USA). A solution containing 50 $\mu g.mL^{-1}$ of XPN, ETN, PETN and NG in methanol was prepared for analysis and 4 µL injections were used.

3.3.9 Gas chromatography-cold electron ionization mass spectrometry

Analyses were conducted using a PerkinElmer Clarus 680 gas chromatograph equipped with a PerkinElmer AxIon iQT MS/MS and a PerkinElmer cold-EI source (Perkin Elmer, Waltham, MA, USA). A 5% phenyldimethylsiloxane column (DB5, 0.25 mm internal diameter with a 0.25 µm film thickness, J&W brand, Agilent Technologies, Victoria, Australia) was cut to 10 m in length. A CTC CombiPal autosampler (CTC Analytics AG, Zwingen, Switzerland) was used with a 0.5 µL injection volume. XPN

was injected as a 0.1 mg.mL^{-1} solution in DCM at an injector temperature of 160°C and a carrier gas (He) flow rate of 1.5 mL.min^{-1}. The oven program began at 40°C, with a 20°C.min^{-1} ramp to 130°C, followed by a 5°C.min^{-1} ramp to 175°C and 20°C.min^{-1} ramp to 280°C. The make-up gas (He) flow rate for the cold-EI accessory was 60 mL.min^{-1}, the source temperature was 150°C and transfer line temperature was 200°C. The electron ionisation energy was 70 eV with a mass range of 45-500 m/z. For MS/MS experiments precursor ions were selected with a filter width of m/z 0,7, the collision gas was Ar (2.0 mTorr) and collision induced dissociation energies in the range 1 - 5 V were used.

3.4 Results & Discussion

3.4.1 Vibrational spectrometry

Figure 27, Figure 28 and Figure 29 show the measured infrared absorption spectra (ATR and transmission) and Raman spectrum of XPN.

An initial attempt to measure a transmission spectrum of single XPN crystals using an infrared microscope was unsuccessful; spectra were distorted by Christiansen bands (data not shown). Then, transmission infrared spectrometry was performed using a thin film of melted XPN between two sodium chloride discs. This produced a spectrum, but it was observed that the extinction coefficients for the three major spectral absorbances were so high that these peaks showed evidence of detector saturation. Therefore, steps had to be taken to reduce greatly the thickness of the film between the discs by separating them, wiping off the film that was present on one disc, remaking the sandwich and then separating it again and repeating the wiping process. The three most intense peaks in the resulting spectrum (Figure 27) were broad and showed no fine structure. Conversely, the spectrum acquired using ATR spectrometry (Figure 28) displayed fine structure and narrower peak widths.

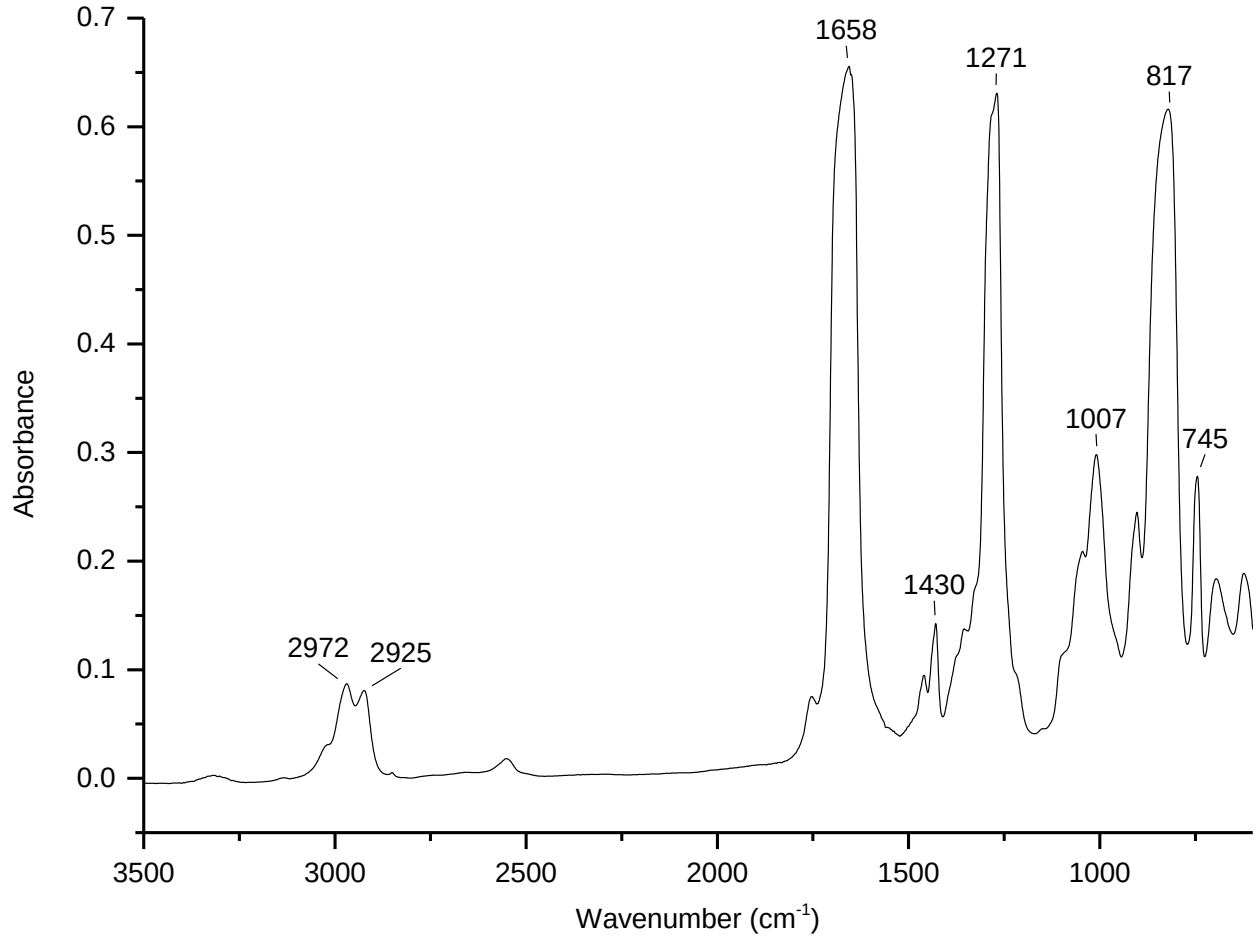

Figure 27: Transmission IR spectrum of XPN acquired from a thin film.

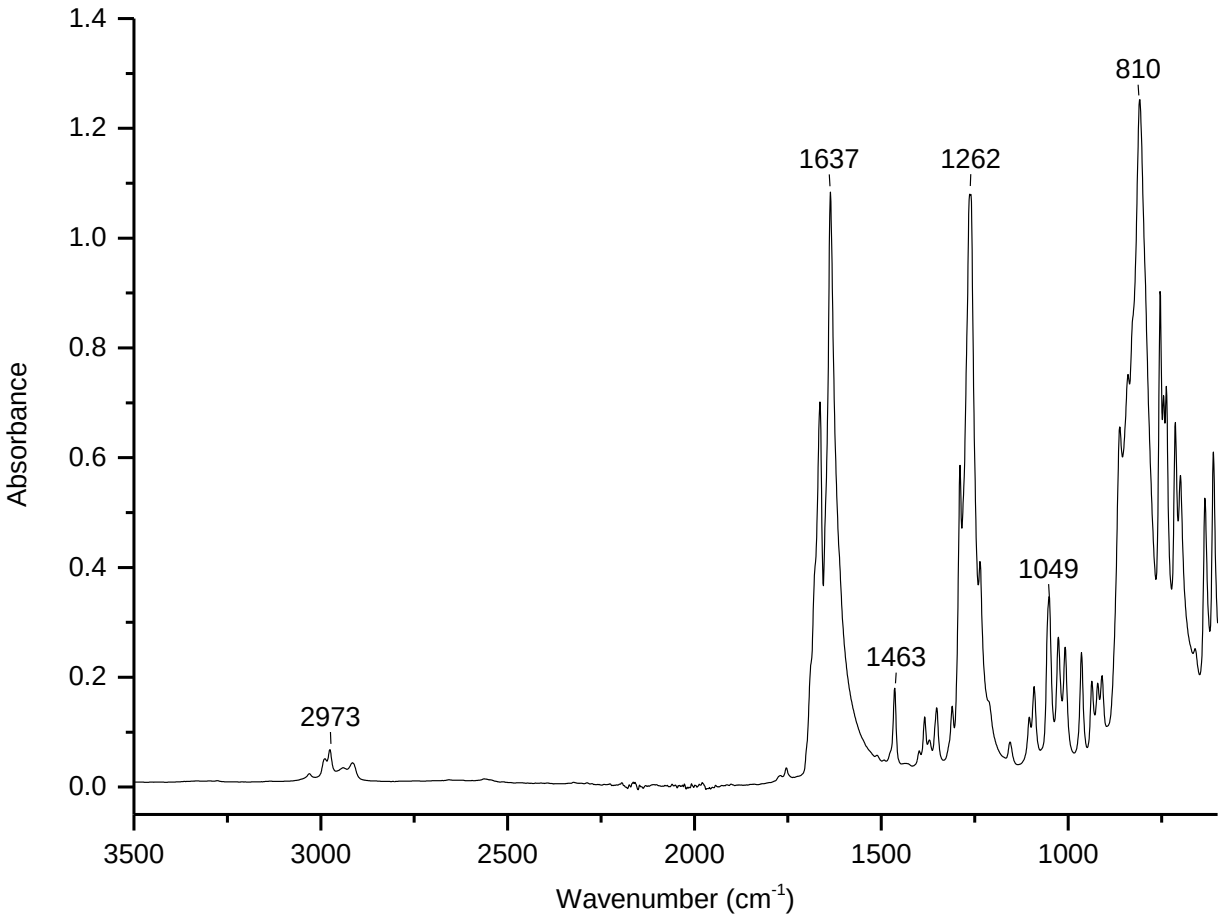

Figure 28: ATR IR spectrum of XPN acquired using solid material.

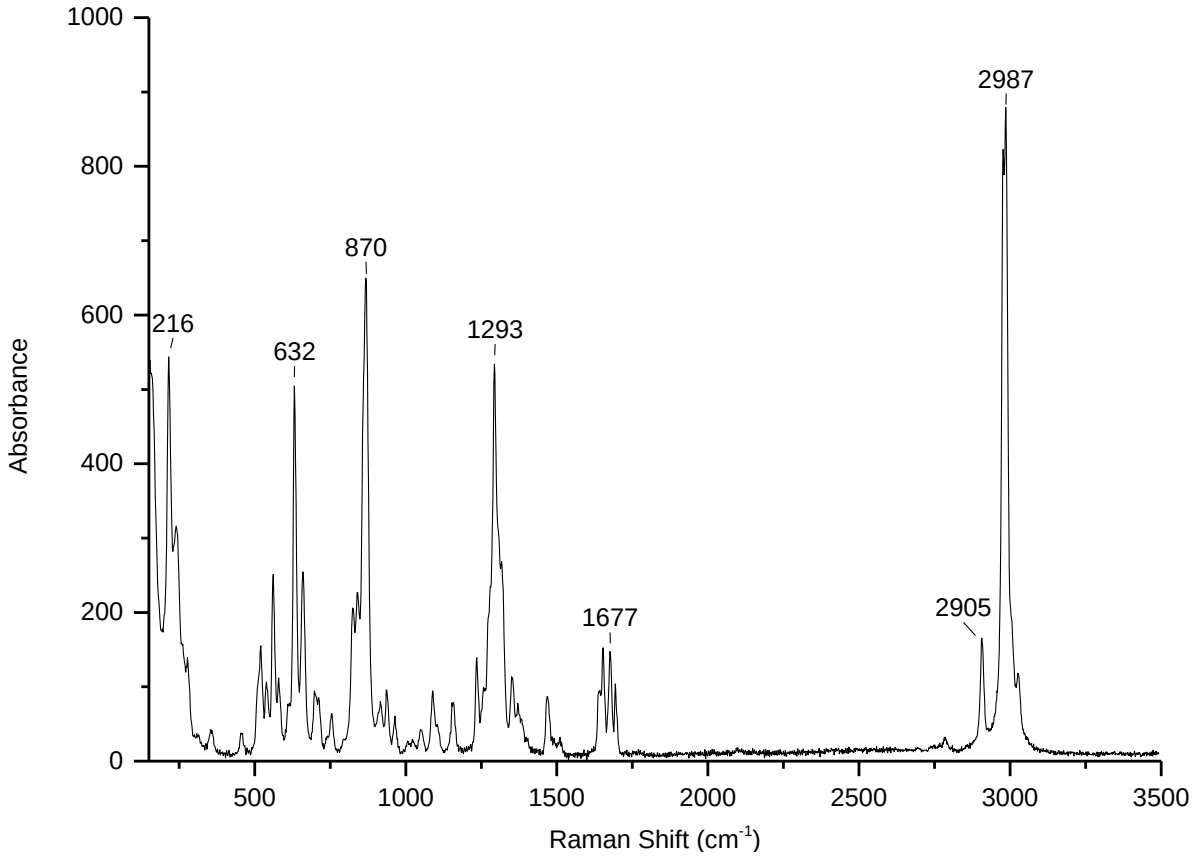

Figure 29: Raman spectrum of solid XPN.

Assignment of the gross features in the measured spectra were made by comparison with theoretically derived spectra and the known characteristic infrared absorptions and Raman transitions for nitroesters [14].

Harmonic vibrational frequencies, infrared intensities, and Raman scattering activities of a single XPN molecule were calculated at the B3LYP/6-31G(d) level of theory. The molecular structure used for the calculation was taken from previously reported crystallographic data [7]. Infrared and Raman spectra derived from the computational data are included in the Supplementary Information together with measured spectra for comparison.

The peaks observed between 500 and 800 cm^{-1} in the Raman and IR spectra are assigned to vibrations and torsions involving the C_5 backbone. Analysis of the normal modes reveal that this region also includes multiple vibrations involving out-of-plane motions of the nitrogen atoms, however these are predicted to have negligible Raman or infrared intensity.

XPN was predicted to have five ONO_2 vibrations where the nitrogen atom moves between the three oxygen atoms of the nitrate group; the O-N (O is attached to the carbon chain) bond stretches and contracts while the NO_2 group executes a scissoring motion. Oxley et al [9], when discussing the

analogous vibrations for the ETN molecule, refer to this as NO_2 scissoring. However, our modelling shows that the ETN molecule executes two combined O-N stretching and NO_2 scissoring vibrations of the type observed for XPN. The measured IR and Raman spectra for XPN show the stretching/scissoring band to be made up of several peaks, with maxima located at 868 cm^{-1} (Raman), 828 cm^{-1} (IR transmission) and 810 cm^{-1} (ATR). Calculations show that the different peaks making up the fine structure have vastly different intensities in the Raman and infrared spectra.

Although XPN is expected to have five NO_2 symmetric stretches (in-phase), the normal mode analysis reveals that these stretches are highly coupled to the motion of the CH_2 groups. This results in 12 normal modes that show significant NO_2 symmetric stretching motions with differing Raman and IR absorption intensities. In all spectra this band appears as a central intense peak with weaker peaks on either side. The maxima are located at 1293 cm^{-1} (Raman), 1278 cm^{-1} (IR transmission) and 1265 cm^{-1} (ATR). Interestingly, the predicted Raman intensity for this band is significantly lower than that observed experimentally. This anomaly was also observed by Gruzdkov and Gupta in PETN using calculations performed at the same level of theory as used here, although a definitive reason was not determined [15].

The five NO_2 asymmetric, or out-of-phase, stretches result in peaks between 1600 and 1700 cm^{-1}. Four resolvable peaks are seen in the Raman spectrum at 1640, 1653, 1676 and 1694 cm^{-1}, whereas one peak is observed in the transmission spectrum (1660 cm^{-1}) and two peaks are seen in the ATR spectrum at 1636 and 1663 cm^{-1}. As is generally seen in organic nitrates, this band is weaker in the Raman spectrum than the infrared spectrum [14]. The predicted frequencies of these bands are more than 60 cm^{-1} higher in energy than experimentally observed. Again, PETN calculations also show this discrepancy where similar calculations resulted in >100 cm^{-1} difference [15]. It is unclear if the difference is due to a limitation in the computational method used or if these vibrational modes are significantly altered in the condensed phase.

Finally, theoretical results predict the C-H stretches to be relatively intense in the Raman spectrum and weak in the infrared spectrum, which is also seen experimentally. The above data are summarized in Table 1.

In summary, Raman and ATR infrared spectrometry were simpler to conduct than transmission infrared spectrometry. They provided well-resolved spectra that were consistent with, and explainable by, theoretical results. Based on available data [1, 9, 16] Raman and ATR spectrometry provided clear differentiation between XPN, PETN and its shorter chain homologue ETN.

Table 1: Assignments of IR and Raman regions

Region	Assignment	Infrared	Raman
550-650	C-C-C bend	w	w
	Backbone torsion	w	w
650-800	N-O stretch	w	w
	N out of plane bend	w	w
800-1150	N-O stretch & NO_2 scissoring	s	s
	C-C stretch	w	w
	C-O stretch	m	w
	CH_2 rocking	w	w
1150-1400	CH_2 twist	w	w
	CH and CH_2 wagging	m	w
	CH_2 scissoring	w	w
	NO_2 symmetric stretch	s	s
1400-1800	NO_2 asymmetric stretch	s	w
2800-3000	CH stretch	w	s
	CH_2 symmetric stretch	w	s
	CH_2 asymmetric stretch	w	m

3.4.2 NMR

Analysis of XPN in $CDCl_3$ using high field proton NMR spectrometry showed the expected 3 proton environments (Figure 30): 1) the signal arising from the four (diastereotopic) methylene protons on the terminal carbon atoms was observed as a ABX multiplet centred at δ 4.66 and 4.91 ppm (J_{AB}= 13.2 Hz, J_{AX} = 5.8 Hz, J_{BX} = 4.0 Hz), 2) the signal from the two methine protons on carbon atoms 2 and 4 was observed as a multiplet at δ 5.62 ppm (2H) and 3) the methine proton on C3 gave rise to a triplet at 5.68 ppm (J = 5.5 Hz). The ^{13}C NMR spectrum of XPN in $CDCl_3$ comprised 3 signals at δ 68.05, 74.59 and 74.65 ppm. In deuteroacetone, the signal for the terminal carbon atoms was found at δ 70.19 ppm while the signals for the three other carbon atoms are observed as a single peak at δ 76.57 ppm; the high field proton NMR spectrum for XPN in deuteroacetone is given in the Supplementary Information. As all the major peaks within the ^{1}H and ^{13}C NMR spectra can be assigned to XPN, and many of the

minor peaks in the ^{1}H NMR can be attributed to satellite peaks, it suggests that the XPN sample used for analysis contained no significant levels of synthesis by-products.

The 500 MHz ^{1}H NMR of ETN in $CDCl_3$ has been reported [14] to give signals at δ 4.63 (doublet of doublets, 2H), 4.96 (doublet of doublets, 2H) and 5.53 (multiplet, 2H). While the chemical shifts for the methine protons in ETN [9] and XPN are close, differentiation between these two compounds using high field NMR in proton mode is trivial; XPN has a triplet at δ 5.68 (integration = 1H) that is absent for ETN.

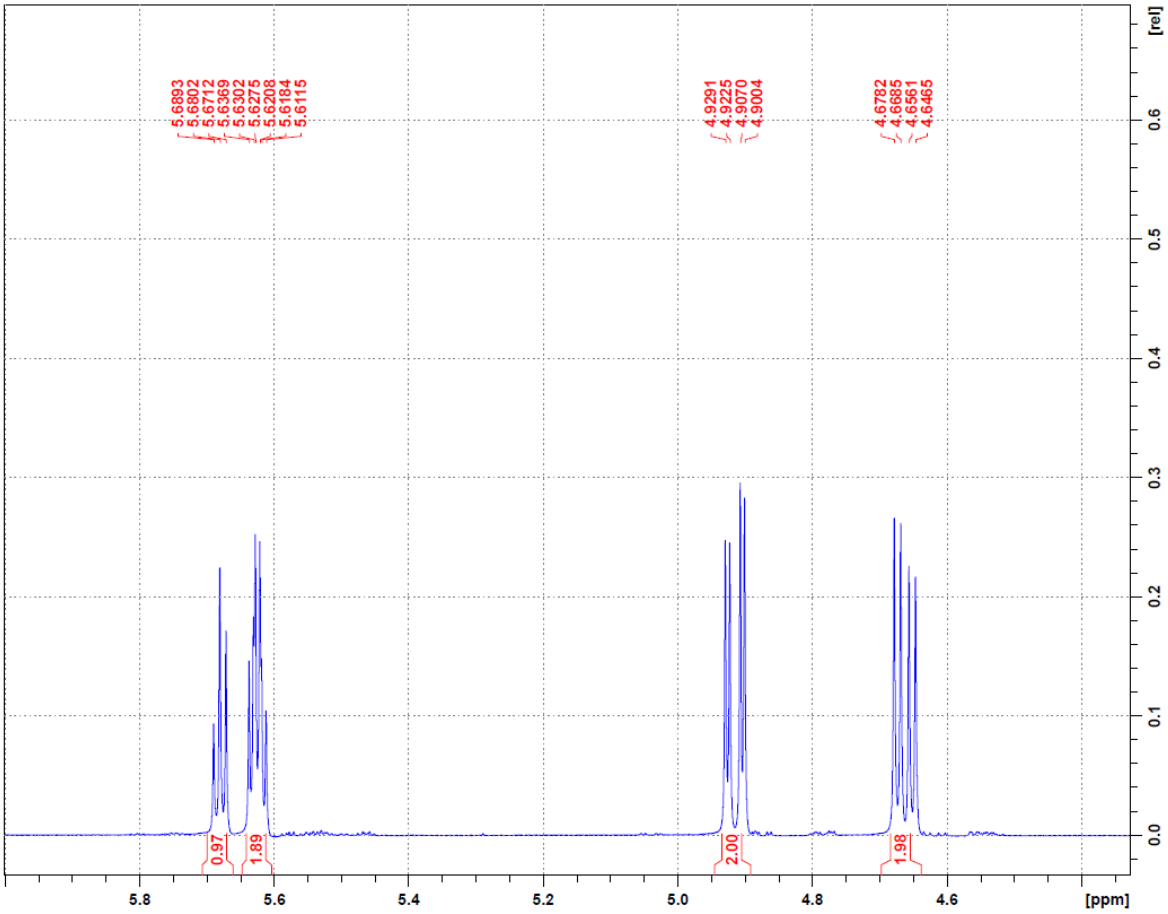

Figure 30: High field ^{1}H NMR of XPN in $CDCl_3$. See supplementary information for a spectrum of XPN in deuteroacetone.

Benchtop NMR spectrometers potentially offer valuable, inexpensive, and transportable analytical capability for first response, defence and forensic operations. Accordingly, a 60 MHz instrument was evaluated for its ability to differentiate between a range of nitrate esters of polyhydric alcohols (Figure 31). For each of the nitrate esters analysed the relevant signals were observed between δ 4.5 and 6.5. Although spectral fine structure that is evident in the high field spectrum in Figure 31 cannot be replicated with the low field instrument, integration for the methylene and methine signal envelopes

allows the four nitrate esters to be readily differentiated. The integration ratio for the low field: high field signals for NG is 1:4, for ETN it is 2:4, for XPN it is 3:4 and for PETN it is 0.

The complete analytical selectivity demonstrated by the benchtop NMR spectrometer with regards to the nitrate esters is likely to be replicated with other important molecular explosives due to the diverse proton environments in nitroaromatics, nitramines, nitroureas and organic peroxides. Therefore, this type of instrument offers potential as a practical tool for screening unknown powders for the presence of explosives. Whilst the sensitivity of these spectrometers would not allow the detection of traces of explosives on surfaces or in post-blast residues, the instrument evaluated here can be used for the analysis of samples of approximately 10 mg in weight, which is a realistic and relatively safe sample size when bulk quantities of unknown powder are under examination.

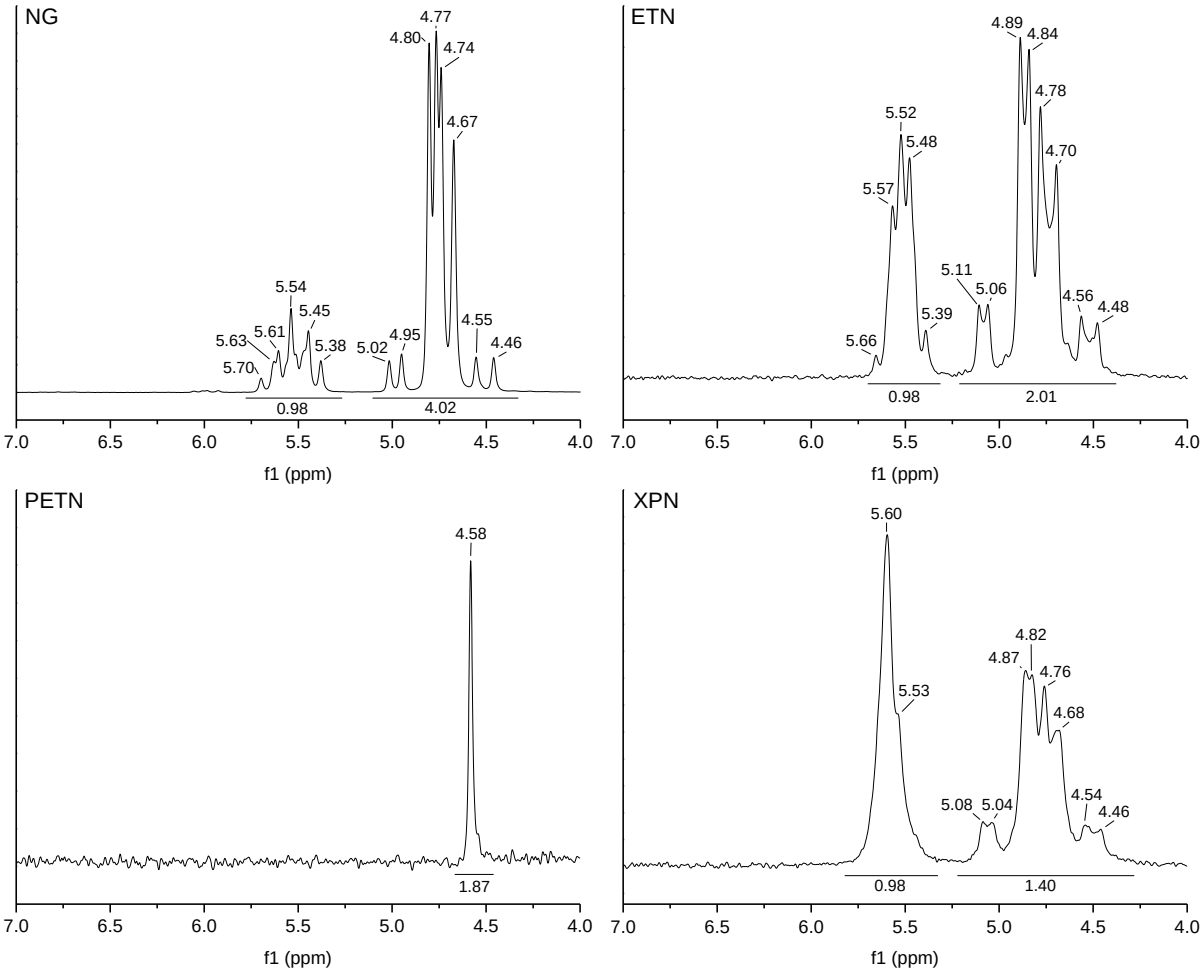

Figure 31: Low field ^{1}H NMR of ETN, NG, XPN and PETN in $CDCl_3$. See supplementary information for spectra of these nitrate esters in deuteroacetone.

3.4.3 Mass spectrometry

3.4.3.1 Direct ESI mass spectrometry

Nitrate esters typically display high electron affinities and consequently some amenability to analysis by negative ion mass spectrometry (see Ostrinskaya et al. [3] for example). Additionally, in the presence of nitrate or chloride ions, even when their presence is adventitious, nitrate esters may form nitrate or chloride adducts. The direct ESI mass spectrum, measured in negative ion mode, for a solution of XPN containing ammonium nitrate is included in Figure 32, with observed peaks, fragments and ppm differences reported in Table 2. The most abundant ions were found at m/z 438.9810 ($[M+NO_3]^-$) and m/z 393.9954. In previous work involving direct ESI mass spectrometry, Matyas et al. [16] proposed that ETN undergoes adduction of hydroxide; if XPN followed an analogous ionization pathway it could account for the formation of the ion at m/z 393.9954. However, in another direct ESI mass spectrometric study, Oxley et al. [1] proposed that ETN undergoes loss of NO followed by adduction of nitric acid. An analogous pathway could also account for the formation of the ion at m/z 393.9954 in the direct ESI mass spectrum of XPN. Yet another possibility (by analogy with ions reported arising during ETN analysis [17]) is that the ion is the nitrate adduct of xylitol tetranitrate (XteN) $[XteN + NO_3]^-$.

Direct ESI mass spectrometry in the presence of ammonium chloride and ammonium acetate produced the expected chloride adduct ions $[M + Cl]^-$ at m/z 411.9605 and 413.9694 (Figure 33, Table 3). An ion at 438.9813 m/z ($[M + NO_3]^-$) was also observed, despite no deliberate introduction of nitrate ion-producing species. The ions at m/z 366.9777 and 368.9743 were attributed to $[M - NO_2 + HCl]^-$, or to a XteN chloride adduct $[XteN + Cl]^-$, and again an ion was observed at m/z ~ 394.

The peaks at m/z 366.9777 and 393.9968 (393.9954 in the previous experiment) were initially considered to have arisen from a tetranitrate species, present as a by-product formed during XPN synthesis. However, this was unlikely, as subsequent liquid chromatographic analysis (see Supplementary Information) did not indicate the presence of lesser-nitrated species. Instead, it is proposed that ions at m/z 366.9777 and 393.9968 originate from XPN as $[M – NO_2 + HCl]^-$.

Of the direct ESI mass spectrometric methods examined, the method that included ammonium chloride and ammonium acetate produced the greater number of high-mass, diagnostic parent ions and hence greater selectivity.

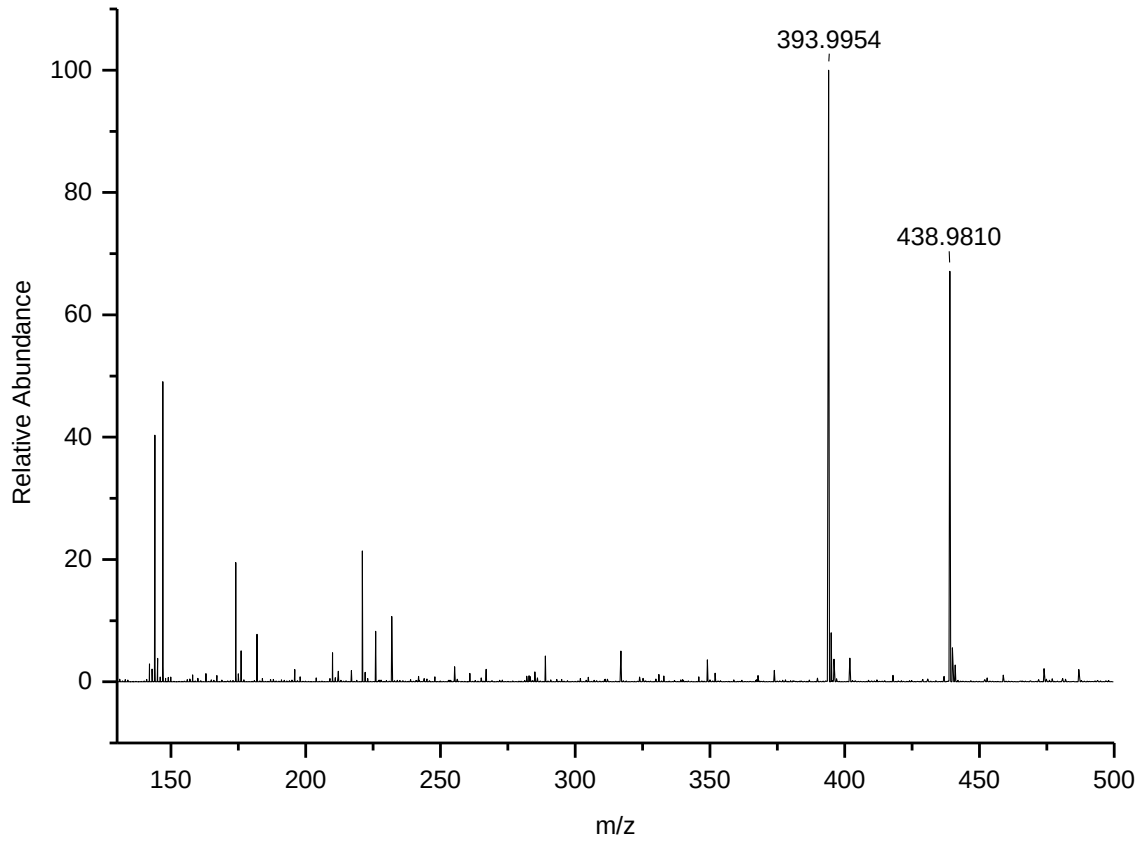

Figure 32: Mass spectrum of XPN with ammonium nitrate obtained by direct injection ESI MS. The peaks below 380 m/z are system peaks.

Table 2: MS peaks of adducts formed during direct injection ESI of XPN with ammonium nitrate as seen in Figure 32.

Mass (m/z)	**ppm difference**	**Ion**	**Relative Abundance (%)**	**Formula**
438.9810	-1.55	$[M+NO_3]^-$	67	$C_5H_7N_6O_{18}$
393.9954	-3.06	$[M-NO_2+HNO_3]^-$, $[M+OH]^-$ or $[XteN+NO_3]^-$	100	$C_5H_8N_5O_{16}$

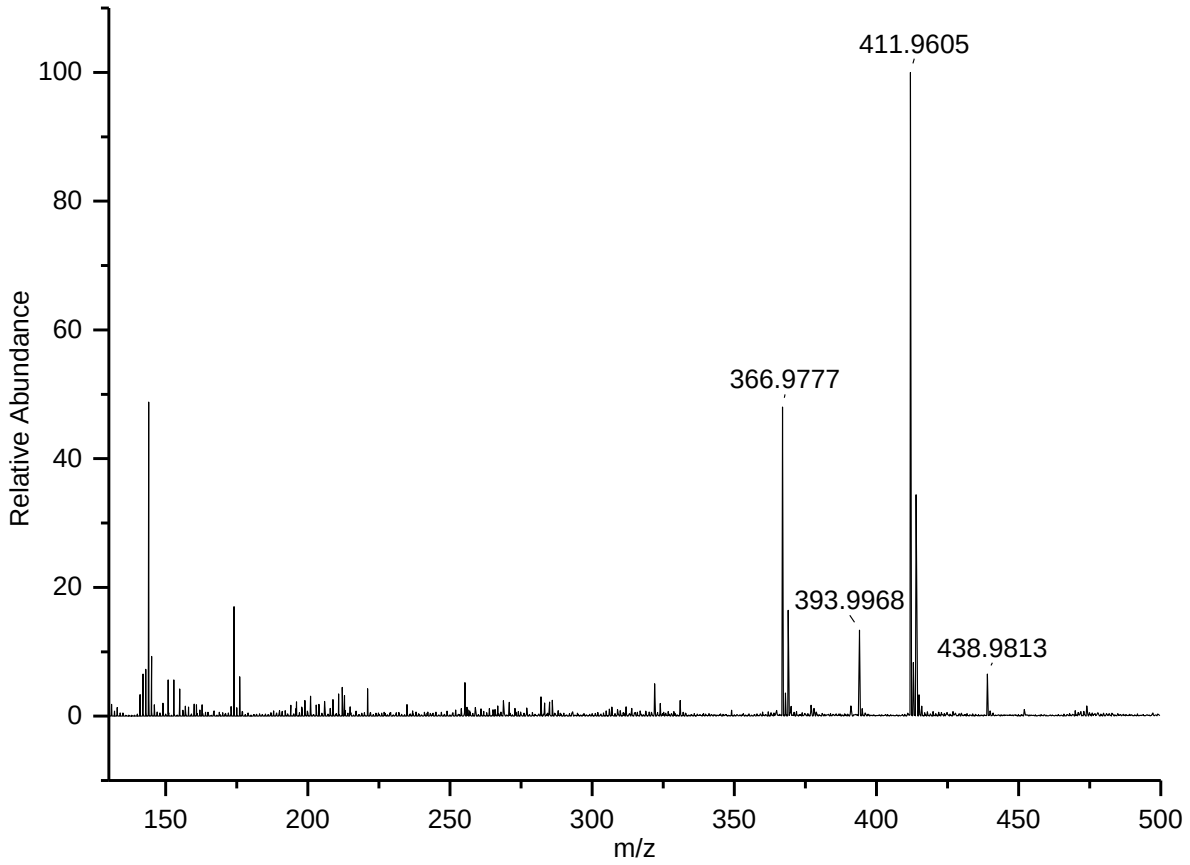

Figure 33: Mass spectrum of XPN with ammonium chloride and ammonium acetate obtained by direct injection ESI MS. The peaks below 360 m/z are system peaks.

Table 3: MS peaks of adducts formed during direct injection ESI of XPN with ammonium chloride and ammonium acetate as seen in Figure 33.

Mass (m/z)	PPM Difference	Ion	Relative Abundance (%)	Formula
438.9813	-0.87	$[M+NO_3]^-$	7	$C_5H_7N_6O_{18}$
411.9605/ 413.9594	-5.38	$[M+Cl^{35}]^-/[M+Cl^{37}]^-$	100	$C_5H_7N_5O_{15}Cl$
393.9968	-0.50	$[M-NO_2+HNO_3]^-$, $[M+OH]^-$ or $[XteN+NO_3]^-$	13	$C_5H_8N_5O_{16}$
366.9777/ 368.9760	0.17	$[XteN+Cl^{35}]^-/[XtenN+Cl^{37}]^-$ or $[M-NO_2+HCl^{35}]^-/[M-NO_2+HCl^{37}]^-$	48	$C_5H_8N_4O_{13}Cl$

3.4.3.2 DSA-ToF MS

A series of nitrate ester explosives, including XPN, have been studied previously using APCI mass spectrometry [3]. Ostrinskaya et al. [3] found that the parent ions $[M + NO_3]^-$ (m/z 439.1) and $[M + CO_3]^-$ (m/z 437.2) were observed when XPN was introduced into the ionisation source in a solution of acetonitrile. Fragmentation peaks were predominantly due to the loss of single or multiple NO_2 groups, although a peak at m/z 317.1 was attributed to fragmentation of the carbon backbone, i.e. $[M - CH_2NO_2]^-$. In the same work, when XPN was introduced into the ionisation source in a mixture of acetonitrile and DCM, the chloride adduct ions $[M + Cl]^-$ (m/z 412.1 and 414.1) and $[M – NO_2 + HCl]^-$ (m/z 367.1 and 369.1) dominated the spectrum [3].

DSA-ToF MS is a direct mass spectrometry technique that involves bombardment of the sample with a stream of nitrogen plasma in order to achieve APCI conditions. It is considered a ‘soft’ ionisation technique, capable of producing accurate mass data for compound identification. Hitherto, its application to the analysis of explosives, including nitrate esters, has not been reported. In many regards, the simple and direct approach offered by DSA-ToF MS resembles that of DART-MS which has

been applied successfully to the analysis of several polyhydric sugars (including xylitol) and some of their nitrate esters (EGDN, NG, PETN and ETN) [18].

Here it is reported that analysis of XPN using DSA-ToF MS shows the nitrate and chloride adducts $[M + NO_3]^-$ (m/z 438.9800) and $[M + Cl]^-$ (m/z 411.9612 and 413.9606) (Figure 34, Table 4). As with the direct ESI experiments (above), an ion at m/z 393.9848 was detected. However, carbonate adducts were not observed, despite the previous identification of these species during the analysis of XPN using APCI [3] and in the analysis of NG, ETN and PETN using DART-MS [18]

A further set of peaks observed at m/z 788.9587, 790.9555 and 815.9783 are consistent with $[2M + Cl]^-$ and $[2M + NO_3]^-$ dimer products, respectively. The source of the adduct-forming chlorine atoms observed by DSA-ToF MS is unclear and analogous ions arising from the DART-MS analysis of NG, ETN and PETN were not reported by Sisco and Forbes [18]. In our experiments the solvent (DCM) was allowed to evaporate before analysis, therefore DCM should not have been available to facilitate the formation of chloride adduct ions. In further experiments, where DCM was completely eliminated from experiments, chloride adduct ions were still observed, which suggests that an adventitious source of chloride is responsible. Unlike the chloride adduct, the nitrate adduct is easily explainable as there is a readily available source of NO_3 in the air and in XPN itself.

The application of DSA-ToF mass spectrometry to ETN resulted in diagnostic ions at m/z 336.9673 $[M+Cl]^-$, 363.9859 $[M + NO_3]^-$ and 638.9653, $[2M + Cl]^-$ (see Supplementary Information). These peaks are consistent with those reported by Matyas et al [16] using ESI mass spectrometry and allow ETN to be discriminated from the longer chain homologue XPN.

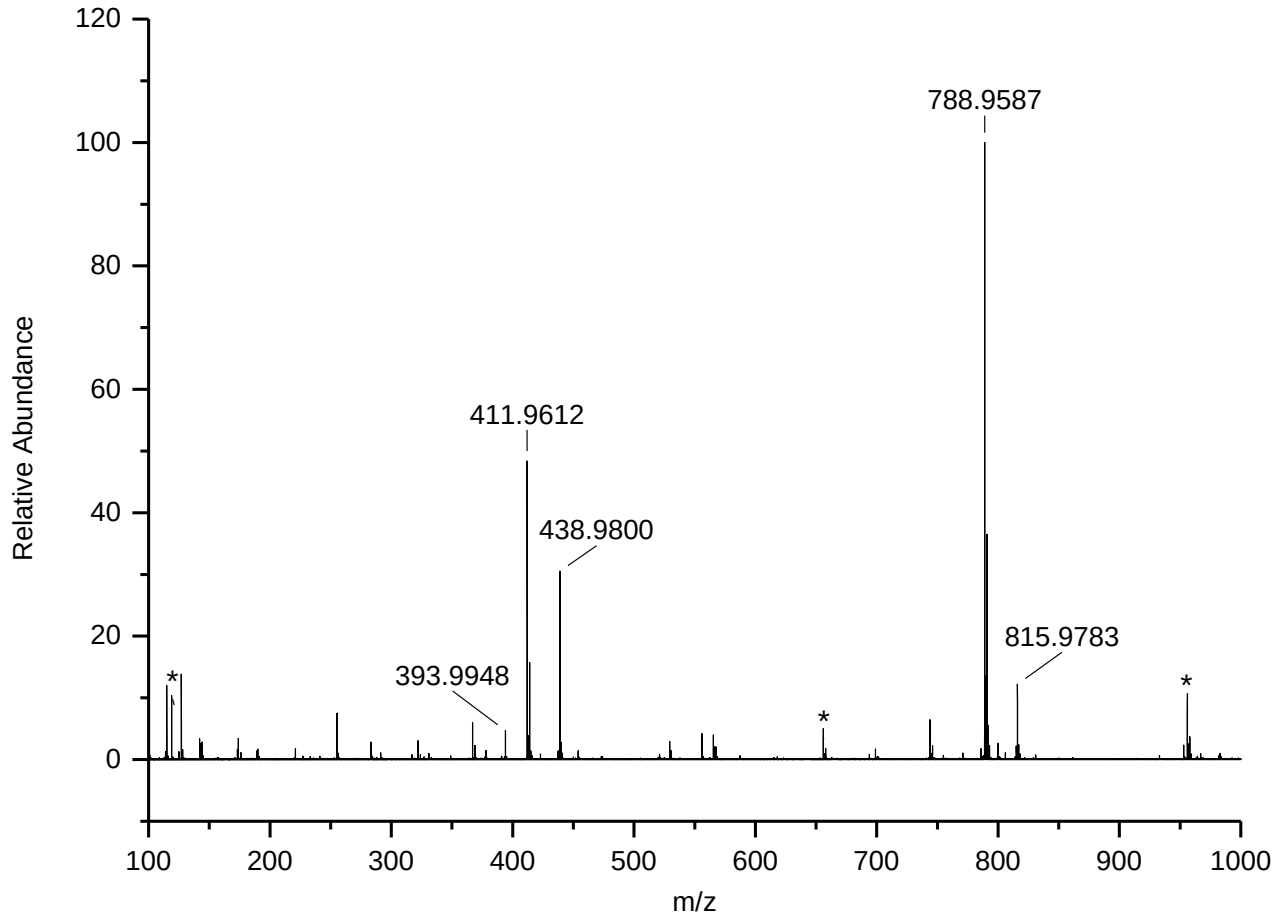

Figure 34: Mass spectrum of XPN obtained using DSA-ToF MS. The unassigned peaks are either calibration peaks (marked with an asterisk) or background peaks.

Table 4: XPN MS peaks observed in Figure 34 obtained using a DSA-ToF MS.

Mass (m/z)	**ppm difference**	**Ion**	**Relative Abundance (%)**	**Formula**
815.9783	3.37	$[2M+NO_3]^-$	12	$C_{10}H_{14}N_{11}O_{33}$
788.9587/790.9555	2.68	$[2M+Cl^{35}]^-/[2M+Cl^{37}]^-$	100	$C_{10}H_{14}N_{10}O_{30}Cl$
438.9800	-3.83	$[M+NO_3]^-$	30	$C_5H_7N_6O_{18}$
411.9612/413.9606	-3.68	$[M+Cl^{35}]^-/[M+Cl^{37}]^-$	48	$C_5H_7N_5O_{15}Cl$
393.9948	-4.58	$[M-NO_2+HNO_3]^-$ or $[M+OH]^-$	5	$C_5H_8N_5O_{16}$

3.4.4 Gas chromatography-cold EI Mass spectrometry

Although nitrate ester explosives can be analysed using GC-MS, they are prone to thermal degradation upon injection, elution and transfer into the ion source [19]. Furthermore, the electron ionization source usually employed in GC-MS typically imparts sufficient energy to those nitrate esters that elute from the column that molecular ions are not observed; instead fragmentation ions are seen at m/z 46 ($^{+}NO_2$) and m/z 76 m ($^{+}CH_2ONO_2$) [19]. An ionization technique referred to as cold-EI has been used for the analysis of energetic materials, including the nitrate esters NG and PETN [20]. A cold-EI source removes thermal and rotational energy from molecules emerging from a GC column by forcing the eluent at high speed through a small pinhole nozzle into a vacuum chamber and then through a pinhole into the ion source. Using this approach, a source temperature equivalent of 20 – 50 K is achieved [21]. For a wide range of compounds, this ionization approach results in an increase in abundance of molecular- and high m/z-ions [20]. The chromatographic behaviour of XPN was investigated using cold-EI GC-MS rather than conventional EI in the hope that some high m/z signals would be detected that could aid in the determination of whether intact XPN or a decomposition product of it elutes from the column.

In order to allow successful detection of XPN, the temperatures that the analyte was exposed to were minimized during injection, chromatography and transfer into the ion source. Similar to the observations reported by Oxley in regard to the analysis of ETN by GC mass spectrometry [1], a peak arising from XPN was not detected when a 30 m GC column was employed. Even with a 10 m column, a high carrier gas flow rate was needed in order to minimize the time the analyte spent in the instrument prior to its detection, which is a strategy recommended by Amirav [21].

Figure 35 shows the spectrum measured from the single peak that eluted using the fast, low temperature GC conditions and cold EI MS. Although the expected molecular ion (m/z 377) was not observed in the spectrum, several ions were detected at relatively high mass, including a signal at m/z 226 and very strong signal at m/z 193. The integral mass of the ion at m/z 193 ion suggests a formula $C_3H_3N_3O_7^{+}$. From these data it is not clear whether intact XPN or a thermal breakdown product of it is detected.

Using tandem mass spectrometry, a scan of product ion arising from m/z 193 was possible if a low collision induced dissociation voltage (1-5 V) was used. This indicated that ion m/z 193 fragmented to yield ions at m/z 146, 130, 84 and 46 (see Supplementary Information). The structure of the ion at m/z 193 is not obvious. However, as it is not present in the mass spectra of NG, ETN or PETN it allows for the unambiguous differentiation of XPN from them. See Stark et al. [22] and Supplementary Information for the mass spectra of NG, ETN and PETN.

Although the use of cold-EI GC-MS for the analysis of nitrate esters provided some interesting results, this method occasionally, and sporadically, produced no diagnostic high mass ions for XPN or ETN, despite manipulating the experimental conditions to minimise thermal exposure of the analytes. Using GC with conventional EI MS retention time would most likely be the only point of differentiation between the nitrate esters.

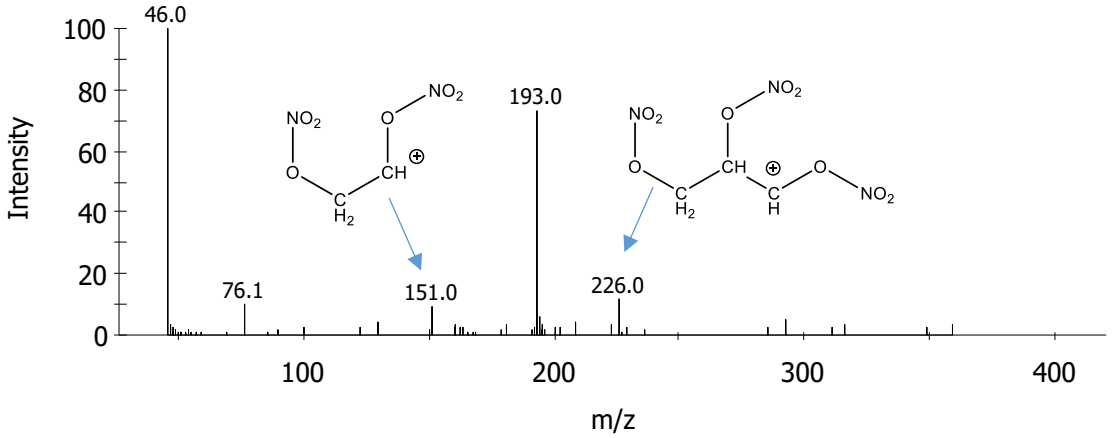

Figure 35: Mass spectrum of XPN obtained using GC Cold EI MS.

3.4.5 Ultra-performance liquid chromatography with diode array detection

Whereas the analysis of XPN and other nitrate esters using gas chromatography was found to be fraught with difficulties, analysis using UPLC was relatively straightforward. Good separation of XPN from PETN and homologous nitrate esters was achieved (see Figure 36) using a column with typical C-18 reverse phase chemistry and a simple mobile phase gradient comprising 0.1 % aqueous formic acid solution and methanol. The chromatogram doesn't display any extra peaks, indicating that the solution contained pure samples of XPN, ETN, PETN and NG. Direct atmospheric ionization mass spectrometry techniques (i.e., direct ESI and DSA-ToF MS, a form of APCI) have been shown in this work to be successful for the differentiation of XPN from other nitrate esters. Therefore, the current leading methods for forensic post-blast explosives screening and confirmation that combine UPLC with atmospheric ionization followed by MS/MS or high resolution MS (e.g., [23]) should also be capable of sensitive and selective analysis of XPN.

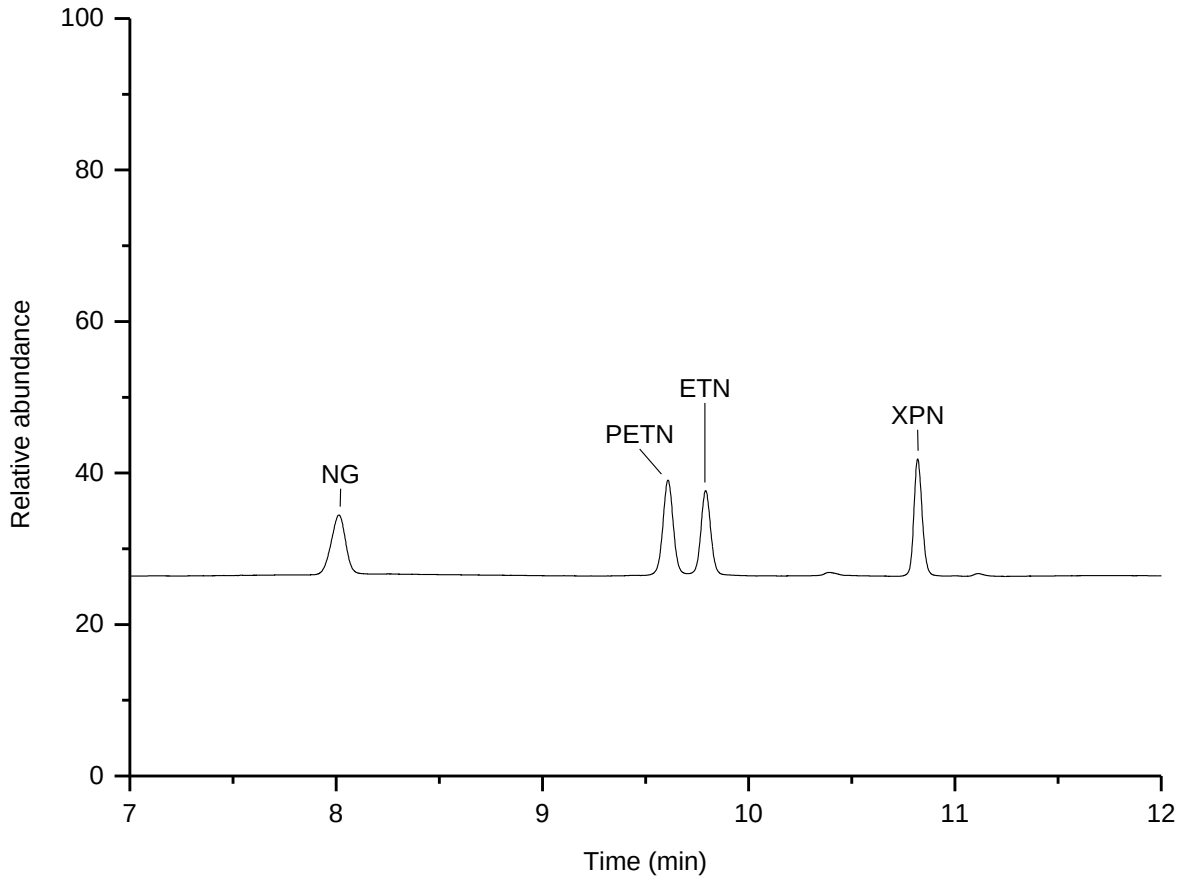

Figure 36: UPLC-DAD separation of nitroglycerine, penterythritoltetranitrate, erythritoltetranitrate and xylitolpentanitrate.

3.4.6 Conclusions

The explosive XPN was synthesised according to a literature procedure and new spectrometric data are reported to aid in its analysis by first responders and forensic specialists.

As expected, the Raman and IR (transmission and ATR) spectra of XPN displayed characteristic vibrations of the N-O and NO_2 moieties; both techniques were capable of distinguishing XPN from its homologue ETN and are therefore of value in the detection of XPN for forensic or first response purposes. Frequencies and signal intensities were consistent with computational results. Compared to transmission infrared measurements, which are difficult to acquire and produce broad spectral features, Raman and ATR measurements are both easier to acquire and provide better-resolved spectral features.

NMR spectrometry was conducted at high field strength (600 MHz) and using a benchtop machine (60 MHz). The high field ^{1}H spectrum revealed rational, characteristic signals that allow unambiguous differentiation between XPN and other nitrate esters. At 60 MHz the peaks of the ABX system arising from the four protons on the termini of the XPN molecule overlapped and were poorly resolved, as were the peaks due to the methine protons. Despite this, the 60 MHz spectra of the nitrate esters NG,

ETN, PETN and XPN were clearly distinguishable from one another by splitting patterns and peak integration. Hence benchtop NMR may be a useful method for distinguishing between bulk samples of these materials and for differentiating the nitrate esters from other improvised organic explosives.

Direct ESI mass spectrometry of XPN in the presence of ammonium chloride and ammonium acetate gave chloride and nitrate adduct ions at high m/z that were diagnostic of molecular XPN. When ammonium nitrate was substituted for ammonium chloride and ammonium acetate, fewer diagnostic parent ions were formed.

DSA-ToF-MS analysis revealed abundant nitrate and chloride adducts that were diagnostic of molecular XPN. As this method required little sample preparation, some advantage over the direct ESI methods may be inferred, despite the source of chloride for adduct formation remaining unknown. The results presented here indicate that DSA-ToF-MS may offer capability similar to DART-MS for the analysis of XPN and other nitrate esters.

Cold-EI MS was utilised to study XPN. Fast, low temperature chromatography was required to allow detection of a signal from XPN, but even under these conditions it was still possible to achieve full separation between it and the signals for the common nitroester explosives NG, ETN and PETN. The cold-EI MS signal for XPN showed an abundance of ions at relatively high m/z, but as a molecular ion was not detected it is not possible to determine whether the signal represents the intact molecule or a thermal degradation product of it. The detection of high m/z ions for XPN sparked further investigation to determine if cold EI MS could be used to distinguish between XPN, NG, ETN and PETN. The presence of a peak at m/z 193 was unique to the spectrum of XPN, and each of the other nitroester produced characteristic ions, hence cold-EI mass spectrometry may be used to distinguish between the common nitroester explosives. Despite the use of experimental conditions that minimised the fragmentation of large mass ions, this method occasionally, and sporadically, produced no diagnostic high mass ions for XPN. More work is required if this technique is to become rugged enough to be used in forensic casework. If conventional EI GC-MS is used it is unlikely that XPN will be able to be discriminated from NG, ETN and PETN except by retention time.

In contrast, ultra-performance liquid chromatography offered trouble-free, reliable separation of XPN from NG, ETN and PETN. As direct atmospheric pressure ionization MS of XPN was readily achieved using APCI and ESI, it is reasonable to expect that combination of these ionization techniques with LC would be effective for the selective and sensitive analysis of XPN.

Chapter 4: Crystal Structure, Sensitiveness and Theoretical Explosive Performance of Xylitol Pentanitrate (XPN)

The research conducted in this chapter were peer-reviewed and published. This first appeared in:

Stark, K. A. S.; Alvino, J. F.; Kirkbride, K. P.; Sumby, C. J.; Metha, G. F.; Lenehan, C. E.; Fitzgerald, M.; Wall, C.; Mitchell, M.; Prior, C., Crystal Structure, Sensitiveness and Theoretical Explosive Performance of Xylitol Pentanitrate (XPN). *Propellants Explos. Pyrotech.* **2019,** *44*, 541-549.

For the purposes of this publication, the approximate contribution of each author was Stark, K.A.S. 55%, Alvino, J.F. 5%, Kirkbride, K.P. 5%, Sumby C.J. 5%, Metha, G.F. 5%, Lenehan, C.E. 5%, Fitzgerald, M. 5%, Wall, C. 5%, Mitchell, M. 5%, and Prior, C. 5%

The full text of the publication has been incorporated in Chapter 5 below.

Please note- Minor formatting amendments have been performed to the presentation of the publication to keep it consistent with the presentation of the thesis, however text and data remain unchanged from the published version

4.1 Chapter Summary

XPN is a little-studied nitrate ester of similar molecular structure to the military energetic materials PETN and NG. XPN was crystallised from a mixture of ethanol and water by slow evaporation and studied by single crystal X-ray diffraction. XPN crystallises in the centrosymmetric monoclinic space group $P2_1/n$, with a calculated density of 1.852 g cm^{-3}. Sensitiveness analysis of the energetic material revealed it to be a primary explosive, significantly more sensitive than PETN to some initiating stimuli. The calculated heat of formation of XPN, -500.48 kJ mol^{-1}, and the density were exploited utilising the Cheetah 7.0 suite of programs to predict explosive performance parameters. The theoretical explosive performances of XPN, ETN, PETN and RDX were comparable.

4.2 Introduction

NG and PETN are nitrate esters which are in common usage by military forces worldwide. ETN has been exhaustively investigated for potential use by conventional armed forces, but has yet to find legitimate applications due to poor chemical stability. In contrast, XPN, a nitrate ester similar in structure to NG, PETN and ETN (Figure 37), only appears sparingly in the scientific literature.

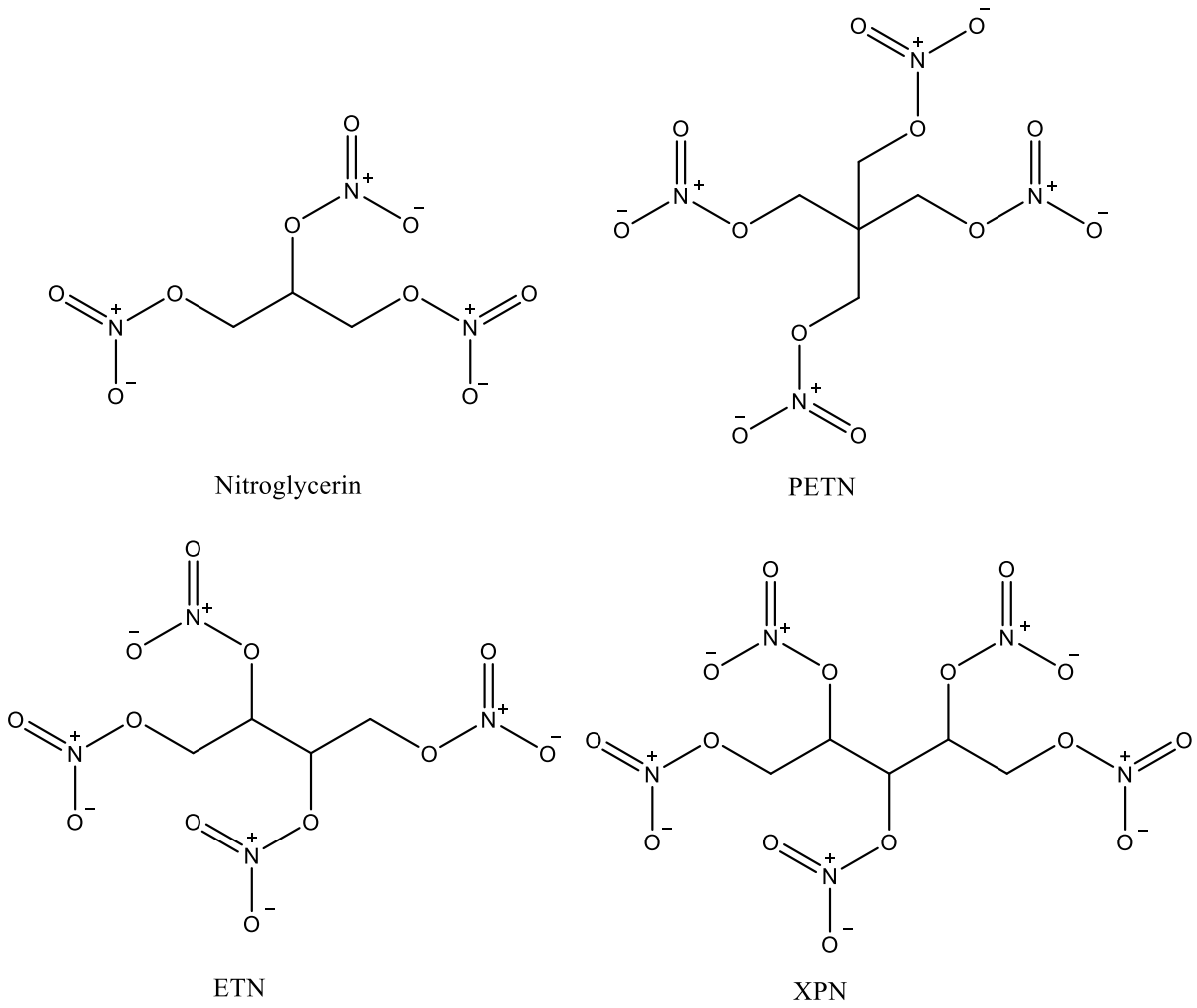

Figure 37: Simple molecular structures of NG, PETN, ETN and XPN.

XPN was first isolated as a crystalline solid in 1960 [100], with a refined synthetic procedure reported three years later [98]. The nitrate, described as a powerful explosive, was formed by the direct nitration of xylitol in a mixture of fuming nitric acid and acetic anhydride, with the structure confirmed by nitrogen content analysis, infra-red spectroscopy, and the near-quantitative catalytic hydrogenation to the parent alcohol.

In 1971 a pharmacological and biochemical evaluation of organic nitrates found XPN was a poor vasodilator compared to NG and PETN [142].

Nearly forty years later, Šarlauskas *et al*. reported the synthesis, electrochemistry and cytotoxicity of a series of nitrate esters and nitramines, including XPN [106-107]. The authors alluded to a synthetic methodology involving the treatment of xylitol with dinitrogen pentoxide in DCM and subsequent characterisation of the isolated product by thin layer chromatography (TLC), IR and NMR spectroscopy; however, neither the detailed synthetic procedure nor the characterisation data were published.

Concomitantly, Wang *et al.* published a theoretical study predicting the spectral, physical, thermodynamic and energetic properties of XPN, and other related compounds [104]. Molecular structures predicted by density functional theory at the B3LYP/6-31G* level of theory were utilised to predict theoretical densities. These results were combined with heats of formation derived from the semiempirical molecular orbital PM3 method to predict detonation velocity and detonation pressure using modified Kamlet-Jacobs equations [143-144]. XPN was suggested as a possible candidate for use in solid rocket propellant formulations.

Qi-Long et al. reported the thermal stability and decomposition mechanism functions of ten nitrate esters, including XPN, by means of non-isothermal Thermal Gravimetric (TG) and DSC techniques [105, 145]. Comparison of mean activation energies indicated that all species shared common decomposition pathways, but analyses of critical temperatures of thermal decomposition revealed XPN as one of the least stable nitrate esters. Other than the abovementioned analyses, no structural characterisation data were provided and it is unclear if XPN was isolated as a crystalline solid.

Herein, the single crystal X-ray diffraction (SCXRD) structure and sensitiveness data for XPN are reported for the first time. The molecular structure from SCXRD was utilised as the starting geometry for CBS-4M quantum chemical calculations to accurately derive heat of formation [3, 146]. The density of XPN, derived from crystallographic analysis, and the calculated heat of formation were subsequently exploited using the thermochemical computer code Cheetah [147] to predict explosive performance. This revealed the theoretical explosive performance of XPN as comparable to some military high explosives.

4.3 Experimental

4.3.1 Reagents

Xylitol, 98% sulfuric acid, acetic anhydride, toluene, and ethanol (Sigma-Aldrich, St Louis, USA) were used as received. Red fuming nitric acid (Sigma-Aldrich, St Louis, USA) was distilled before use.

4.3.2 Synthetic Procedure

Caution: XPN is a sensitive primary explosive and as such should only be synthesised in minimal quantities by experienced and appropriately trained chemists, in purpose-built explosive laboratories.

XPN was synthesized using a literature procedure [98].

4.3.3 Instruments

A single XPN crystal was mounted under paratone-N oil on a nylon loop, and X-ray diffraction data were collected at 150(2) K with Mo Kα radiation (λ = 0.7107 Å) on an Oxford Diffraction X-calibur small molecule diffractometer [148]. The data set was corrected for absorption and the structure solved by direct methods using SHELXS-2014 and refined by full matrix least-squares on F^2 by SHELXL-2014, interfaced through the program X-Seed [149-151]. In general, all non-hydrogen atoms were refined anisotropically, and hydrogen atoms were included as invariants at geometrically estimated positions. CCDC number 1869403 contains the supplementary crystallographic data for this paper. These data can be obtained free of charge from The Cambridge Crystallographic Data Centre via www.ccdc.cam.ac.uk/data_request/cif.

Crystal data for XPN. $C_5H_7N_5O_{10}$, F.w. 377.16, monoclinic, $P2_1/n$, a 8.0945(3), b 15.9392(6), c 10.4903(5) Å, β 91.684(3)°, V 1352.87(10) Å^3, Z = 4, D_{calc} = 1.852 Mg/m^3, μ 0.191 mm^{-1}, F(000) 768, crystal size 0.50 × 0.22 × 0.14 mm^3, θ range for data collection 3.39 to 29.37°, Ind. reflns 3331, Obs. reflns 2634, R_{int} 0.0381, GoF 1.043, R_1 [I>2σ(I)] 0.0356, wR_2 (all data) 0.0803, largest diff. peak and hole 0.274 and -0.245 e.Å^{-3}.

Sensitiveness data were measured in accordance with established protocols [152]. Sensitiveness to friction was measured using a Julius Peters BAM (German Federal Institute for Testing Materials) friction apparatus (Berlin, Germany). The values reported are the lowest setting at which the 10 mg samples initiated; six repetitions of the experiment at the next lower setting produced nil initiations. Sensitiveness to impact was measured using a Rotter Impact apparatus (Defence Science and Technology Group, Edinburgh, Australia). The experiment was repeated 50 times utilizing 30 mg samples with a standard drop weight of 2 kg and reported values [Figure of Insensitiveness (F of I)] standardized to RDX (F of I = 80) [153]. Sensitiveness to elevated temperatures [Temperature of

Ignition (T of I)] was determined utilizing 50 mg samples (unless stated otherwise) heated (in duplicate) at 5 °C min^{-1} to decomposition within a shielded heating block. Sensitiveness to electrostatic discharges (ESD) was measured by passing electrical discharges of 4.5, 0.45 and 0.045 J through 10 mg samples utilizing equipment purpose built by the Defence Science and Technology Group. The figure reported is the lowest setting at which the samples ignited. DSC was conducted with a TA Instruments (New Castle, Pennsylvania, USA) DSC Q10 scanning from 20 °C to 250 °C at 10 °C min^{-1} under nitrogen.

4.3.4 Theoretical Methods

The molecular structure derived from X-ray crystal analysis was optimized in its singlet and triplet states by the Becke 3LYP method and 6-31+G(d,p) basis set using the Gaussian 03 program [154-157]. Stationary points were characterized as minima (no imaginary frequencies) by calculation of the frequencies using analytical gradient procedures. The global minimum was then probed using the CBS-4M (complete basis set) method, which is based on the theoretical extrapolation of the basis set to an infinite limit (to completion) [146]. The enthalpy (H) from the CBS calculation was then used to predict the gas phase heat of formation of XPN using the atomisation method; subsequent conversion to the condensed phase was done by applying Trouton's rule using the melting point as measured by DSC [3, 158-162]. Crystal density, from X-ray crystallographic analysis, and the calculated solid phase heat of formation were inputted to the Cheetah 7.0 program suite to predict detonation parameters [147]. Cheetah is a physics- and chemistry-based tool that employs thermochemical computer code to predict detonation characteristics.

4.4 Results and Discussion

4.4.1 Crystal Structure

Rod-shaped crystals of XPN suitable for X-ray diffraction were grown by slow evaporation from a concentrated solution of the compound in ethanol and water. XPN crystallises in the centrosymmetric monoclinic space group $P2_1/n$ with a single molecule in the asymmetric unit.

(a)

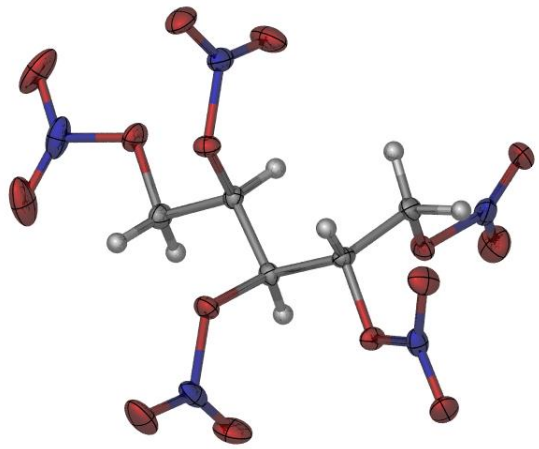

(b)

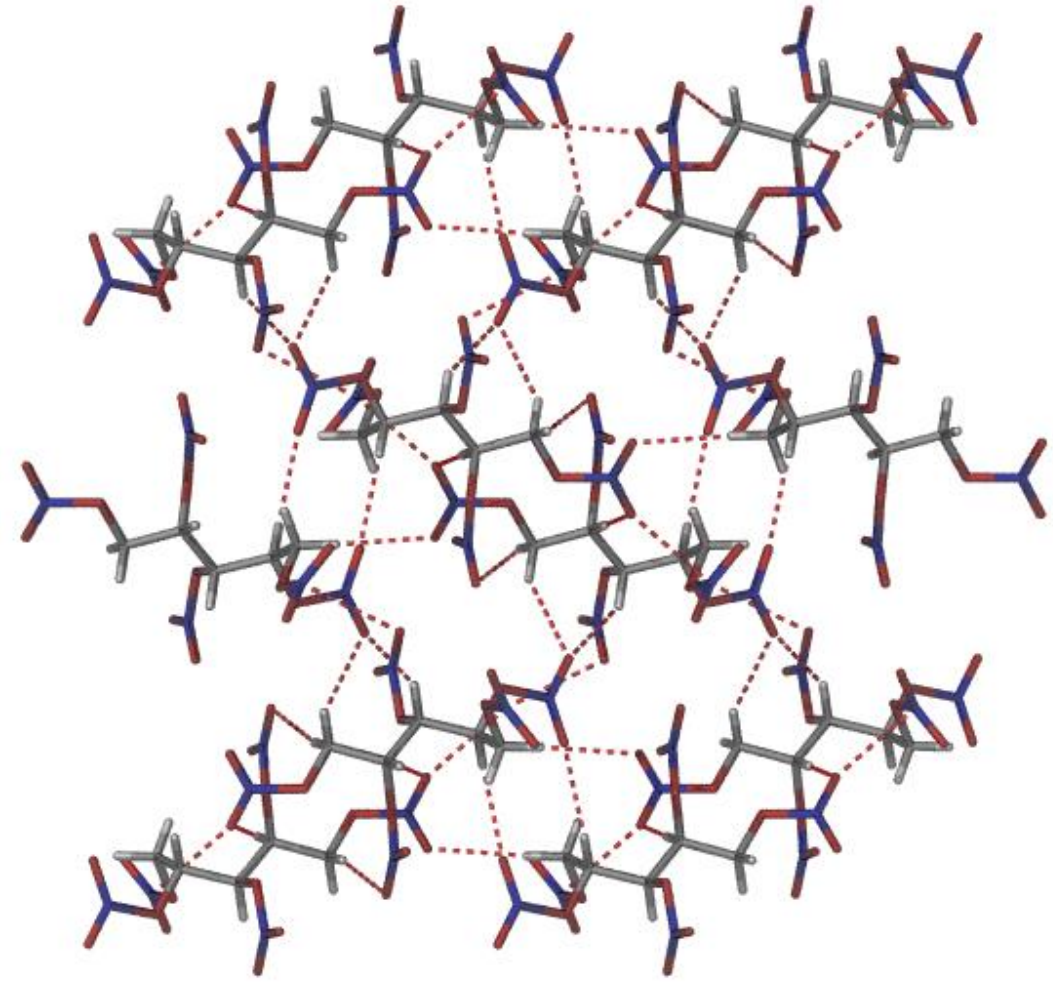

Figure 38: (a) A representation of the structure of XPN with ellipsoids presented with 50% probability level. (b) The packing of XPN viewed down the *a*-axis with the weak CH---O hydrogen bonds and NO---N interactions shown with dashed red bonds. Carbon- grey; hydrogen- white; nitrogen- blue; and oxygen- red.

The density of XPN calculated from the crystal structure is 1.852 g.cm^{-3} at 150 K, which is very close to the value reported for ETN (1.851 g cm^{-3} at 140 K [81]]) and for PETN (1.845 g cm^{-3} at 100 K [163]). As can be seen from Table 5, the carbon-carbon bond angles for XPN indicate that bonds are more distorted than those in PETN but less distorted than those in ETN. For O-C bonds, distortion in XPN is slightly lower than ETN but significantly higher than PETN.

Table 5: Comparison of Bond Lengths (Å) and Angles (°) for XPN, ETN and PETN.

BOND	**BOND LENGTH RANGE (Å)**		
	XPN	ETN[a]	PETN[b]
C - C	1.5135(18) - 1.5275(18)	1.5142(16)−1.541(2)	1.53169(13)
C - O	1.4456(17) - 1.4542(15)	1.4466(14)−1.4481(14)	1.44634(18)
O_2N - O	1.3977(16) - 1.4417(15)	1.3968(13)−1.4246(13)	1.40088(17)
O_2N	1.1923(15) - 1.2062(15)	1.1902(13)−1.2080(14)	1.19941(19), 1.2057(2)
	BOND ANGLE RANGE (°)		
C - C - C	111.53(11) - 114.97(11)	114.10(12)−114.16(12)	107.998(5), 112.46(1)
C - O - N	112.88(10) - 115.52(10)	113.04(9)−114.54(8)	112.95(1)
O - C - C	103.27(10) - 108.60(10)	102.37(11)−104.38(9)	106.774(8)
NO_2	129.74(12) - 130.82(14)	129.30(11)−130.35(11)	129.53(2)
O_2N - O	111.33(13) - 118.10(11)	111.33(9)−118.59(9)	118.01(1), 112.46(1)

[a] [81]
[b] [163]

Close analysis of the crystal structure (Figure 38b) indicates that weak intermolecular hydrogen bonding (CH···O) and NO- -ON and NO- -N interactions govern crystal packing (Table 6). All but one of the hydrogen atoms are involved in intermolecular CH···O hydrogen bonding with parameters as shown in Table 6.

Table 6: Weak intermolecular interactions in the crystal packing of XPN.

INTERACTION	D-A DISTANCE (Å)	D-H···A ANGLE (°)
C1-H1B···O24	3.550	177.32
C2-H2···O12	3.309	137.49
C3-H3···O113	3.451	145.47
C4-H4···O25	3.502	175.85
C5-H5A···O13	3.360	147.79
C5-H5B···O20	3.475	163.28
O16···N7	2.857	
O25···N7	2.758	

4.5 Sensitiveness Testing

Sensitiveness testing data for XPN are included in Table 7, along with previously reported results for PETN, RDX and lead azide [152, 164-165]. For comparison, Table 7 also includes sensitiveness data for ETN, measured at the Defence Science and Technology Group explosive testing facility [166]. It should be noted that while a universally accepted classification system to distinguish primary from secondary explosives is yet to be realised, species that are more sensitive to initiating stimuli than PETN may be considered primary explosives, whereas those less sensitive, as secondary explosives. Lead azide is generally considered a sensitive primary explosive [153].

Table 7: Sensitiveness data for XPN, ETN, PETN, Lead Azide and RDX.

	T of I (°C)	F of I (evolved gas, mL)	Friction (N)	ESD (J)
XPN	167	25(6)	18	4.5
ETN	173	40(11)	40	4.5
PETN	181	50(6)	42	0.45
Lead Azide[a]	330	30	5	<0.02
RDX	220	80(12)	80	4.5

[a]T of I, F of I and ESD taken from reference [152], Friction Sensitiveness data from reference [165].

A 50 mg sample of XPN, heated during a T of I experiment at 5 °C min^{-1} [from an initial temperature of 20 °C], did not noticeably evolve vapour or undergo an energetic event before the experiment was terminated at 250 °C. Upon cooling and subsequent inspection of the sample, the originally white crystalline solid had decomposed to form a dark viscous liquid. To examine if a more vigorous

decomposition reaction was observable at a larger scale, the T of I experiment was repeated in duplicate using 100 mg samples. At the increased scale, an evolution of a dark vapour began at 163 °C and was accompanied by an explosive "cracking" sound at 167 °C, consistent with a low-moderate energetic/explosive event. This is consistent with the DSC results whereby a 9.4 mg sample heated at 10 °C min^{-1}, having melted at 45.5 °C, exhibited an exothermic decomposition beginning at 169.4 °C, reached a peak maximum at 185.8 °C, and evolved 353 J g^{-1} (see Figure 39). The exotherm is consistent with the previous published DSC results of [105], however herein is reported for the first time the full DSC trace, including the melt at 45.5 °C. Under similar experimental (DSC) conditions, RDX and lead azide underwent more vigorous exotherms, evolving 2100 and 1298 J g^{-1}, respectively, whereas PETN and ETN produced 240 and 167 J g^{-1}, respectively [15, 167-168].

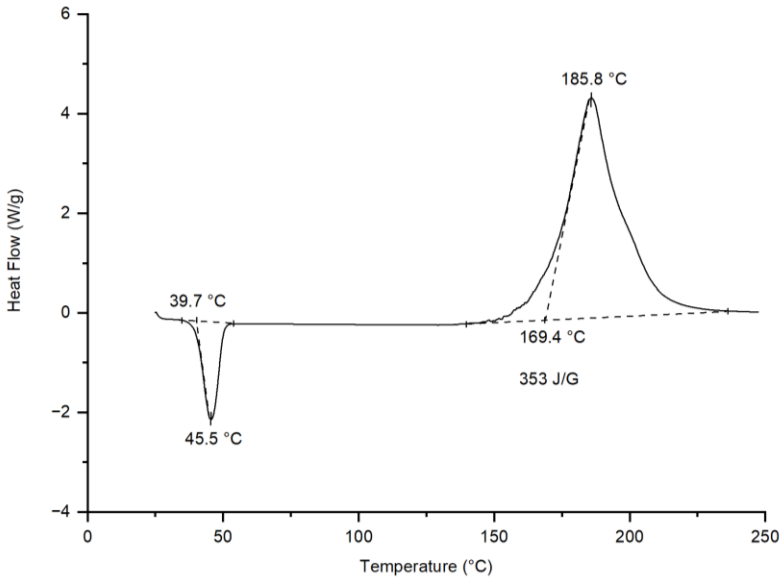

Figure 39: DSC curve of XPN with an open pan measured at a heating rate of 10°C.min^{-1} from 20°C to 250°C under nitrogen.

Comparison of the T of I points of XPN, ETN, PETN and lead azide show XPN to be significantly more sensitive to elevated temperatures compared to lead azide, and similarly sensitive compared to ETN and PETN [152-153, 164-165]. It should be noted, however, that the T of I and DSC experiments should not be viewed as exhaustive analyses of the hazards associated with XPN at elevated temperatures. It remains possible that a change in experimental conditions, such as the heating regime or scale of the experiment, may lead to significantly different results.

Rotter Impact analysis of XPN produced an F of I of 25 (standardized to RDX, F of I = 80, Table 7) from 50 repetitions of the experiment with an average gas evolution of 6 mL. This is significantly more sensitive than PETN (40) and similarly impact sensitive compared to lead azide (30), indicative of a primary explosive [164-165]. Intuitively, the volume of gas evolved from an energetic event may be

diagnostic of the performance of an explosive [164]. An average gas evolution of 6 mL for XPN is consistent with a moderate- to high-performance explosive and is similar to that observed for PETN.

Approximately 10 mg samples of XPN consistently initiated producing a low report (faint cracking sound) when 18 N of frictional force was applied using a BAM friction apparatus (Table 7). The explosive did not initiate when subjected to 16 N of frictional force. This is more sensitive than PETN (42 N) and ETN (40 N), but not as sensitive as lead azide (5 N), which is highly susceptible to ignition by frictional stimuli [164-165]. As with Rotter Impact analysis, BAM friction results depict XPN as a primary explosive.

ESD measurements showed that XPN samples repeatedly initiated upon application of 4.5 J, but failed to initiate at 0.45 J. Likewise, the minimum points at which ETN and RDX initiated due to electrical discharges are also in the range of 4.5-0.45 J, typical of insensitive energetic materials or secondary explosives (Table 7) [164-165]. PETN was more sensitive, initiating at between 0.45 and 0.045 J.

In summary, based on the sensitiveness data, XPN may be classified as a primary explosive. While it displayed similar test results during T of I experiments when compared to the PETN and ETN, and was insensitive to electrical discharge, XPN is significantly more sensitive to impact and frictional stimuli compared to PETN.

4.6 Computational Results

The molecular structure determined by X-ray crystallography was used as the input geometry for both the B3LYP/6-31+G(d,p) and CBS-4M calculations. For completeness, density functional calculations were conducted on singlet and triplet states of XPN. The singlet state (point group = C_1; dipole moment = 0.86 D) was 289.1 kJ mol^{-1} lower in energy than the triplet state (point group = C_1; dipole moment = 0.57 D) and hence the latter species has not been considered further. A lower energy stereoisomer of XPN could not be found and data for the optimized [B3LYP/6-31+G(d,p)] global minimum is included in

Table 8. For comparison,

Table 8 also includes the key bond lengths, bond angles and dihedral angles for XPN derived from X-ray analysis and complete basis set calculation (CBS-4M).

As seen in

Table 8, the calculated bond lengths and angles for the B3LYP and CBS-4M calculations were in good agreement with the single crystal X-ray structure. For example, bond lengths C_1C_2 were 1.514 Å, 1.527 Å and 1.514 Å for X-ray, B3LYP and CBS-4M results, respectively. Likewise, bond lengths for C_4O_{12} were 1.450 Å, 1.446 Å and 1.475 Å and N_3O_8 were 1.193 Å, 1.200 Å and 1.204 Å. Bond angles were likewise

in good agreement, for example $C_3O_9N_3$ were 115.5° (X-ray), 115.7° (B3LYP) and 114.2° (CBS-4M), whereas $O_{12}N_4O_{10}$ were 117.8°, 117.7° and 116.2° and $C_5O_{13}N_5$ were 113.8°, 113.8° and 113.3°.

As with the bond lengths and angles depicted in

Table 8, the experimental and computational dihedral angles were generally in good agreement. For example, dihedral $C_1C_2C_3C_4$ were 53.1° (X-ray), 54.8° (B3LYP) and 54.7° (CBS-4M) and $C_1O_3N_1O_2$ were -1.0°, -1.6° and -2.5°. However, the $C_3O_9N_3O_7$ and $C_3O_9N_3O_8$ dihedral angles for the X-ray results depict this part of the molecule as almost planar, whereas the computational results skew the NO_2 group by approximately 10° (B3LYP) and 20° (CBS-4M). A similar phenomenon, albeit less pronounced, was observed for $C_4O_{12}N_4O_{10}$ and $C_4O_{12}N_4O_{11}$.

Table 8: The experimental (X-ray) and calculated (B3LYP/6-31+(d,p) and CBS-4M) structures of XPN.

	X-ray	B3LYP	CBS-4M			X-ray	B3LYP	CBS-4M
Bond Length (Å)					*Bond Angle(°)*			
C_1C_2	1.514	1.527	1.514		$C_5O_{13}N_5$	113.8	113.8	113.3
C_2C_3	1.527	1.542	1.520		$O_{13}N_5O_{14}$	117.7	116.9	116.0
C_3C_4	1.525	1.534	1.514		$O_{13}N_5O_{15}$	112.1	112.5	114.1
C_4C_5	1.515	1.527	1.511		*Dihedral Angle (°)*			
C_1O_3	1.447	1.444	1.471		$C_1C_2C_3C_4$	53.1	54.8	54.7
0_3N_1	1.406	1.435	1.411		$C_2C_3C_4C_5$	-179.3	174.8	162.0
N_1O_1	1.200	1.203	1.212		$C_3C_2C_1O_3$	48.0	45.6	40.9
N_1O_2	1.199	1.212	1.231		$C_2C_1O_3N_1$	177.8	173.2	174.2
C_2O_6	1.454	1.445	1.469		$C_1O_3N_1O_1$	179.4	178.4	177.4
O_6N_2	1.417	1.444	1.413		$C_1O_3N_1O_2$	-1.0	-1.6	-2.5
N_2O_4	1.199	1.200	1.207		$C_4C_3C_2O_6$	173.5	176.0	172.6
N_2O_5	1.206	1.212	1.241		$C_3C_2O_6N_2$	154.4	146.9	157.9
C_3O_9	1.446	1.439	1.469		$C_2O_6N_2O_4$	175.0	-177.0	-173.9
O_9N_3	1.442	1.460	1.422		$C_2O_6N_2O_5$	-4.0	3.6	6.9
N_3O_7	1.196	1.208	1.240		$C_1C_2C_3O_9$	170.1	175.0	173.0
N_3O_8	1.193	1.200	1.204		$C_2C_3O_9N_3$	105.0	108.0	118.9
C_4O_{12}	1.450	1.446	1.475		$C_3O_9N_3O_7$	1.3	11.5	20.8
$O_{12}N_4$	1.441	1.452	1.425		$C_3O_9N_3O_8$	-179.2	-170.0	-161.2
N_4O_{10}	1.193	1.211	1.241		$C_2C_3C_4O_{12}$	62.4	54.9	45.2
N_4O_{11}	1.192	1.200	1.202		$C_3C_4O_{12}N_4$	-141.9	-134.7	-140.8
C_5O_{13}	1.445	1.441	1.466		$C_4O_{12}N_4O_{10}$	18.9	14.3	34.7
$O_{13}N_5$	1.398	1.432	1.410		$C_4O_{12}N_4O_{11}$	-163.4	-167.6	-148.3
N_5O_{14}	1.196	1.213	1.234		$C_3C_4C_5O_{13}$	-192.2	170.7	173.9
N_5O_{15}	1.203	1.203	1.211		$C_4C_5O_{13}N_5$	167.0	175.0	175.3
Bond Angle (°)					$C_5O_{13}N_5O_{14}$	1.6	2.1	2.0
$C_1C_2C_3$	115.0	115.3	113.4		$C_5O_{13}N_5O_{15}$	-178.9	-178.3	-178.3
$C_2C_3C_4$	113.0	114.0	113.1					

$C_3C_4C_5$	111.5	111.5	112.8		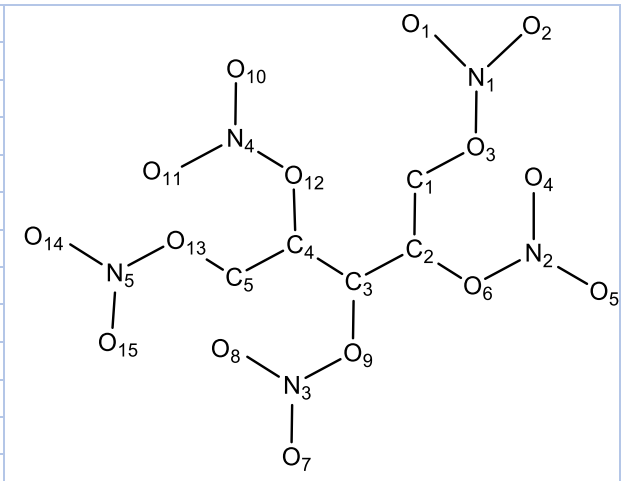
$C_2C_1O_3$	105.5	106.5	104.0		
$C_1O_3N_1$	112.9	114.1	113.6		
$O_3N_1O_1$	112.3	112.3	113.8		
$O_3N_1O_2$	117.8	116.9	116.1		
$C_3C_2O_6$	103.3	103.6	101.5		
$C_2O_6N_2$	114.2	115.1	113.9		
$O_6N_2O_4$	112.2	111.9	114.1		
$O_6N_2O_5$	118.1	117.4	116.2		
$C_4C_3O_9$	106.4	108.6	109.0		
$C_4O_{12}N_4$	115.3	116.0	113.9		
$O_{12}N_4O_{10}$	117.8	117.7	116.2		
$O_{12}N_4O_{11}$	111.6	111.6	114.0		
$C_4C_5O_{13}$	103.7	104.8	102.3		

The enthalpy (H^{298}= 1594.360004 a.u.) from the CBS calculation and the DSC data were used to derive the solid phase heat of formation ($\Delta_f H^0_{(s,\ Molecule)}$ = -500.48 kJ mol^{-1}); see Theoretical Methods section for details. The heat of formation was inputted into the Cheetah 7.0 program suite, with the calculated crystal density (1.852 g cm^{-3}) derived from the measured crystal structure, to calculate explosive parameters for XPN (Table 9). For comparison, Table 9 also includes calculated (Cheetah) and experimental literature detonation parameters for ETN, PETN and RDX [12, 80, 83, 163, 169-171].

Table 9: Computational and experimental parameters for XPN, ETN, PETN and RDX.

	XPN		**ETN**		**PETN**		**RDX**	
	Cal.	Cal.[6]	Cal.[a]	Exp.[39]	Cal. [a]	Exp.[40]	Cal.[a]	Exp.[40]
Density (g cm^{-3})	1.852	1.750	1.827[38]	1.740	1.845[30]	1.770	1.816[41]	1.800
Detonation Pressure (GPa)	32.6	32.3	31.6	(b)	33.8	33.3	33.6	34.7
Detonation Velocity (km s^{-1})	8.780	8.610	8.706	8.030	8.843	8.500	8.727	8.800

[a]Heat of formation data for calculation taken from [12]; [b]Data not available.

The calculated (Cheetah) detonation velocity of XPN, 8.780 km s^{-1}, and detonation pressure, 32.6 GPa, are in good agreement with the entirely computationally derived predictions of Wang et al. of 8.610 km s^{-1} and 32.3 GPa (Table 9) [104]. The detonation velocity is also comparable to the values calculated for ETN (8.706 km s^{-1}), RDX (8.727 km s^{-1}) and PETN (8.843 km s^{-1}). The Chapman-Jouguet (CJ) pressures were similar for the four explosives. Superficially, XPN displays similar detonation characteristics to the experimental and theoretical data reported for RDX. However, the crystal density of RDX at 1.816 g cm^{-3} is close to the charge packing density achieved for this explosive during experimentation (Table

9), and hence the calculated theoretical detonation velocity and pressure are similar to those measured experimentally. This is not the case for ETN, which has a theoretical detonation velocity of 8.706 km s^{-1} and a measured value of 8.030 km s^{-1} reported for a pressed charge [12]. The detonation velocity for melt cast ETN was similar to that of the pressed material [170-171]. It may be that further experimentation will narrow the gap between experiment and theory for ETN, however it is also possible that a significantly higher detonation velocity (e.g. >8.500 km s^{-1}) may be impractical due to the sensitivity of the explosive, i.e. it may be too sensitive to sustain significantly greater pressing loads. If this is the case, then it is probable that future experimentally derived explosive performance data for XPN, a significantly more sensitive explosive than ETN, may never approach the maximum theoretical values reported herein.

4.7 Summary and Conclusion

The explosive XPN has been synthesized following a literature procedure and slowly re-crystallized from ethanol and water to produce a crystalline material suitable for single crystal X-ray diffraction and sensitiveness analyses. The crystal forms a close-packed structure sustained by weak intermolecular packing constraints and has a density of 1.852 g cm^{-3} at 150 K. XPN is more sensitive to impact and frictional stimuli than ETN and PETN and is classified as a primary explosive. The calculated theoretical explosive performance of XPN is similar to predicted detonation characteristics of ETN, PETN and RDX. Due to the sensitivity of XPN, it may be challenging to realise the predicted performance by experimentation.

4.8 Acknowledgments

The authors would like to thank: Ben Hall and Arthur Provatas for their assistance in reviewing this manuscript; the Centre of Expertise in Energetic Materials (CEEM), a partnership between DST Group and Flinders University, for funding and material support; and The University of Adelaide for time on The Phoenix High Performance Computing (HPC) facility. C.J.S. acknowledges the Australian Research Council for equipment provided under grant LE0989336.

Chapter 5: Degradation and stabilisation of ETN

5.1 Chapter Summary

Degradation of ETN was investigate at 40, 60, 80 and 100 °C with studies being conducted in the presence and absence of acid vapour and with DPA and EC as potential stabilisers. Over a 28 day period, neat ETN was stable at 60 °C, however, at 80 and 100 °C, no detectable ETN was observed at the 28 day and 14 day time points respectively. The presence of acid vapour was found to increase the degradation rate of ETN significantly with no detectable ETN remaining at the 7 day time point at 80 °C and at the 24 hour time point at 100 °C. Stabilisation attempts of ETN with 0.2 %w/w DPA and EC were unsuccessful.

5.2 Introduction

ETN (Figure 40) is a crystalline nitrate ester explosive first discovered in 1849 [172], is a longer chain homologue of NG and has similar physical and explosive properties to PETN [12, 17]. Although ETN is one of the oldest known nitrate ester explosives, it has not been utilised for military or commercial use because 1) its precursor, erythritol (Figure 41), was expensive to manufacture [15] and 2) ETN can readily undergo chemical degradation [17, 84]. However, a new manufacturing method has been developed, allowing for erythritol to be widely obtainable in supermarkets as a sugar alternative [15, 77]. As ETN can be easily synthesised using either the mixed acid or acetyl nitrate method and due to the availability of its precursor [12, 78], ETN has gained interest in the commercial industry as a military explosive and in forensic science as an improvised explosive. Recent studies have examined the explosive performance of ETN, as well as combining ETN with other explosives, such as PETN and RDX, to improve its explosive performance [15, 80-81, 83, 89-90]. It has also gained traction in amateur online forums with many references to the synthetic procedure and the instability of the explosive, with mentions of possible ways to improve its stability [173-177].

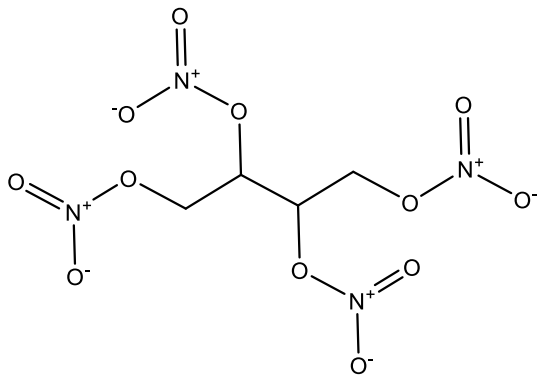

Figure 40: Structure of ETN

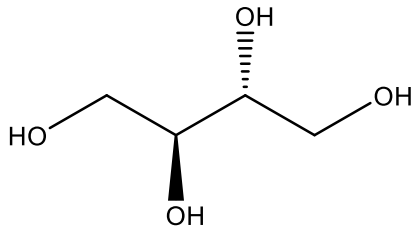

Figure 41: Structure of erythritol

It has been suggested that ETN decomposes in a similar manner to NC (homolytic cleavage of the O-NO_2 bond) (Figure 42) [22], rather than through the exothermic release of a HONO molecule [17]. The former process has an activation energy 37 $kJ.mol^{-1}$ lower than that of the latter [17]. It is suggested that the NO_2 radical produced by the O-NO_2 cleavage may cause further decomposition of ETN in a process analogous to that observed for NC [17]. To delay autocatalysis in NC based propellants, stabilisers such as DPA (Figure 43 (1)) and EC (Figure 43 (2)) are added to the formulation to capture NO_2 radicals [28, 36]; it is hypothesised that these stabilisers may similarly delay autocatalytic degradation of ETN.

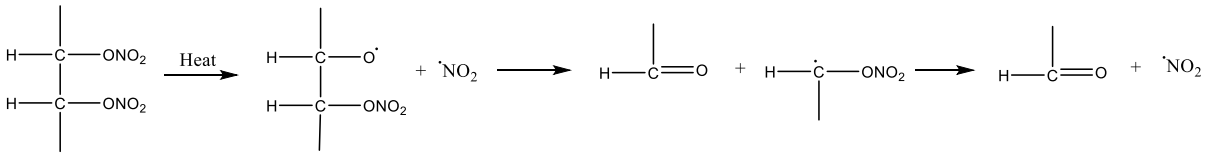

Figure 42: The decomposition of NC through thermolysis [22].

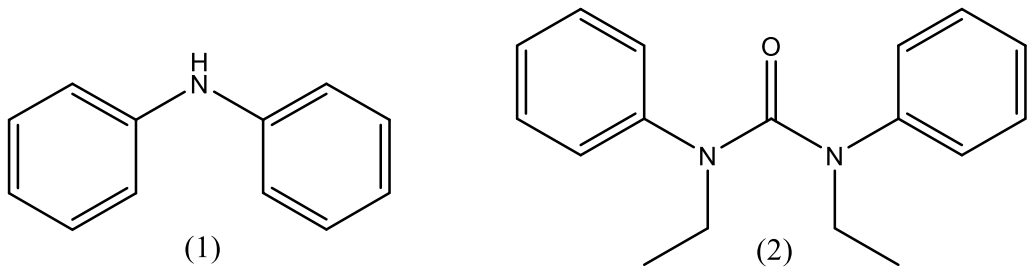

Figure 43: Structures of diphenylamine (1) and ethyl centralite (2).

The effect of different heating and humidity regimes on the chemical stability of ETN has been investigated by Sisco et al [84]. The results of the study indicated that elevated temperatures and humidity increase the rate of decomposition of ETN, with less than 5% by weight remaining after 7 days at 47 °C and no detectable ETN remaining after 4 days at 90% humidity (stored at 30 °C). The study also found that while ETN was most stable below -4 °C, the percentage of ETN remaining after 7 days at that temperature was 76% [84]. This study was conducted on unsealed samples at the nanogram scale, and it is unclear if these results are translatable to the degradation of larger quantities

of ETN in sealed containers. There is also a lack of information on the affect that residual acid has on the degradation of ETN.

This chapter examines the chemical degradation of ETN at various heating regimes, as well as in the presence of a mixed acid (nitric and sulfuric acid) solution. The stabilisers DPA and EC were investigated to determine if they could slow the chemical degradation of ETN.

5.3 Experimental

5.3.1 Reagents

Erythritol, 98% sulfuric acid, acetic anhydride, DPA, EC, DCM, toluene, diethyl ether, 2-butanone, dimethylformamide (DMF) (Sydney, NSW, Australia; all reagents were the purest available) were used as received. Red fuming nitric acid (Sigma-Aldrich, St Louis, MO, USA) was distilled before use. Both HPLC grade methanol and 98% formic acid were purchased from either Sigma-Aldrich (Sydney, Australia) or Honeywell (purchased from ChemSupply, Gillman, SA, Australia). Ammonium chloride was purchased from Sigma-Aldrich (Sydney, NSW, Australia). Ammonium acetate was purchased from BDH Laboratory Supplies (Poole, Dor, England).

5.3.2 Sample preparation

ETN was synthesis and purified by scientists at DST Group using a reference procedure [12]. Aliquots of ETN were prepared in 20 mL SPME vials (Bellefonte, PA, USA) either by weighing out approximately 10 mg of solid ETN, or by taking accurately measured amounts of a standard solution of ETN and removing the solvent by applying a gentle flow of nitrogen for 8 min using a Ratek 2 block digital heater (Ratek, Adelab Scientific, Thebarton, SA, Australia) set at 30°C to leave approximately 10 mg of solid explosive. Standard solutions were made using diethyl ether, 2-butanone, toluene or DMF to determine if the solvent type influenced the decomposition rate of ETN.

The effect of acid vapour on the degradation rate of ETN was investigated by placing ETN and a small vial containing 20 µL of mixed acid into a sealed vial (Figure 44). Samples containing DPA or EC were prepared by adding 0.2% concentration based on the weight of the ETN to the standard solution before solvent evaporation.

Calibration solutions (5, 10, 20, 40, 60 and 80 $\mu g.mL^{-}$) for UPLC were prepared using ETN from the same batch as the heating experiment samples. This was to eliminate the effect of any batch to batch variation.

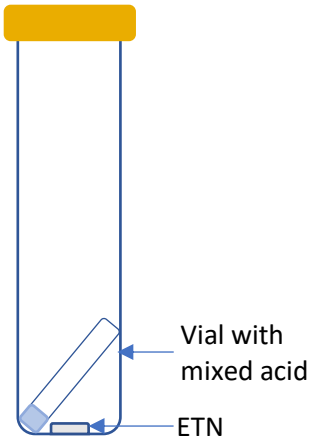

Figure 44: Sealed vial of solid ETN showing the small vial containing mixed acid.

5.3.3 Chemical degradation studies of ETN

Ageing studies were conducted using various ovens at DST Group and Flinders university. The ovens were set to 40, 60, 80 or 100°C. Four replicates for each timepoint were aged for 1 hr, 2 hrs, 4 hrs, 1 day, 2 days, 3 days, 4 days, 7 days, 2 weeks, or 4 weeks, unless otherwise stated. At the fixed time points, samples were removed from the oven and residual ETN dissolved in methanol (50 $\mu g.mL^{-1}$ based on the initial weight) for further analysis. The availability of the ovens placed limitations on the number of experiments conducted.

5.3.4 UPLC

A Waters Aquity liquid chromatograph (Waters, Milford, MA, USA) was used with a Kinetex C18 UPLC column (2.6 µ, 50 x 2.10 mm, Phenomenex, Torrance, CA, USA). A gradient separation using 0.1 % aqueous formic acid solution (A) and methanol (B) was used. The mobile phase was 98 % A for 1 minute, ramping linearly to 100 % B at 8 minutes, and back to 98 % A at 8.5 minutes where it was maintained until 12 minutes. A constant flow rate of 0.200 $\mu L.min^{-1}$ was maintained with a column temperature of 30°C and absorbance detection between 210 and 400 nm was achieved using a Waters photodiode array deuterium UV-lamp detector (Waters, Milford, MA, USA).

5.3.5 LC-MS

The liquid chromatograph described in 2.2.3 was combined with a Waters Synapt HDMS (Waters, Milford, MA, USA) to identify the single by-product peak observed in the LC chromatogram. Chromatography experiments were conducted as described in 2.2.3, with the exception that 0.2 mM ammonium chloride and 0.2 mM ammonium chloride were added to both mobile phases.

A Waters Synapt HDMS (Waters, Milford, MA, USA) was used in negative ion mode to obtain a mass chromatogram of the single degradation product peak observed in the chromatogram of degraded ETN. The sodium formate calibration solution was prepared using 9 mL of isopropanol, 1 mL of milliQ water, 100 µL sodium hydroxide and 100 µL of formic acid (calibration peaks m/z: 112.9850, 180.9725, 248.9599, 316.94734, 384.9348, 452.9222, 520.9096, 588.8970, 656.8845, 724.8719, 792.8593, 860.8467, 928.8341 and 996.8216). Lockspray MS was used as it allows for the sodium formate calibration solution to be injected into the mass spectrometer every 30 seconds for 1 second. The calibration is then updated based on the data obtained over the 1 second allowing for higher mass accuracy. The mass spectrometer was used with a desolvation temperature of 200°C, desolvation gas flow rate of 500 $L.h^{-1}$, a source temperature of 80°C and a capillary voltage of 3.5 kV. The mass scan range was set to 60 to 1000 m/z.

5.3.6 DSA-ToF-MS

An AxION 2 Time of Flight (ToF) Mass Spectrometer, equipped with a "Direct Sample Analysis" (DSA) sample introduction system (Perkin Elmer, Waltham, MA, USA), was operated in negative ionisation mode with a heater temperature of 150°C and a corona current of 4 µA. The voltage used for the endplate was 200 V with a capillary entrance of 800 V and a capillary exit of -100 V. Spectra were acquired with an acquisition rate of 1 Hz.

An APCI ToF Tuning mix (G1969-85010, Supelco/Agilent Technologies, Santa Clara, CA, USA), diluted 1:10 in milliQ water, was continuously nebulised into the nitrogen flow to enable accurate mass calibration (m/z 955.971923, 655.991085, 119.036320). Aged ETN samples were dissolved in dichloromethane or methanol to a concentration of 1 $\mu g.mL^{-1}$, of which 10 µL was pipetted onto sampling mesh (Perkin Elmer, Waltham, MA, USA) and allowed to dry. All samples were analysed in triplicate. No further reagents were added to promote adduct formation.

Spectra were analysed using the "ToF MS Driver" software (Perkin Elmer, Waltham, MA, USA, version 8.1) by averaging ~5 spectra/sample and calculating the accurate mass to $\pm$0.00005 amu. The measured mass was then compared to the calculated accurate mass for the relevant ions, with discrepancies reported in ppm.

5.4 Results and Discussion

5.4.1 Method Development

The chemical degradation pathway of ETN is suggested to follow the same pathway as that of NC, with homolytic cleavage of the O-NO_2 bond. However, unlike nitrocellulose, ETN and its degradation

products may be separated, detected, and quantified using LC and hence it is possible to observe the chemical degradation of ETN using this method.

Aliquots (1 mL) taken from a standard solution (10 $mg.mL^{-1}$) of ETN in diethyl ether were placed in SPME vials and the solvent removed by heating (30°C) under a gentle nitrogen flow (see Experimental Section). The vials were then capped, before being subjected to heating in an oven at either 40, 60, 80 or 100°C. Samples were removed from the oven at 1 hr, 2 hrs, 4 hrs, 1 day, 2 days, 3 days, 4 days, 7 days, 2 weeks, and 4 weeks and analysed via UPLC. Four replicates of each experiment were conducted.

Initial experiments conducted at 60°C showed inconsistent results with high variability observed between replicates at all time points. Typically, two replicates had no detectable ETN remaining, and two replicates showed no signs of degradation. In all cases, samples that had undergone significant degradation showed the presence of a brown-orange vapour consistent with the presence of NO2.

It was hypothesised that the cause(s) of the inconsistent results may be due to – 1) light accelerating the rate of chemical degradation, 2) inconsistencies in the thin film deposition of ETN in the sample vials influencing surface area and hence reaction/degradation rate, and 3) the type of solvent used for the standard solution or impurities therein. Each of these possibilities were investigated experimentally.

A standard solution of ETN in diethyl ether was prepared, then aliquots were separated into SPME vials, and the solvent evaporated as previously described. The vials were sealed, half of the vials were wrapped in aluminium foil to protect the contents from light, and all samples were then heated at 60°C and analysed by UPLC at set time points (0 hr, 1 hr, 2 hr, 4 hr, 1 day, 2 days, 4 days, and 7 days)). The results for samples that were exposed to light showed high variation between replicates at all time points which is consistent with the previous experiments (Figure 45). Similarly, the samples which were wrapped in aluminium foil showed high variability between replicated also, indicating that under the chosen experimental conditions exposure to light has no significant effect on the chemical degradation of ETN.

To examine if the standard solution preparation method was causing the inconsistent results, experiments were conducted in which 10 mg of crystalline ETN were manually weighed into the SPME vials. Again, half of the samples were protected from light. These experiments were conducted concurrently with experiments on ETN samples prepared using the standard solution preparation method (see experimental section). It can be seen in Figure 45(A), that the samples prepared from a standard solution showed high variation between replicates. There was also significant chemical degradation over the 7 day period (Figure 7A). However, the samples that were weighed, showed

significantly less inconsistencies between replicates and showed no signs of chemical degradation over the 7 day period [Figure 45 (B)]. It was also observed for the weighed samples, that the samples exposed to light showed no significant difference compared to those wrapped in aluminium foil, similar to the light experiments conducted using the standard solution preparation method. Clearly, the degradation rate and repeatability of the results was influenced by how the samples were prepared. While this may be due to one series of samples being aged as a thin film, whereas the other as a bulk material, another possibility is that the solvent, or an impurity within it, may have caused the inconsistent results and hence further experimentation was necessary.

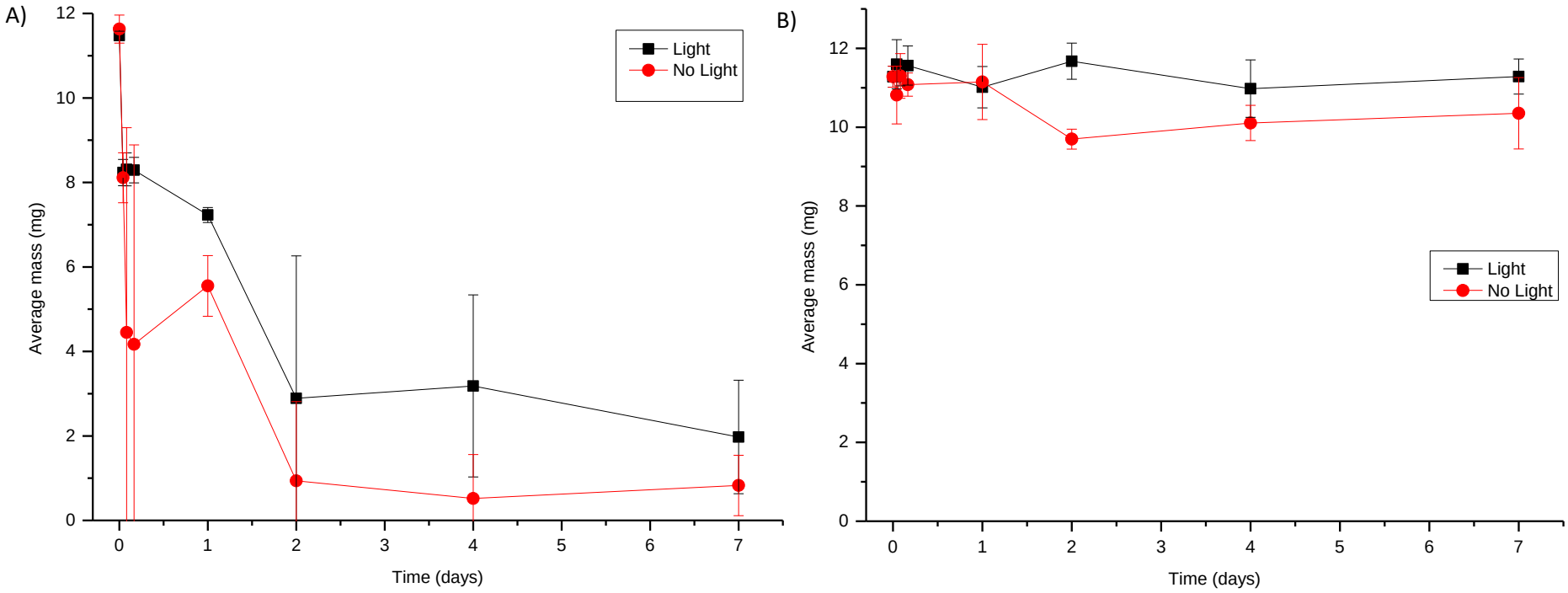

Figure 45: Decomposition of ETN at 60°C comparing samples exposed to light and samples wrapped in aluminium foil. A) Samples were prepared using a 10 mg.mL^{-1} standard solution of ETN in diethyl ether. B) Samples were prepared by weighing 10 mg of crystalline ETN into the SPME vials.

Standard solutions (10 mg.mL^{-1}) of ETN were made using diethyl ether, toluene, 2-butanone and DMF. For each solution, aliquots of 1 mL were transferred into ten SPME vials. The solvent was then evaporated under gentle nitrogen flow and the vials capped. The samples were then heated in a 60 °C oven for 7 days, before being removed from the oven and visually examined. Samples were considered to have undergone significant degradation if an orange/brown gas was observed within the vials.

At the seven-day timepoint, the ten samples that were evaporated from the diethyl diether solution displayed obvious discoloration (brown/orange gas), whereas the samples deposited using the other solvents showed no sign of degradation. A possible rationale for this observation is that the degradation of ETN may have been catalysed by a peroxide, which is a common contaminant in diethyl ether. For all subsequent experiments, standard solutions of ETN were made using 2-butanone as the solvent.

5.4.2 Degradation of ETN

Sealed vials containing ETN (1mg) were heated at 40°C, 60°C, 80°C, or 100°C, before being removed from the oven at predetermined time points and analysed by UPLC (Figure 46). It can be seen from Figure 46, that significant degradation occurs at 100 °C, with no ETN detected after 14 days. When the temperature of storage is lowered to 80 °C, ETN is stable until approximately 14 days, however no ETN was detected by LC at the 28 day timepoint. At 60 °C there was no noticeable degradation of ETN at 28 days; degradation after 28 days was not measured. As the ETN was stable at this temperature, lower temperatures were not tested.

The results described herein differ from those reported previously by Sisco et al. (2017), who found that ETN had nearly fully decomposed or was lost due to sublimation when heated at 47°C for 7 days [84]. The study also found that ETN stored at -4 °C underwent partial degradation (approximately 24% degraded) after 42 days. Due to the rapid decrease in detectable ETN, Sisco et al. concluded that the main pathway for ETN loss was by sublimation [84].

In a study by Oxley et al. (2017), the chemical degradation of 1 mg samples of ETN sealed in melting point capillaries was examined [17]. This study found that the rate of ETN degradation accelerated after 25% of the sample degraded, with samples rarely surviving past 75% degradation, indicating that most samples beyond this, showed complete decomposition. It was suggested that this acceleration was due to NO_2 radicals cleaved from the ETN molecule causing further degradation by autocatalysis [17]. Unfortunately, the study by Oxley et al. (2017) did not report the time it took for degradation to occur, making comparison to this study difficult.

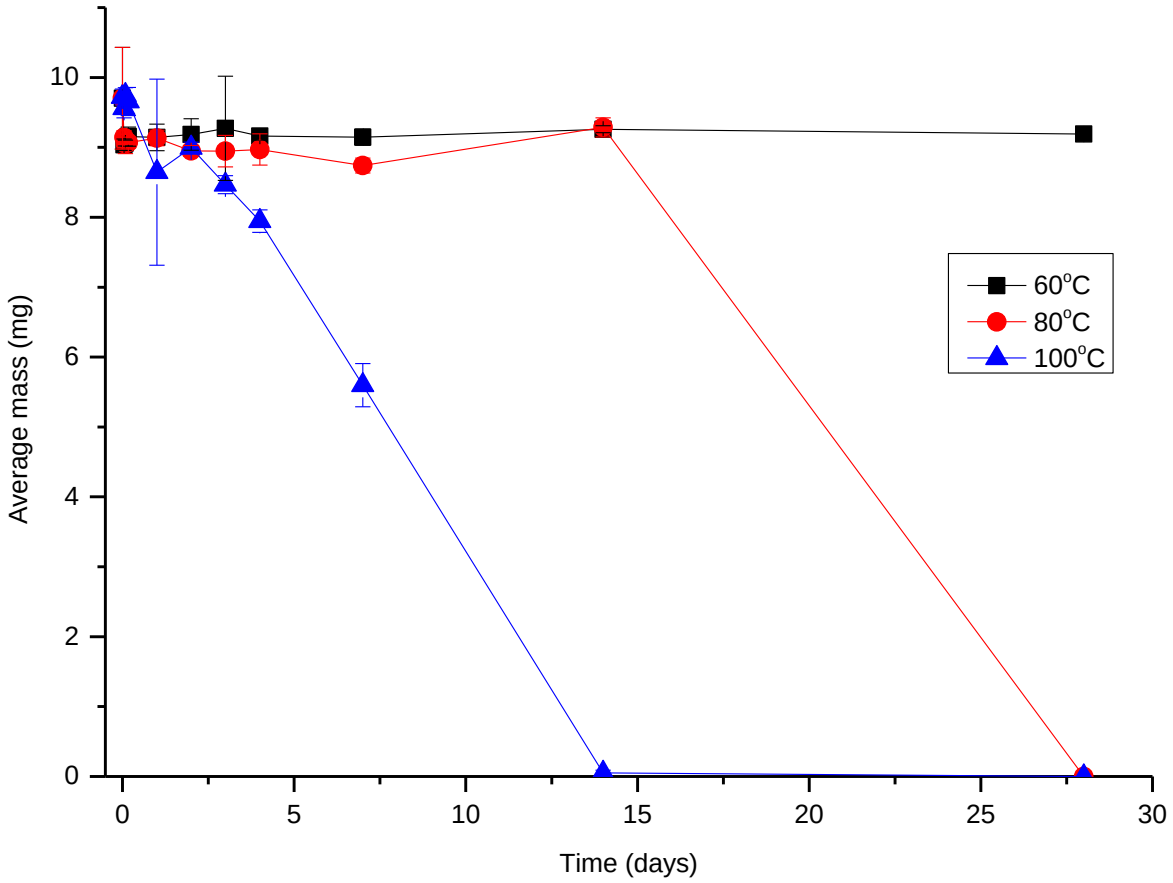

Figure 46: ETN decomposition at 60, 80 and 100 °C over 28 days with samples prepared using the standard solution method.

5.4.3 Degradation of ETN in the presence of mixed acid vapour

Clandestine samples of ETN may not be rigorously purified and hence may contain residual acid from the synthesis procedure. To determine the effect that the acid may have on the rate of degradation of ETN, vials containing mixed acid were introduced to the samples.

Samples of ETN (10 mg) were transferred to SPME vials as described previously (above). Each of the SPME vials had an unsealed vial containing 20 µL of mixed acid solution (sulphuric and nitric acid; mole ratio 1:1) placed inside it before it was hermetically capped (see Figure 44). Samples were then aged at 40°C, 60°C, 80°C or 100°C and analysed at set timepoints by UPLC. Four repetitions of each temperature and time point were measured (see Figure 47).

The samples aged at 100 °C displayed less than 5% ETN remaining at the 24 hour timepoint (Figure 47). This is similar to the observed degradation noted at the 14 day time point for samples which had not been acidified. For acidified samples at 80 °C, the ETN had degraded to less than 1% remaining at the 7 day time point (Figure 47), and at 60 °C near-complete degradation occurred at the 14 day time point. This again showed more rapid degradation than that observed for unacidified samples at these

temperatures, indicating that mixed acid vapour increased the degradation rate of ETN. ETN with residual acid was stable at 40 °C for up to 28 days.

From the results described herein, it reasonable to infer that forensic samples of ETN which have been poorly purified, i.e. samples which contain residual acid from the synthetic process, which was not adequately removed during experimental workup, may degrade at a faster rate than rigorously purified material. Therefore, for ETN of unknown origin or purity, it may be prudent to neutralise any residual acid before storing the samples at or below 40 °C; preferably below 0 °C.

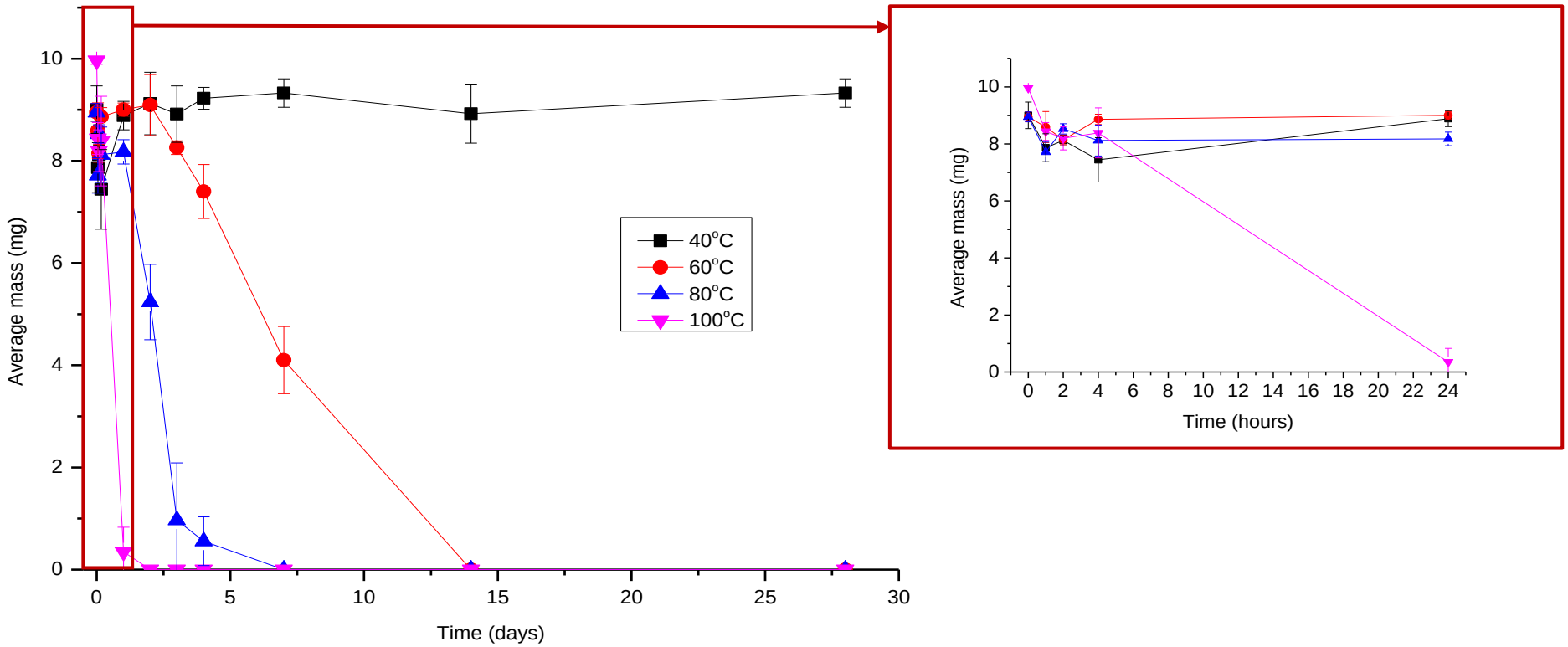

Figure 47: ETN decomposition at 40, 60, 80 and 100 °C over a 28 day period with acid vapour with samples prepared using the standard solution method.

5.4.4 Effect of batch to batch variation and the effect of storage vessel on the decomposition of ETN

Another factor that was considered to be important was the effect of the storage vessel and the effect of possible batch to batch variation. Two different batches of ETN were produced using the mixed acid method and prepared for heating studies using the standard solution method with 2-butanol. The samples were subjected to heating at 80 °C for up to 28 days. At the same time, the second batch of ETN was studied using two different storage vials, one set with gold caps and another set with blue caps (as seen in Figure 48), at the same temperature for the same time period. The different vials were used due to limitations in stock; initially gold lid vials were used, however due to a shortage, blue cap vials were used as well. Both vial caps were described by the vendor to be a match for the vials used. This allowed for an investigation into the effect the vial cap might have on the decomposition of ETN. Batch to batch variation was tested using all gold capped vials. From Figure 49, the effect of batch to batch variation was determined to be negligible, with the rate of decomposition being similar for both batches. The storage vessel however, had a much larger effect on the rate of decomposition and the replicate variability. For the majority of time points, it can be seen that the ETN samples contained in vials capped with blue caps gave much larger standard deviations than the samples in the containers capped with gold lids. One of the important things to note about the blue lid containers was the ease at which the lids could be removed from the vial along with the observation of tears in many of the lids after they had been crimped. This suggests that the seal on the vials was not good and hence the environment inside the vial may have changed over time or that the ETN may have sublimed and escaped the containers.

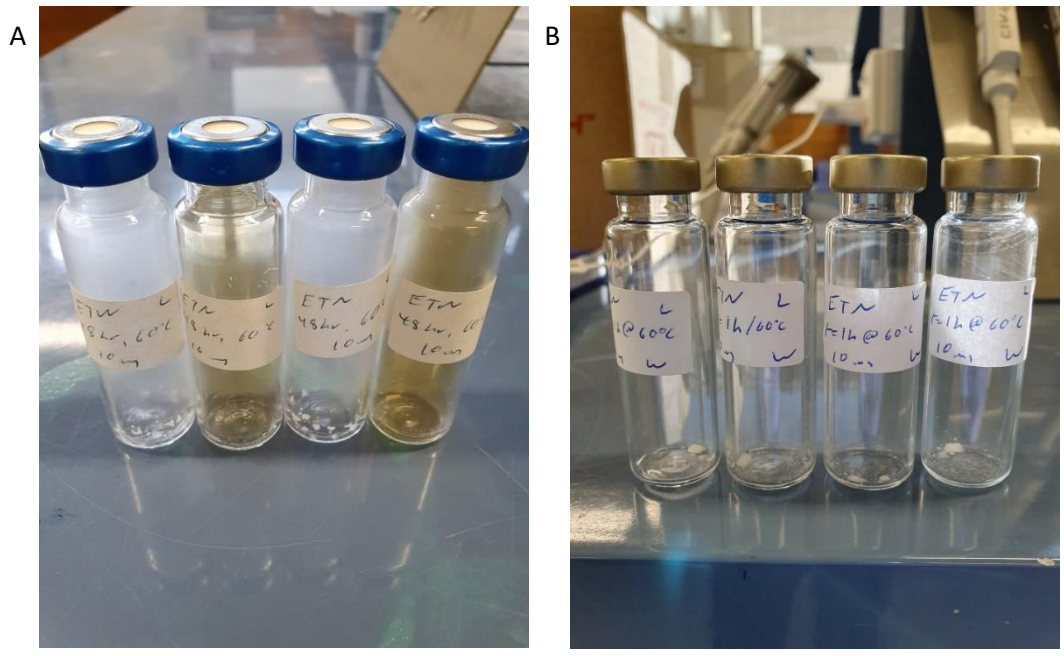

Figure 48: A depiction of the different vials and vial lids used for experiments. A) Blue capped vials. B) Gold capped vials

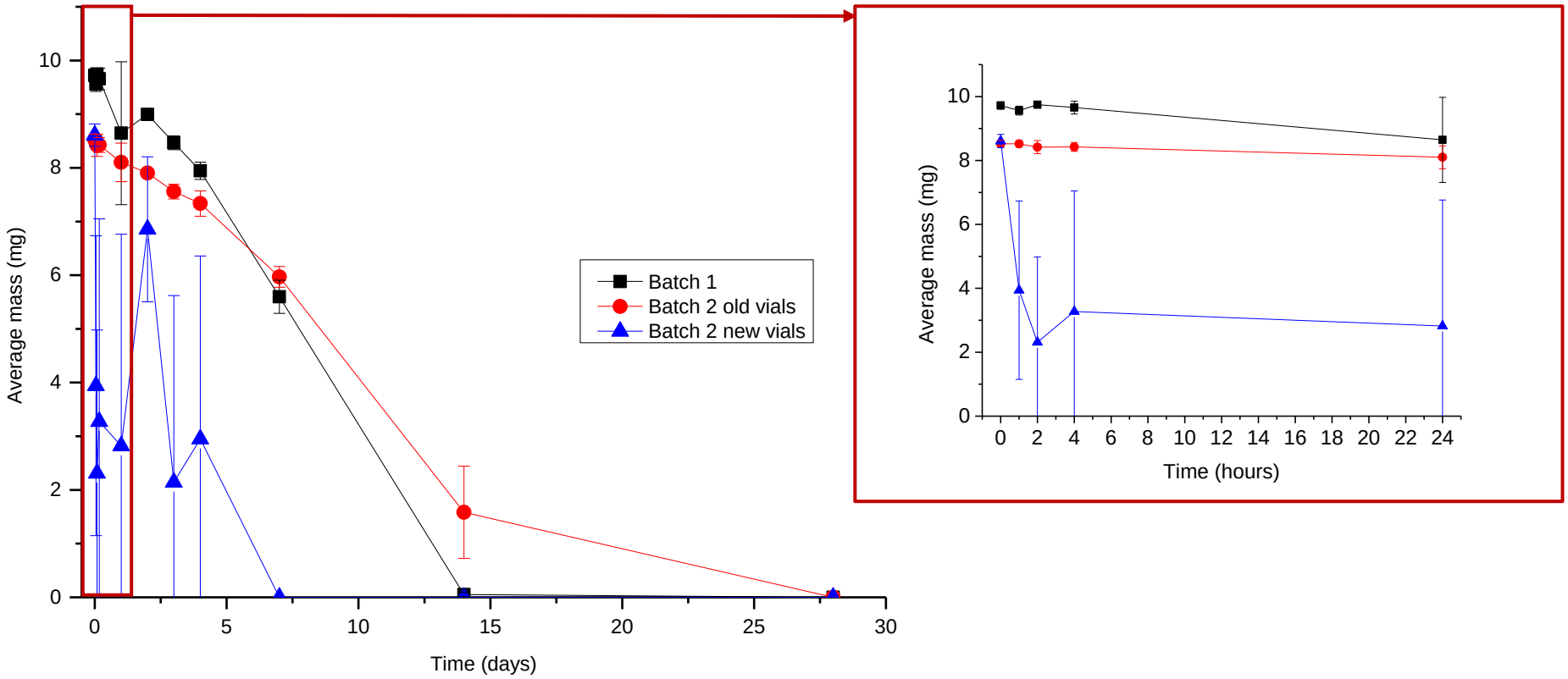

Figure 49: A comparison of the decomposition of ETN at 80 °C from two different batches (prepared using the same synthesis and purifying methods) and a comparison of new vials (blue lid) and old vials (gold lid).

5.4.5 Identification of ETN degradation products

Throughout this study, only one degradation product was observed in the LC chromatograms (Figure 50). Additionally, this species was only observable when some ETN was also visible in the chromatograms. Once the ETN had completely decomposed, the peak attributed to the degradation product was also no longer visible. It has been reported in literature that ETN decomposes to form lesser nitrated species such as erythritol trinitrate, dinitrate and mononitrate [17]. It should be noted that all samples at time zero showed no by-product peaks within the UPLC-DAD chromatogram. This suggests that ETN used for these studies is pure and contains no synthesis by-products.

LC-MS and DSA-TOF-MS were used to determine if the degradation peak could be attributed to a lesser nitrated species. As ETN does not readily ionise in mass spectrometry, 0.2 mM of ammonium chloride and 0.2 mM ammonium acetate were added to the mobile phase to achieve preferential adduct formation in LC-MS.

Figure 51 and Table 10 show the mass spectrum of the degradation species measured using lockspray LC-MS. The peak observed at 318.9994 is attributed to the nitrate adduct of the trinitrate $[EtriN+NO_3]^-$ and the peak at 291.9825 is likely due to an analogous chloride adduct $[EtriN+Cl]^-$. The presence of an $[NO_3]^-$ ion at 61.9881 suggests the degradation product may be related to a nitrate ester. The spectrum shown in Figure 51 is the result of an average of 5 repeated injections into the LC-MS and as such, individual ppm differences (the difference between the observed and calculated m/z values) were higher than acceptable for positive identification of the unknown species. This may have been due to the calibration drifting during the experiment, although lockspray MS should have compensated for this. Due to the high ppm differences, there is a chance that the degradation product was misassigned as the trinitrate despite reports describing EtriN as a degradation product of ETN.

As has been previously addressed in Chapter 3, DSA-TOF-MS provides chloride and nitrate adducts of the nitrate ester explosives without the need to purposely add these ions to the system. From Figure 52 and Table 11, DSA-TOF-MS analysis of a sample of ETN aged at 80°C for 14 days, showed evidence of the presence of ETN, EtriN and EdiN. The peak at 336.9587 m/z is indicative of $[ETN+Cl^{35}]^-$ while the peaks at m/z 319.0024 and 291.9781 are indicative of $[EtriN+NO_3]^-$ and $[EtriN+Cl^{35}]^-$ respectively. A peak at m/z 246.9914 is tentatively assigned to $[EdiN+Cl^{35}]^-$. Like the data for LC-MS, the data shown here for DSA-TOF-MS is the result of 5 averaged spectra. The ppm differences shown in Table 11 are higher than acceptable for positive identification and hence there is a possibility that compounds other than EtriN and EdiN are present, however, as mentioned previously, they are known products of the decomposition of ETN.

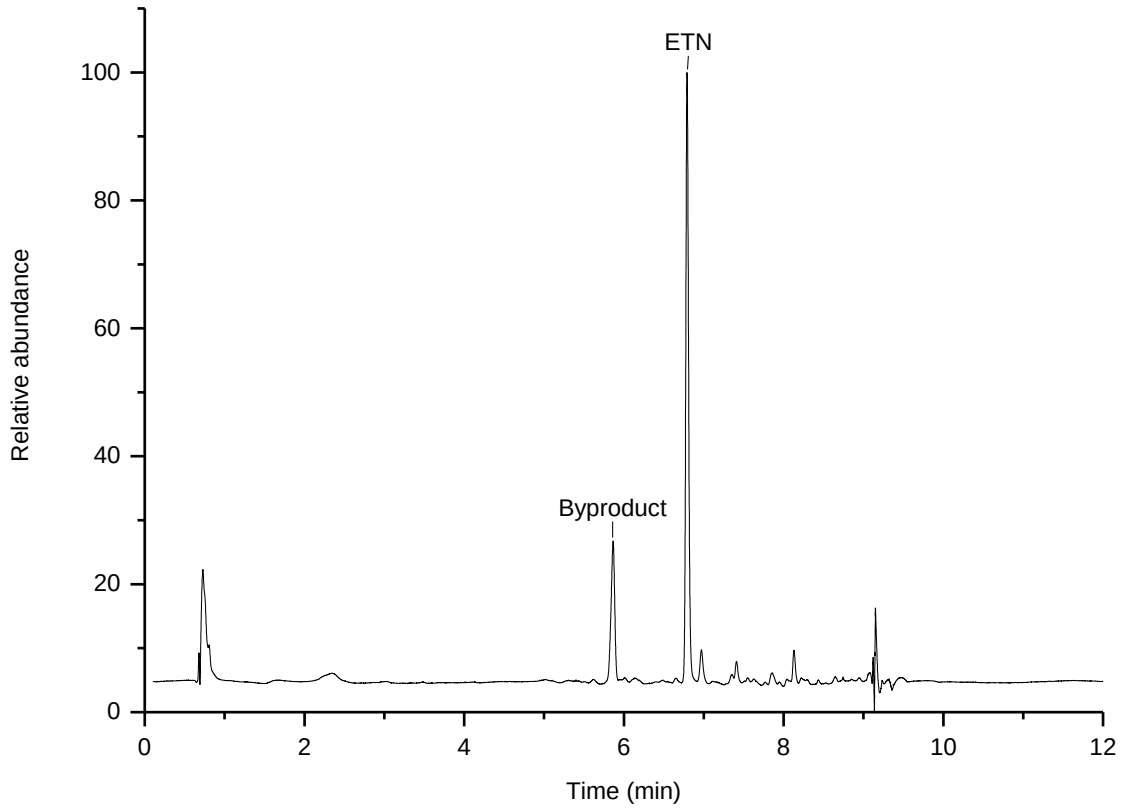

Figure 50: Liquid chromatogram of ETN heated at 100 °C for 7 days, displaying the peak for ETN at 6.8 minutes and the by-product peak at 5.9 minutes. All other peaks are observed in a blank run.

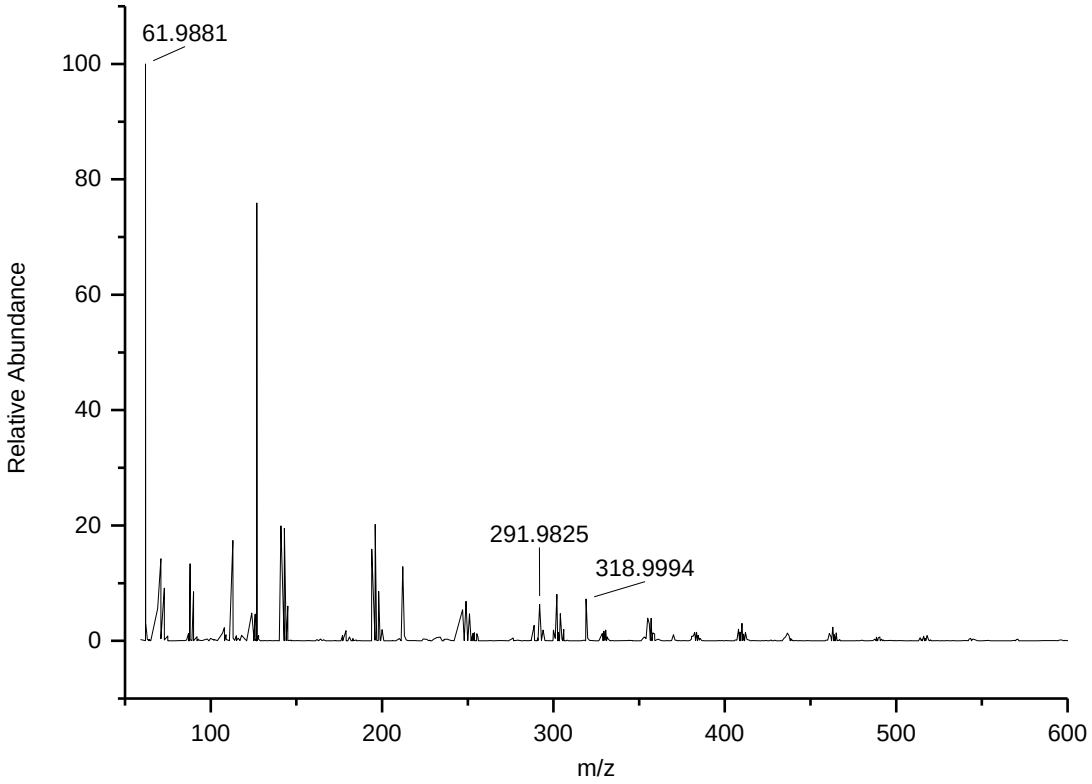

Figure 51: Mass spectrum obtained using lockspray LC-MS of the by-product peak at 5.9 minutes from Figure 50. The peak at 61.9881 m/z is assigned to $[NO_3]^-$ and the peaks at 291.9825 and 318.9994 m/z are due to Cl^- and NO_3^- adducts of EtriN. The unassigned peaks are background peaks.

Table 10: The observed and theoretical m/z values of LC peak at 5.9 minutes obtained through LC-MS with lockspray

Fragment	**Observed (average m/z)**	**Theoretical (m/z)**	**Ppm difference**
$[NO_3]^-$	61.9881	61.9878	4.6
$[EtriN+Cl]^-$	291.9825	291.9820	1.8
$[EtriN+NO_3]^-$	318.9994	319.0010	-5.2

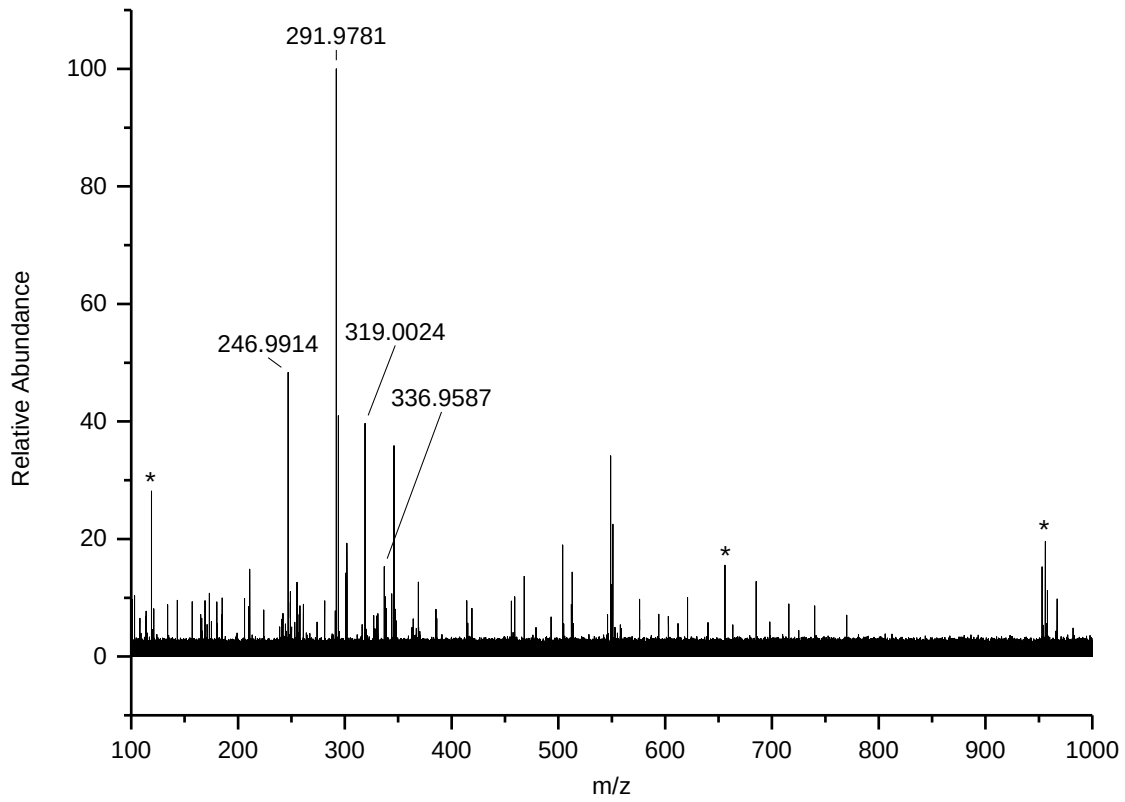

Figure 52: Mass spectrum of ETN, aged at 80°C for 14 days, obtained using DSA-ToF-MS. The peak at 336.9587 m/z is assigned to $[ETN+Cl]^-$, the peaks at 291.9781 and 319.0024 m/z are due to Cl^- and NO_3^- adducts of EtriN and the peak at 246.9914 m/z is assigned to $[EdiN+Cl]^-$. The unassigned peaks are either calibration peaks (marked with an asterisk) or background peaks.

Table 11: MS peaks observed in Figure 52 obtained using a Perkin Elmer DSA-ToF MS.

Mass (m/z)	**ppm difference**	**Ion**	**Relative Abundance (%)**	**Formula**
336.9587	-24.9	$[ETN+Cl^{35}]^-$	15	$C_{10}H_{14}N_{11}O_{33}$
319.0024	4.23	$[EtriN+NO_3]^-$	41	$C_{10}H_{14}N_{10}O_{30}Cl$
291.9781/293.9745	-13.5	$[EtriN+Cl^{35}]^-/[EtriN+Cl^{37}]^-$	100	$C_5H_7N_6O_{18}$
246.9914/248.9874	-22.5	$[EdiN+Cl^{35}]^-/[EdiN+Cl^{37}]^-$	47	$C_5H_7N_5O_{15}Cl$

Interestingly, in many of the samples aged at elevated temperatures, sublimed crystals were clearly observed in the vials. These crystals were typically observed when no ETN or degradation products were detected by LC, indicating these crystals weren't sublimed ETN or a lesser nitrated species. The appearance of these crystals changed with temperature. Samples aged at 60 °C displayed thin crystals protruding from the side to the middle of the vial (Figure 53 A and B). For samples aged at 80 °C, the crystals were small and powder-like (Figure 53 C). Further work to identify the crystals may employ a different LC column, GC-MS, or IR microspectrometry. In addition to this, gas phase IR or SPME GC-MS may provide insight into the gaseous products formed during the degradation of ETN.

A)  B) 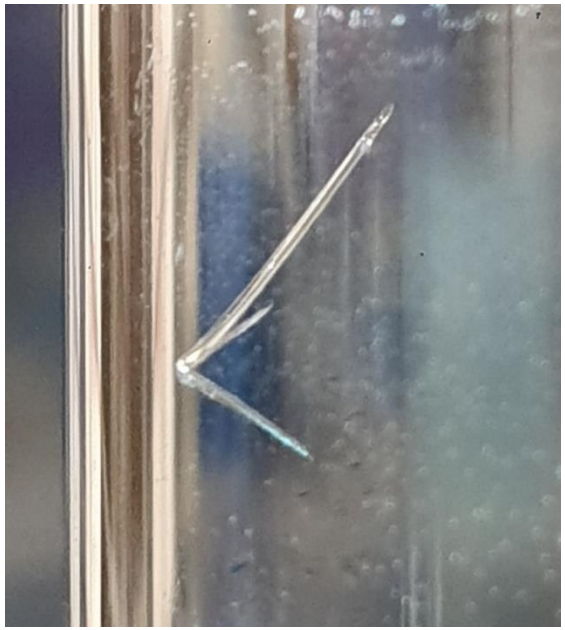 C) 

Figure 53: A) Fine sharp crystals observed at 60°C. B) A sublimated crystal observed at 60°C showing how the crystal grows from the side of the vial into the middle. C) Powder like crystals observed at 80°C.

5.4.6 Stabilisation studies

Samples (10 mg) of rigorously purified ETN were transferred into SPME vials as previously described. DPA or EC (0.2 % w/w of stabiliser/ETN) was added to each of the vials, before they were hermetically capped and aged at either 80°C or 100°C. From Figure 54 and Figure 55 it can be seen that both DPA and EC have little effect on the degradation rate of ETN; in fact it appears as though they may have a slight negative effect due to the increase in replicate variability. It is possible that the concentration of the stabiliser was too low as the presence of the stabiliser- and any degradation products - were not observed after approximately 14 days at 80 °C. It was hypothesised that using higher concentrations of stabiliser may result in a stabilising effect being observed, however, this was not tested due to time restraints.

As has been mentioned previously, residual acid has the potential to significantly increase the degradation rate of crude ETN, therefore, it may be beneficial to add a base to retard this effect. Since DPA is basic, there is the potential that it will slow the degradation of ETN by neutralising the residual acid *and* by retarding autocatalysis. Therefore, further investigation of the effect of adding DPA to crude or acidified samples of ETN should be considered.

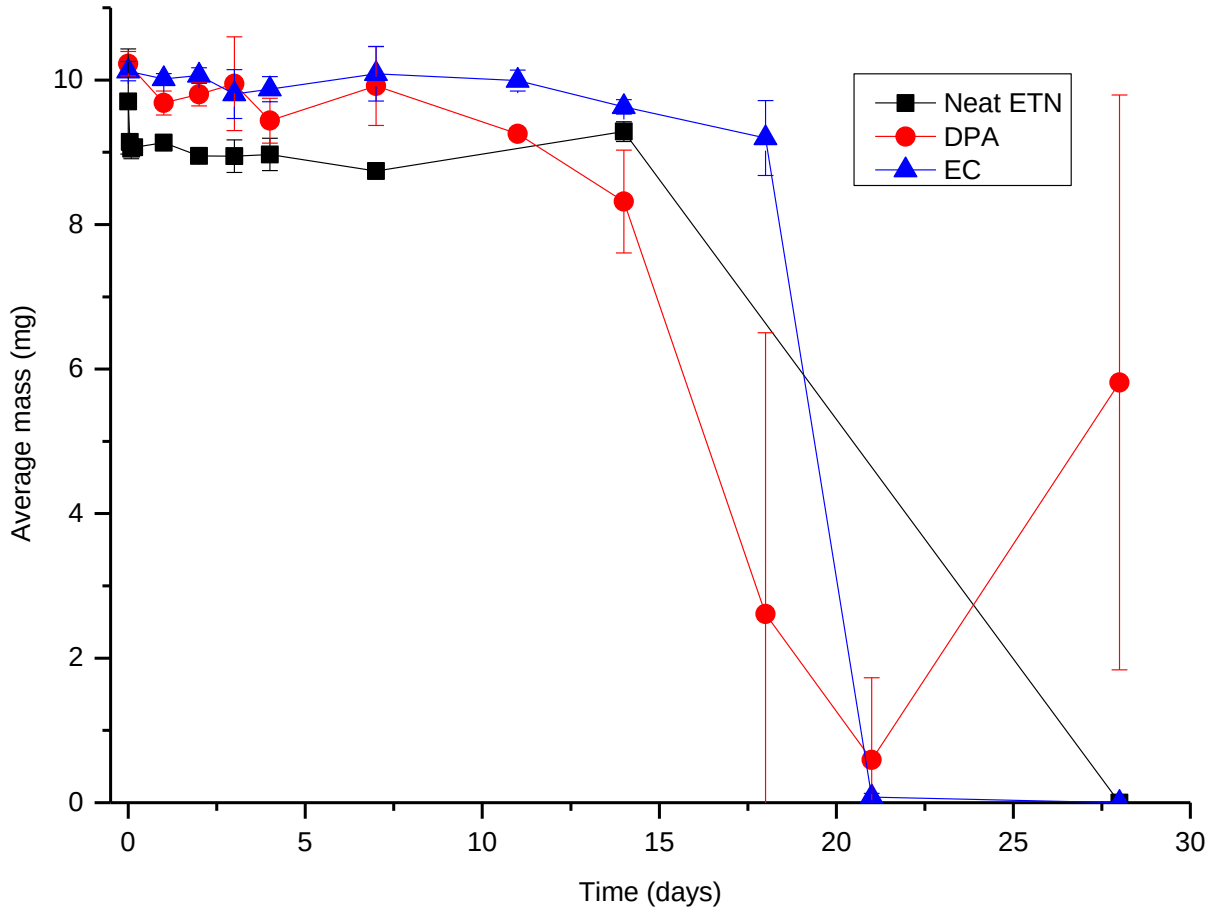

Figure 54: Effect of the stabilisers, DPA and EC, on the decomposition of ETN at 80 °C.

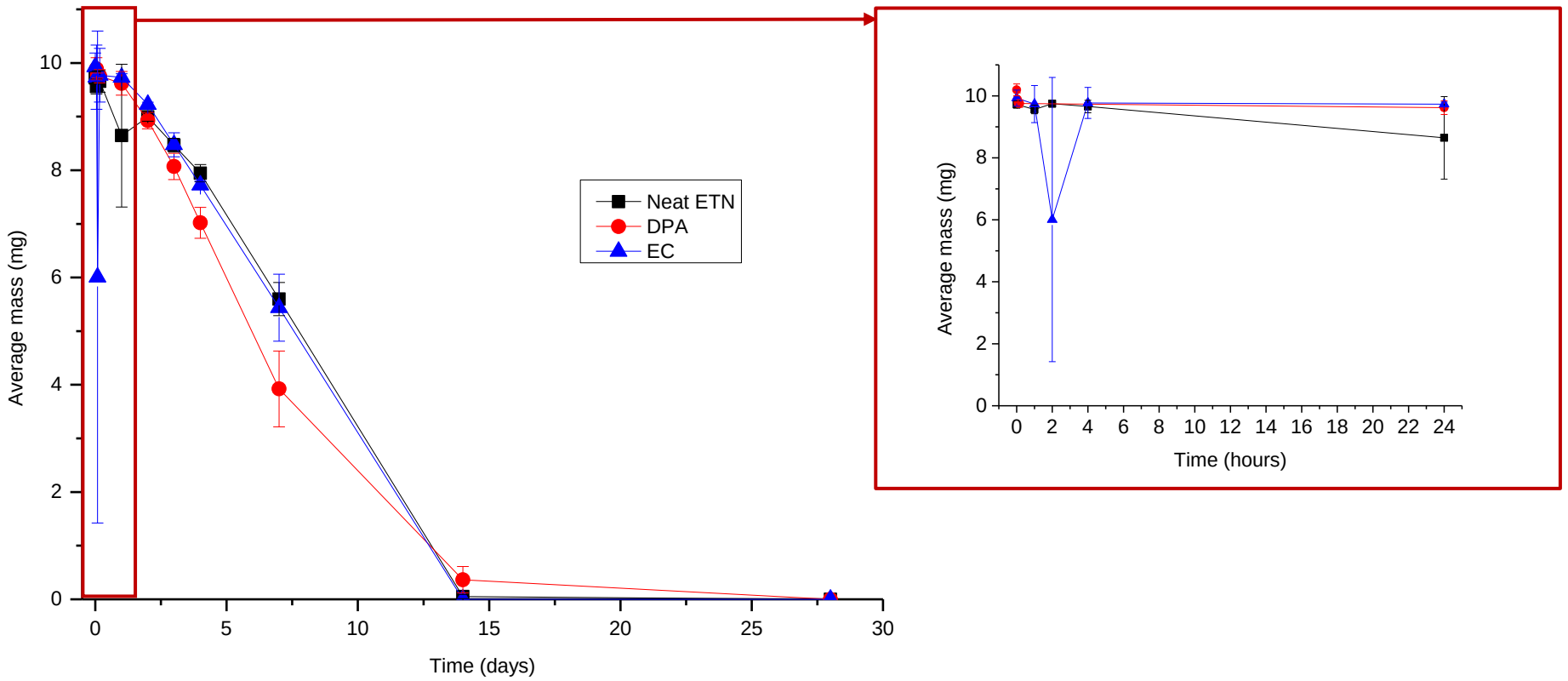

Figure 55: The effect of DPA and EC on the decomposition of ETN at 100 °C.

5.5 Conclusions and future work

The degradation of ETN was examined at various temperatures. Studies were undertaken in the presence and absence of acid vapour and with DPA and EC as potential stabilisers. It was found that pure ETN had completely degraded by 28 days at 80 °C and by 14 days at 100 °C. The presence of acid vapour was shown to significantly increase the rate of ETN degradation, with no detectable ETN remaining by 7 days at 80 °C and after 24 hours at 100 °C. Other factors were determined to affect the rate of degradation, such as the solvent used to prepare the samples and whether the storage vessel was well sealed, however exposure to light did not alter the results. A single degradation product of ETN, identified using ESI-LC-MS and DSA-ToF-MS was tentatively identified as EtriN.

The results of the experiments detailed in this chapter suggest that while acid-free ETN is stable at 60C for 28 days, in the presence of acid ETN is less stable at this temperature. Therefore ETN of unknown origin (e.g., a forensic sample) or a crude material should be stored at 40 °C or below; preferably below 0 °C. ETN should also be stored in containers that can be properly sealed and be extensively purified to remove any residual acid and any solvent used to dissolve or store ETN should be considered carefully to ensure it doesn't cause an increase in the decomposition rate.

Results showed that stabilisation of ETN was not achieved using DPA and EC at a concentration of 0.2 %w/w; however, it is possible a higher concentration may provide more favourable results. Hence future work testing higher concentrations of DPA and EC, along with other stabilisers, is required in order to determine whether ETN may have some use in military or commercial applications or establish whether criminals may be able to produce a stabilised product. Experiments using a base to eliminate the effect of the residual acid are also of interest, with DPA being a possible candidate.

Chapter 6: Conclusions and Future Work

Well-characterised explosives, such as triacetone triperoxide and hexamethylene triperoxide diamine, continue to pose a threat to the public due to ease of manufacture and the availability of precursor chemicals. However, perhaps of greater threat are so-called '*emerging explosives*' for which little characterisation, stability and detection data is known. In this thesis, the emerging nitrate ester explosives XPN and ETN were examined. Chromatographic, mass spectrometric and vibrational spectroscopy data was reported for XPN, as well as LC, crystallographic, sensitiveness and theoretical explosive performance.

Defence expressed an interest in examining the stability of ETN during prolonged storage and its potential use as a melt castable explosive. Consequently, this thesis investigated the chemical degradation of ETN at various storage temperatures for up to 28 days, along with the effect that residual acid had on the rate of degradation. As other nitrate esters, such as NC, have been successfully stabilised, studies were conducted to determine whether ETN could be stabilised in a similar manner. Although there is currently a gap in literature for the chemical degradation of XPN, this was not addressed here due to time constraints.

6.1 XPN

XPN was recrystallised using a slow evaporation method to form a highly pure crystalline product. Previous to the studies described herein, there was little characterisation data for XPN in literature. This thesis provides and abundance of characterisation data such as LC, LC-MS, GC-MS, NMR, and vibrational spectroscopy have been collected and can be used by Defence and first responders as reference materials. All techniques were able to distinguish XPN from ETN, PETN and NG, although conventional EI GC-MS could only do so by retention times; the mass spectra did not contain unique, characteristic ions. However, a technique known as cold-EI GC-MS can provide higher m/z fragment ions, perhaps even the molecule ion for certain explosives. It was observed that cold-EI GC-MS of ETN, NG, PETN and XPN was not able to provide molecular ions but did provide unique mass spectra for each explosive. However, due to the high temperatures used in GC-MS and due to nitrate esters being thermally labile, the results obtained were inconsistent and hence this technique is not recommended for analyses of this class of compounds. Further work could be conducted using a GC technique which utilised a high vacuum ultra violet detector (GC-VUV). This technique has been explored previously for the post blast detection and intact detection of nitrate ester explosives, such as NG, PETN, and ETN, hence the applicability of this technique for newer nitrate ester is warranted for first responders and the forensic community [178-179]. The results obtained from cold-EI GC-MS within this thesis, indicate that for the method to be successful, close attention to the inlet temperature, low temperature transfer line and low temperature and fast throughput in the column are required. Therefore, it may

be necessary to consider a narrow bore size column for use in GC-VUV. The nitrate ester results shown in literature by Cruse and Goodpaster (2019) suggest that they are difficult to differentiate when analysed with a flow cell temperature of 170 °C, however at 190 °C, the relative peak height ratios were a source of differentiation [178]. As this study showed that GC-VUV can be used to differentiate nitrate ester explosives, it would be beneficial to expand on this information by analysing newer nitrate ester explosives for inclusivity.

Although differentiation of nitrate esters by GC-MS is difficult, achieving this using UPLC is relatively straightforward. Along with UPLC, direct MS using either ESI-MS or DSA-ToF-MS has also been successful at differentiating XPN from PETN, ETN and NG. It was possible to obtain molecular ions with chloride or nitrate adducts in negative ion mode ($[M + NO_3]^-$= m/z 438.9810 and 438.9800, $[M + Cl]^-$= m/z 411.9605/413.9694] and 411.8612/413.9606 for direct ESI-MS and DSA-ToF-MS respectively).

Proton NMR spectrometry of XPN in $CDCl_3$ gave rise to 3 proton environments- an ABX multiplet at δ 4.66 and 4.91 ppm (J_{AB}= 13.2 Hz, J_{AX} = 5.8 Hz, J_{BX} = 4.0 Hz), a multiplet at δ 5.62 ppm (2H) and a triplet at δ 5.68 ppm (J= 5.5 Hz). The ^{13}C NMR spectrum of XPN in $CDCl_3$ showed 3 signals at δ 68.05, 74.59, and 74.65 ppm, whereas in deuteroacetone the ^{13}C NMR spectrum showed 2 signals at δ 70.19 and 76.57 ppm. The ^{1}H NMR spectra of ETN and XPN are similar, however, a triplet at δ 5.68 ppm only appears in the XPN spectrum. Therefore high field NMR can differentiate between the two nitrate esters.

As benchtop NMR spectrometry is useful for first response, defence and forensic industries, a 60 MHz NMR was evaluated for its potential to differentiate between XPN, ETN, PETN and NG. Although the low field instrument was unable to show fine structure, the integration of the methylene and methine signals allowed for the nitrate esters to be differentiated. The benchtop NMR is able to be used for the analysis of nitrate ester samples of approximately 10 mg, however, it would not be of use for analysis of trace residues or post blast analysis.

Theoretical and experimental Raman and IR spectra of XPN showed the expected NO and NO_2 functional groups and were able to differentiate it from ETN. Transmission IR spectra were more difficult to measure and displayed poorly resolved peaks compared to ATR IR spectra and hence it is recommended that ATR and Raman spectroscopy be used in preference to transmission IR. The molecular structure of XPN was modelled using the Becke 3LYP method and 6-31+G(d,p) basis set in Gaussian 03. The molecular structure was then used to complete calculations in Gaussian 09 to simulate Raman and IR spectra with the simulation allowing the approximate assignments of functional groups to regions in the spectra.

The crystal structure of XPN was determined using X-ray diffraction with XPN crystallising in the centrosymmetric monoclinic space group $P2_1/n$. The density calculated from the crystal structure was determined to be 1.852 g.cm^{-3} at 150 K. The enthalpy of XPN (H^{298}= 1594.360004 a.u.) was calculated using the CBS-4M method. The enthalpy and melting point (45.5 °C) obtained from DSC measurements were used to determine the heat of formation (-500.48 kJ.mol^{-1}). The density and heat of formation were then inputted into Cheetah 7.0 to calculate the theoretical detonation parameters of XPN. The calculated detonation velocity and detonation pressure were 8.780 km.s^{-1} and 32.6 GPa, respectively. These values are in agreement with those reported by Wang et al. (8.610 km.s^{-1} and 32.3 GPa respectively) [104].

The sensitiveness of XPN was also investigated. The T of I was measured at 167 °C, which was consistent with the DSC results that showed an exothermic decomposition reaction occurring at 169.4 °C with a peak maximum at 185.8 °C. The DSC exotherm is consistent with previously reported data [105]. The T of I value of XPN was like those reported for ETN and PETN, and significantly lower than those reported for lead azide and RDX. [152-153, 164-165]. XPN, with an F of I of 25, is significantly more sensitive to impact than PETN which has an F of I value of 50 [164]. During the Rotter impact testing of XPN, the average gas evolution was 6 mL which is consistent with an explosive of moderate to high performance. XPN displayed a low crackling noise when 18 N was applied during friction testing, however when 16 N was applied XPN did not initiate. This indicates that XPN is significantly more sensitive to friction than ETN and PETN, but is less sensitive than lead azide [164-165]. The ESD measurements showed that XPN has a similar sensitivity to electrostatic discharge as ETN and RDX [164-165]. From the results of the sensitiveness testing, XPN can be classified as a primary explosive and this would present difficulties in the application of XPN to criminal or terrorist activities.

Experimental detonation parameters, measured at or near the maximum theoretical density, have not been reported for XPN. It may be that the experimentally derived detonation velocity never approaches the theoretical value because the explosive is too sensitive to achieve sufficient pressing loads.

Obtaining experimental density and detonation parameters and comparing them to the theoretical data provided in this thesis is the topic of future investigations.

6.2 ETN

The chemical degradation of rigorously purified ETN was investigated at 60, 80 and 100 °C. It was determined that ETN is stable at 60 °C for at least 28 days, with no significant degradation observed by UPLC analysis. At 80 °C, there was no detectable ETN at 28 days and at 100 °C there was no detectable ETN at the 14 day timepoint. When ETN was in the presence of acid vapour, there was an

increase in the degradation rate. Samples stored at 100 °C showed less than 5 % ETN at the 24 hour timepoint. For samples stored at 80 °C there was less than 1 % ETN detected at 7 days and at 60 °C there was no detectable ETN remaining after 14 days. As ETN degraded at 60 °C in the presence of acid vapour, 40 °C was also tested. It was observed that at this temperature, ETN is stable for at least 28 days in the presence of acid vapour.

During initial studies, high variations between replicates was observed, which was ascribed to the involvement of peroxide impurities in the solvent used in experiments (diethyl ether). It is theorised that degradation was catalysed by a peroxide contaminant, a common impurity in diethyl ether.

Throughout the chemical degradation studies, there was one degradation product observed by UPLC analysis; this was identified as EtriN using LC-MS and DSA-ToF-MS.

Samples heated at 60 °C and 80 °C, which had no detectable ETN, sporadically showed the presence of sublimed crystals The crystals were not attributable to EtriN as they could not be observed using UPLC.

These crystals could be investigated in future studies using a different column and chromatographic conditions, IR microscopy if crystals can be collected, or *in situ* using Raman microscopy.

Stabilisation studies of ETN with either DPA or EC were unsuccessful. There was no significant change in the rate of degradation at 80 °C and 100 °C when DPA and EC were added to samples of ETN. However, further studies could be conducted which employ a higher concentration of stabiliser, as the stabiliser was depleted after approximately 14 days at 80 °C.

Stabilisers were also not investigated using ETN samples exposed to acid vapour. It is possible that since DPA is basic, it could reduce the effect that the acid vapour has on the degradation rate of ETN. Therefore a future investigation of DPA as a stabilizer for ETN is warranted.

If future studies involving the stabilisation of ETN are not successful, it could indicate that ETN does not follow the same degradation pathway as NC. As purified ETN is stable at 60 °C for up to 28 days and at 80 °C for approximately 14 days, it may be amenable to melt-casting. As it has a melting point of 61 °C, ETN could be melted at 65 °C - 70 °C and then cast before any significant decomposition occurs. If stabilisation is successful and the resultant product can be melt-cast, tests to determine whether the addition of stabiliser effects the explosive properties of ETN should be conducted.

Longer sugar alcohols, such as mannitol and sorbitol, have been nitrated to form the hexanitrate esters mannitol hexanitrate (MHN) and sorbitol hexanitrate (SHN). However, studies have shown that MHN and SHN are significantly more prone to thermal decomposition than ETN, with SHN showing signs of degradation (appearance of brown gas) after a week at room temperature [145, 180]. The

melting point of MHN is 110 °C which is close to the decomposition temperature onset of 143 °C [181]. This most likely makes it unsuitable for melt-casting. The melting point and decomposition onset temperature of SHN have been reported by Lease et al. as 55 °C and 145 °C respectively [181], however, Gribanov et al. report them as 53 °C and 163 °C respectively [182]. Regardless, the temperature difference indicated that SHN may be suitable for melt casting. However, it is more sensitive than ETN and stabilisation may also be needed.

While XPN is more sensitive than ETN, the chemical degradation has not been investigated. Due to the difference between then melting point and degradation onset temperature of XPN, it could be a candidate for melt-casting. However, the chemical degradation would need to be studied and the low melting point of XPN (45.5 °C) may cause the resultant melt-cast product to melt under certain storage or application conditions.

References:

1. Akhavan, J., *The chemistry of explosives*. 2nd ed. ed.; Cambridge, U.K. : Royal Society of Chemistry: Cambridge, U.K., 2004.
2. Meyer, R.; Köhler, J.; Homburg, A., *Explosives*. John Wiley & Sons: 2016.
3. Klapötke, T. M., *Chemistry of high-energy materials*. 3rd ed. ed.; Berlin, Germany

Boston, Massachusetts : De Gruyter: 2015.
4. Siegel, J. A., Forensic Chemistry: Fundamentals and Applications. 1st ed.. ed.; New York: John Wiley & Sons, Incorporated: 2015.
5. Doyle, S., *Improvised Explosives*. 2013; p 98-103.
6. Mehta, N.; Oyler, K.; Cheng, G.; Shah, A.; Marin, J.; Yee, K., Primary Explosives. *Z. Anorg. Allg. Chem.* **2014,** *640*, 1309-1313.
7. Laska, P. R., *Bombs, IEDs, and explosives : identification, investigation, and disposal techniques*. Boca Raton, Florida : CRC Press: 2016.
8. Vernon, A., Response to Homemade Explosives. *Fire Engineering* **2011,** *164*, 65-70.
9. Gill, P.; Horgan, J.; Lovelace, J., Improvised Explosive Device: The Problem of Definition. *Studies in Conflict & Terrorism* **2011,** *34*, 732-748.
10. Agrawal, J. P.; Hodgson, R. D., *Organic Chemistry of Explosives*. 2007; p 1-384.
11. Boschan, R.; Merrow, R. T.; Van Dolah, R. W., The Chemistry of Nitrate Esters. *Chemical Reviews* **1955,** *55*, 485-510.
12. Oxley, J. C.; Smith, J. L.; Brady Iv, J. E.; Brown, A. C., Characterization and analysis of tetranitrate esters. *Propellants Explos. Pyrotech.* **2012,** *37*, 24-39.
13. Drake, G. W.; Bolden, S.; Dailey, J.; McQuaid, M. J.; Parrish, D., New takes on nitrate ester chemistry: Salts with oxygen-rich ammonium cations. *Propellants, Explosives, Pyrotechnics* **2012,** *37*, 40-51.
14. Badgujar, D. M.; Talawar, M. B.; Asthana, S. N.; Mahulikar, P. P., Advances in science and technology of modern energetic materials: An overview. *Journal of Hazardous Materials* **2008,** *151*, 289-305.
15. Künzel, M.; Yan, Q. L.; Šelešovský, J.; Zeman, S.; Matyáš, R., Thermal behavior and decomposition kinetics of ETN and its mixtures with PETN and RDX. *Journal of Thermal Analysis and Calorimetry* **2014,** *115*, 289-299.
16. Makashir, P. S.; Kurian, E. M., Spectroscopic and thermal studies on pentaerythritol tetranitrate (PETN). *Propellants, Explosives, Pyrotechnics* **1999,** *24*, 260-265.
17. Oxley, J. C.; Furman, D.; Brown, A. C.; Dubnikova, F.; Smith, J. L.; Kosloff, R.; Zeiri, Y., Thermal Decomposition of Erythritol Tetranitrate: A Joint Experimental and Computational Study. *Journal of Physical Chemistry C* **2017,** *121*, 16145-16157.
18. Pouretedal, H. R.; Damiri, S.; Ravanbod, M.; Haghdost, M.; Masoudi, S., The kinetic of thermal decomposition of PETN, Pentastite and Pentolite by TG/DTA non-isothermal methods. *Journal of Thermal Analysis and Calorimetry* **2017,** *129*, 521-529.
19. Yamawaki, H.; Fujihisa, H.; Wakabayashi, K.; Honda, K.; Gotoh, Y., Thermal decomposition of pentaerythritol tetranitrate under static high pressure. *Propellants, Explosives, Pyrotechnics* **2013,** *38*, 394-398.
20. Bailey, A.; Murray, S., *Explosives, propellants, and pyrotechnics*. Potomac Books Inc: 1989; Vol. 2.
21. Fernández de la Ossa, M. T.; López-López, M.; Torre, M.; García-Ruiz, C., Analytical techniques in the study of highly-nitrated nitrocellulose. *TrAC - Trends in Analytical Chemistry* **2011,** *30*, 1740-1755.
22. Saunders, C. W.; Taylor, L. T., A review of the synthesis, chemistry and analysis of nitrocellulose. *Journal of Energetic Materials* **1990,** *8*, 149-203.
23. MacMillan, D. K.; Majerus, C. R.; Laubscher, R. D.; Shannon, J. P., A reproducible method for determination of nitrocellulose in soil. *Talanta* **2008,** *74*, 1026-1031.

24. Alinat, E.; Delaunay, N.; Archer, X.; Mallet, J. M.; Gareil, P., A new method for the determination of the nitrogen content of nitrocellulose based on the molar ratio of nitrite-to-nitrate ions released after alkaline hydrolysis. *Journal of Hazardous Materials* **2015,** *286*, 92-99.
25. López-López, M.; de la Ossa, M. A. F.; Galindo, J. S.; Ferrando, J. L.; Vega, A.; Torre, M.; García-Ruiz, C., New protocol for the isolation of nitrocellulose from gunpowders: Utility in their identification. *Talanta* **2010,** *81*, 1742-1749.
26. Siochi, E. J.; Ward, T. C., Absolute molecular weight distribution of nitrocellulose. *J. Macromol. Sci., Rev. Macromol. Chem. Phys.* **1989,** *C29*, 561-657.
27. Berthumeyrie, S.; Collin, S.; Bussiere, P. O.; Therias, S., Photooxidation of cellulose nitrate: New insights into degradation mechanisms. *Journal of Hazardous Materials* **2014,** *272*, 137-147.
28. López-Ĺopez, M.; Bravo, J. C.; Garciá-Ruiz, C.; Torre, M., Diphenylamine and derivatives as predictors of gunpowder age by means of HPLC and statistical models. *Talanta* **2013,** *103*, 214-220.
29. Boers, M. N.; De Klerk, W. P. C., Lifetime prediction of EC, DPA, akardite II and MNA stabilized triple base propellants, comparison of heat generation rate and stabilizer consumption. *Propellants Explos. Pyrotech.* **2005,** *30*, 356-362.
30. Bohn, M. A. In *Kinetic description of the ageing of gun and rocket propellants for the prediction of their service lifetime*, Workshop on the Microcalorimetry of Energetic Materials, Leeds, UK, Leeds, UK, 1997.
31. Volk, F.; Bohn, M. A. In *Ageing behaviour of propellants by measuring heat generation, stabilizer consumption and molar mass degradation*, ADPA symposium on Compatibility and Processing, Virginia, USA, Virginia, USA, 1989.
32. Trache, D.; Khimeche, K., Study on the influence of ageing on thermal decomposition of double-base propellants and prediction of their in-use time. *Fire and Materials* **2013,** *37*, 328-336.
33. Volk, F.; Bohn, M. A. In *Ageing behaviour of propellants determined by mass loss, heat generation, stabilizer consumption and molar mass decrease*, 87th Symposium of the Propulsion and Energetics Panel of the AGARD, Athens, Greece, Athens, Greece, 1996.
34. De Klerk, W.; Haye, E. K., Applicability of Microcalorimetry on Energetic Materials.
35. Organisation, N. A. T., Standardisation Agreement 4178. 2009.
36. Zhou, S.; Wang, Z.; Lu, L.; Yin, Q.; Yu, L.; Deng, G., Rapid quantification of stabilizing agents in single-base propellants using near infrared spectroscopy. *Infrared Phys. Technol.* **2016,** *77*, 1-7.
37. Bergens, A.; Danielsson, R., Decomposition of diphenylamine in nitrocellulose based propellants—I. Optimization of a numerical model to concentration-time data for diphenylamine and its primary degradation products determined by liquid chromatography with dual-amperometric detection. *Talanta* **1995,** *42*, 171-183.
38. Jelisavac, L.; Filipovic, M., Determination of diphenylamine and its mono-derivatives in single-base gun propellants during aging by High Performance Liquid Chromatography. *Chromatographia* **2002,** *55*, 239-241.
39. Druet, L.; Angers, J., LC/MS Studies of ethyl centralite stabilized propellants. *Propellants Explos. Pyrotech.* **1988,** *13*, 87-94.
40. Matečić-Muśanić, S.; Sućeska, M.; Čuljak, R., The applicability of chromatographic methods in the investigation of ageing processes in double base rocket propellants. *Central European Journal of Energetic Materials* **2013,** *10*, 245--262.
41. Laza, D.; Nys, B.; Kinder, J. D.; Kirsch-De Mesmaeker, A.; Moucheron, C., Development of a quantitative LC-MS/MS method for the analysis of common propellant powder stabilizers in gunshot residue. *Journal of forensic sciences* **2007,** *52*, 842-850.
42. Lindblom, T.; Christy, A. A.; Libnau, F. O., Quantitative determination of stabiliser in a single base propellant by chemometric analysis of Fourier transform infrared spectra. *Chemometrics and intelligent laboratory systems* **1995,** *29*, 243-254.
43. Lindblom, T. In *Use of FT-IR for Chemometric Determination of Stabilizer and Chemical Reactions in Single-base and Double-base propellants*, Symp. Chem. Probl. Connected Stabil. Explos, 1995; pp 83-120.

44. Pristera, F., Analysis of propellants by infrared spectroscopy. *Analytical Chemistry* **1953,** *25*, 844-856.
45. López-López, M.; Ferrando, J. L.; García-Ruiz, C., Comparative analysis of smokeless gunpowders by Fourier transform infrared and Raman spectroscopy. *Anal. Chim. Acta* **2012,** *717*, 92-99.
46. Farley, C.; Kassu, A.; Mills, J.; Bibb, J.; Curley, M.; Ruffin, P.; Sharma, A.; Rice, J.; McDonald, B. In *Raman studies for stockpile reliability of missiles by detecting degradation of propellant stabilizers*, Photonic Fiber and Crystal Devices: Advances in Materials and Innovations in Device Applications X, International Society for Optics and Photonics: 2016; p 99580P.
47. Yan, Q.; Zhu, W.; Pang, A.; Chi, X.; Du, X.; Xiao, H., Theoretical studies on the unimolecular decomposition of nitroglycerin. *J. Mol. Model.* **2013,** *19*, 1617-1626.
48. Katoh, K.; Nakahama, M.; Kawaguchi, S.; Wada, Y.; Ogata, Y.; Arai, M., The effects of conventional stabilizers and phenolic antioxidants on the thermal stability of nitroglycerine. *Science and Technology of Energetic Materials* **2010,** *71*, 17-23.
49. Chin, A.; Ellison, D. S.; Poehlein, S. K.; Ahn, M. K., Investigation of the Decomposition Mechanism and Thermal Stability of Nitrocellulose/Nitroglycerine Based Propellants by Electron Spin Resonance. *Propellants, Explosives, Pyrotechnics* **2007,** *32*, 117-126.
50. Zhu, Y. L.; Ding, L.; An, J.; Liang, Y.; Zhang, Y. J.; Hu, R. Z., A safety way to measure the thermal properties of nitroglycerin dissolved in ethyl acetate and ethanol. *Journal of thermal analysis and calorimetry* **2017,** *127*, 2545-2552.
51. Sun, S.; Ma, S.; Zhao, B.; Zhang, G.; Luo, Y., A facile way to prolong service life of double base propellant. *Materials* **2018,** *11*.
52. Liu, J., *Nitrate esters chemistry and technology*. 2019; p 1-683.
53. Murray, J. S.; Lane, P.; Nieder, A.; Klapötke, T. M.; Politzer, P., Enhanced detonation sensitivities of silicon analogs of PETN: Reaction force analysis and the role of σ-hole interactions. *Theoretical Chemistry Accounts* **2010,** *127*, 345-354.
54. Foltz, M. *Aging of pentaerythritol tetranitrate (PETN)*; Lawrence Livermore National Lab.(LLNL), Livermore, CA (United States): 2009.
55. Bhattacharia, S. K.; Maiti, A.; Gee, R. H.; Nunley, J.; Weeks, B. L., Effect of homolog doping on surface morphology and mass-loss rates from PETN crystals: Studies using atomic force microscope and thermogravimetric analysis. *Propellants Explos. Pyrotech.* **2014,** *39*, 24-29.
56. Bhattacharia, S. K.; Maiti, A.; Gee, R. H.; Weeks, B. L., Sublimation properties of pentaerythritol tetranitrate single crystals doped with its homologs. *Propellants Explos. Pyrotech.* **2012,** *37*, 563-568.
57. Zhang, X.; Weeks, B. L., Improved thermal stability and reduced sublimation rate of pentaerythritol tetranitrate through doping graphene oxide. *Journal of Thermal Analysis and Calorimetry* **2015,** *122*, 1061-1067.
58. Hikal, W. M.; Bhattacharia, S. K.; Weeks, B. L., Effect of porphyrin doping on thermodynamic parameters of pentaerythritol tetranitrate (PETN) single crystals. *Propellants Explos. Pyrotech.* **2012,** *37*, 718-723.
59. Mridha, S.; Weeks, B. L., Effect of Zn doping on the sublimation rate of pentaerythritol tetranitrate using atomic force microscopy. *Scanning: The Journal of Scanning Microscopies* **2009,** *31*, 181-187.
60. Pitchimani, R.; Zheng, W.; Simon, S.; Hope-Weeks, L.; Burnham, A.; Weeks, B., Thermodynamic analysis of pure and impurity doped pentaerythritol tetranitrate crystals grown at room temperature. *Journal of thermal analysis and calorimetry* **2007,** *89*, 475-478.
61. Pitchimani, R.; Hope-Weeks, L.; Zhang, G.; Weeks, B., Effect of impurity doping on the morphology of pentaerythritol tetranitrate crystals. *Journal of energetic materials* **2007,** *25*, 203-212.
62. Overton, I.; Davies, R.; Tumchewics, L. *IEDs: past, present and future*; Action on Armed Violence: 2020.
63. Marcus, W., Shoe bomber pleads guilty: National Edition. *National post (Toronto)* **2002**.

64. United States District, C., Shoe Bomber Attempts Airliner Explosion. In *Terrorism: Essential Primary Sources*, Lerner, K. L.; Lerner, B. W., Eds. Gale: Detroit, MI, 2006; pp 293-296.
65. Tim, D., NCA bombing a 'personal' attack. *AAP General News Wire* **2020**.
66. Beveridge, A., *Forensic investigation of explosions*. 2nd ed. ed.; Boca Raton, Fla. : CRC Press: 2012.
67. Royds, D.; Lewis, S. W.; Taylor, A. M., A case study in forensic chemistry: The Bali bombings. *Talanta* **2005,** *67*, 262-268.
68. Greene, M., Recipe for Disaster: The characteristics & components of home-made explosives. *Fire Rescue Magazine* 2011.
69. Treleven, E., Former student charged with possessing homemade explosive. *Wisconsin State Journal* 2014.
70. Vella, V., Explosions in Bucks County tied to chemical-company owner David Surman Jr. *The Philadelphia Inquirer* 2018.
71. Bennett, G., Recap: Man who had 250 bombs in Bedminster home in court. *Bristol News* 2018.
72. Aspinall, A., 'Misguided' binman caged for hoarding over 250 homemade bombs in family home. *Daily record* 2018.
73. Osbourne, S., Teenage schoolboy under investigation for selling uranium online and producing explosives. *Independent* 2019.
74. Man further remanded on terror-related charges. *Ballymena Daily* 2019.
75. Man facing terror charges is released on continuing bail at Ballymena Magistrates Court. *Ballymena Daily* 2019.
76. Stenhouse, J., Ueber die naheren Bestandtheile einiger Flechten *Justus Liebigs Ann. Chem.* **1849,** *70*, 218-228.
77. Moon, H. J.; Jeya, M.; Kim, I. W.; Lee, J. K., Biotechnological production of erythritol and its applications. *Appl. Microbiol. Biotechnol.* **2010,** *86*, 1017-1025.
78. Oleske, J. B.; Smith, B. T.; Barber, J.; Weatherall, J. C., Identifying Raman and Infrared Vibrational Motions of Erythritol Tetranitrate. *Applied spectroscopy* **2015,** *69*, 1397-1402.
79. Freye, C. E.; Kinman, W. S.; Tiemann, C.; McDonald, D.; Manner, V. W.; Bowden, P. R.; Tappan, B. C.; Greenfield, M. T., Linking chemical precursors to the synthesis of erythritol tetranitrate. *Forensic chemistry* **2020,** *19*, 100246.
80. Manner, V. W.; Preston, D. N.; Tappan, B. C.; Sanders, V. E.; Brown, G. W.; Hartline, E.; Jensen, B., Explosive performance properties of erythritol tetranitrate (ETN). *Propellants Explos. Pyrotech.* **2015,** *40*, 460-462.
81. Manner, V. W.; Tappan, B. C.; Scott, B. L.; Preston, D. N.; Brown, G. W., Crystal structure, packing analysis, and structural-sensitivity correlations of erythritol tetranitrate. *Crystal Growth and Design* **2014,** *14*, 6154-6160.
82. Matyáš, R.; Lyčka, A.; Jirásko, R.; Jakový, Z.; Maixner, J.; Mišková, L.; Künzel, M., Analytical Characterization of Erythritol Tetranitrate, an Improvised Explosive. *Journal of Forensic Sciences* **2016,** *61*, 759-764.
83. Matyáš, R.; Künzel, M.; Růžička, A.; Knotek, P.; Vodochodský, O., Characterization of erythritol tetranitrate physical properties. *Propellants Explos. Pyrotech.* **2015,** *40*, 185-188.
84. Sisco, E.; Najarro, M.; Samarov, D.; Lawrence, J., Quantifying the stability of trace explosives under different environmental conditions using electrospray ionization mass spectrometry. *Talanta* **2017,** *165*, 10-17.
85. Yan, Q. L.; Künzel, M.; Zeman, S.; Svoboda, R.; Bartošková, M., The effect of molecular structure on thermal stability, decomposition kinetics and reaction models of nitric esters. *Thermochimica Acta* **2013,** *566*, 137-148.
86. Furman, D.; Kosloff, R.; Zeiri, Y., Effects of Nanoscale Heterogeneities on the Reactivity of Shocked Erythritol Tetranitrate. *The Journal of Physical Chemistry C* **2016,** *120*, 28886-28893.
87. Rapp-Wright, H.; McEneff, G.; Murphy, B.; Gamble, S.; Morgan, R.; Beardah, M.; Barron, L., Suspect screening and quantification of trace organic explosives in wastewater using solid phase

extraction and liquid chromatography-high resolution accurate mass spectrometry. *Journal of Hazardous Materials* **2017,** *329*, 11-21.
88. Khrapkovskii, G. M.; Shamsutdinov, T. F.; Chachkov, D. V.; Shamov, A. G., Energy of the O-NO 2 bond dissociation and the mechanism of the gas-phase monomolecular decomposition of aliphatic alcohol nitroesters. *Journal of Molecular Structure: THEOCHEM* **2004,** *686*, 185-192.
89. Oxley, J. C.; Smith, J. L.; Brown, A. C., Eutectics of Erythritol Tetranitrate. *Journal of Physical Chemistry C* **2017,** *121*, 16137-16144.
90. Künzel, M.; Matyáš, R.; Vodochodský, O.; Pachman, J., Explosive properties of melt cast erythritol tetranitrate (ETN). *Central European Journal of Energetic Materials* **2017,** *14*, 418-429.
91. Ravi, P.; Badgujar, D. M.; Gore, G. M.; Tewari, S. P.; Sikder, A. K., Review on Melt Cast Explosives. *Propellants Explos. Pyrotech.* **2011,** *36*, 393-403.
92. Sun, D.; Annapragada, S. R.; Garimella, S. V.; Singh, S. K., Analysis of Gap Formation in the Casting of Energetic Materials. *Numerical heat transfer. Part A, Applications* **2007,** *51*, 415-444.
93. McDonald, D. L.; Manner, V. W.; Tappan, B. C.; Lease, N.; Brown, G. W.; Mueller, A., Thermal stability of solid and molten erythritol tetranitrate (ETN). 2020; Vol. 2272.
94. Global Xylitol Market Analysis, Trends, Share, Size, Growth, Opportunity & Forecast 2018-2023, With an Expected CAGR of 5.7% - ResearchAndMarkets.com. *Biotech Business Week* **2018**, 61.
95. Ur-Rehman, S.; Mushtaq, Z.; Zahoor, T.; Jamil, A.; Murtaza, M. A., Xylitol: A Review on Bioproduction, Application, Health Benefits, and Related Safety Issues. *Crit Rev Food Sci Nutr* **2015,** *55*, 1514-1528.
96. Felipe Hernández-Pérez, A.; de Arruda, P. V.; Sene, L.; da Silva, S. S.; Kumar Chandel, A.; de Almeida Felipe, M. d. G., Xylitol bioproduction: state-of-the-art, industrial paradigm shift, and opportunities for integrated biorefineries. *Crit. Rev. Biotechnol.* **2019,** *39*, 924-943.
97. Rafiqul, I. S. M.; Sakinah, A. M. M., Processes for the Production of Xylitol-A Review. *Food reviews international* **2013,** *29*, 127-156.
98. Hayward, L. D.; Wright, I. G., Xylitol Pentanitrate Preparation and Denitration. In *Methods in Carbohydrate Chemistry*, Academic Press Inc.: New York, 1963; p 258.
99. Ostrinskaya, A.; Kelley, J. A.; Kunz, R. R., Characterization of nitrated sugar alcohols by atmospheric-pressure chemical-ionization mass spectrometry. *Rapid Communications in Mass Spectrometry* **2017,** *31*, 333-343.
100. Wright, I. G.; Hayward, L. D., The Pentitol Pentanitrates. *Can. J. Chem.* **1960,** *38*, 316-319.
101. Xylitol pentanitrate. https://en.wikipedia.org/wiki/Xylitol_pentanitrate (accessed December 2019).
102. Stark, K. A. S.; Alvino, J. F.; Kirkbride, K. P.; Sumby, C. J.; Metha, G. F.; Lenehan, C. E.; Fitzgerald, M.; Wall, C.; Mitchell, M.; Prior, C., Crystal Structure, Sensitiveness and Theoretical Explosive Performance of Xylitol Pentanitrate (XPN). *Propellants Explos. Pyrotech.* **2019,** *44*, 541-549.
103. Stark, K. A. S. In *Characterisation of Xylitol Pentanitrate*, 50th International Annual Conference of ICT, Karlsruhe, Germany, Karlsruhe, Germany, 2019.
104. Wang, G.-X.; Gong, X.-D.; Du, H.-C.; Liu, Y.; Xiao, H.-M., Theoretical prediction of properties of aliphatic polynitrates. *The journal of physical chemistry. A* **2011,** *115*, 795-804.
105. Dong, J.; Yan, Q.-L.; Liu, P.-J.; He, W.; Qi, X.-F.; Zeman, S., The correlations among detonation velocity, heat of combustion, thermal stability and decomposition kinetics of nitric esters. *An International Forum for Thermal Studies* **2018,** *131*, 1391-1403.
106. Šarlauskas, J.; Krikštopaitis, K.; Miliukiene, V.; Čenas, N.; Anusevičius, Ž.; Šaikunas, A., Investigation on the electrochemistry and cytotoxicity of organic nitrates and nitroamines. *Central European Journal of Energetic Materials* **2011,** *8*, 15-24.
107. Šarlauskas, J.; Krikštopaitis, K.; Miliukiene, V.; Anusevičius, Ž.; Šaikunas, A.; Čenas, N. In *Organic nitrates and nitramines: synthesis, electrochemistry and cytotoxicity*, New Trends Res. Energ. Mater., Czech Republic, Czech Republic, 2010.
108. Christian, G. D., *Analytical chemistry*. Seventh edition. ed.; Hoboken, New Jersey : Wiley: 2014.

109. Saitman, A., Overview of analytical methods in drugs of abuse analysis: Gas chromatography/mass spectrometry, liquid chromatography combined with tandem mass spectrometry and related methods. In *Critical Issues in Alcohol and Drugs of Abuse Testing*, 2019; pp 157-171.
110. Munjanja, B. K., Gas chromatography-mass spectrometry basic concepts and instrumentation. In *Chromatographic Analysis of the Environment: Mass Spectrometry Based Approaches, Fourth Edition*, 2017; pp 3-24.
111. Qian, M. C.; Peterson, D. G.; Reineccius, G. A., Gas Chromatography. Cham: Springer International Publishing: Cham, 2017; pp 227-253.
112. McNair, H. M.; Miller, J. M.; Snow, N. H., *Basic Gas Chromatography*. Newark: John Wiley & Sons, Incorporated: Newark, 2019.
113. Curtis, N. In *The chemical basis for gun propellant stability testing*, Fouth Gun Propellant Conference, Mulwala, NSW, Mulwala, NSW, 1990.
114. Fryš, O.; Bajerová, P.; Eisner, A.; Mudruňková, M.; Ventura, K., Method validation for the determination of propellant components by Soxhlet extraction and gas chromatography/mass spectrometry. *J. Sep. Science* **2011,** *34*, 2405-2410.
115. Yücel, A.; Inal, E. K.; Akay, M. A.; Atakol, O.; Öz, S., Chromatographic Determination of Stabilizer in Nitrocellulose Based Propellants.(A new extraction based chromatographic method for the determination of stabilizers in propellants). *Central European Journal of Energetic Materials* **2011,** *8*, 183-192.
116. Zhao, X.; Yinon, J., Identification of nitrate ester explosives by liquid chromatography–electrospray ionization and atmospheric pressure chemical ionization mass spectrometry. *J. Chromatogr. A* **2002,** *977*, 59-68.
117. Bayne, S., *Forensic Applications of High Performance Liquid Chromatography*. 1st ed. ed.; Baton Rouge : Taylor & Francis Group: 2010.
118. Vitha, M. F., *Chromatography: Principles and Instrumentation*. Newark: John Wiley & Sons, Incorporated: Newark, 2016.
119. Bruins, A. P., Mechanistic aspects of electrospray ionization. *Journal of Chromatography A* **1998,** *794*, 345-357.
120. Cech, N. B.; Enke, C. G., Practical implications of some recent studies in electrospray ionization fundamentals. *Mass Spectrom. Rev.* **2001,** *20*, 362-387.
121. Cole, R. B., Some tenets pertaining to electrospray ionization mass spectrometry. *Journal of Mass Spectrometry* **2000,** *35*, 763-772.
122. Larkin, P., *Infrared and raman spectroscopy principles and spectral interpretation*. Amsterdam Netherlands

Boston : Elsevier: Amsterdam [Netherlands]

Boston, 2011.
123. Chalmers, J. M.; Edwards, H. G. M.; Hargreaves, M. D., *Infrared and Raman Spectroscopy in Forensic Science*. 2012.
124. Chang, R., *Basic principles of spectroscopy*. New York, McGraw-Hill: New York, 1970.
125. Hufziger, K. T.; Bykov, S. V.; Asher, S. A., Ultraviolet raman wide-field hyperspectral imaging spectrometer for standoff trace explosive detection. *Applied Spectroscopy* **2017,** *71*, 173-185.
126. Banas, K.; Banas, A.; Moser, H. O.; Bahou, M.; Li, W.; Yang, P.; Cholewa, M.; Lim, S. K., Multivariate analysis techniques in the forensics investigation of the postblast residues by means of fourier transform-infrared spectroscopy. *Analytical Chemistry* **2010,** *82*, 3038-3044.
127. Zapata, F.; López-López, M.; García-Ruiz, C., Detection and identification of explosives by surface enhanced Raman scattering. *Applied Spectroscopy Reviews* **2016,** *51*, 207-242.
128. Botti, S.; Almaviva, S.; Cantarini, L.; Palucci, A.; Puiu, A.; Rufoloni, A., Trace level detection and identification of nitro-based explosives by surface-enhanced Raman spectroscopy. *Journal of Raman Spectroscopy* **2013,** *44*, 463-468.

129. Lipinska-Kalita, K. E.; Pravica, M. G.; Nicol, M., Raman scattering studies of the high-pressure stability of pentaerythritol tetranitrate, C(CH 2ONO 2) 4. *J. Phys. Chem. B* **2005,** *109*, 19223-19227.
130. Gruzdkov, Y. A.; Gupta, Y. M., Vibrational properties and structure of pentaerythritol tetranitrate. *Journal of Physical Chemistry A* **2001,** *105*, 6197-6202.
131. Contini, A. E.; Flood, N.; McAteer, D.; Mai, N.; Akhavan, J., Low hazard small-scale synthesis and chemical analysis of high purity nitroglycerine (NG). *RSC Advances* **2015,** *5*, 87228-87232.
132. Meenakshi, R.; Jaganathan, L.; Gunasekaran, S.; Srinivasan, S., Molecular structure and vibrational spectroscopic investigation of nitroglycerin using DFT calculations. *Molecular Simulation* **2012,** *38*, 204-210.
133. Abraham, R. J., *Proton and carbon-13 NMR spectroscopy : an integrated approach*. London

Philadelphia : Heyden: London

Philadelphia, 1978.
134. Munjal, P.; Sharma, B.; Sethi, J. R.; Dalal, A.; Gholap, S. L., Identification and analysis of organic explosives from post-blast debris by nuclear magnetic resonance. *Journal of Hazardous Materials* **2021,** *403*.
135. Bruker NMR Instruments: Fourier 80. https://www.bruker.com/en/products-and-solutions/mr/nmr/fourier80.html (accessed 15th June 2021).
136. Jin, L. Q.; Xu, W.; Yang, B.; Liu, Z. Q.; Zheng, Y. G., Efficient Biosynthesis of Xylitol from Xylose by Coexpression of Xylose Reductase and Glucose Dehydrogenase in Escherichia coli. *Applied Biochemistry and Biotechnology* **2019,** *187*, 1143-1157.
137. Yinon, J.; Zitrin, S., *Modern Methods and Applications in Analysis of Explosives*. John Wiley & Sons Ltd: England, 1994; p p. 123-133.
138. Amirav, A.; Gordin, A.; Poliak, M.; Fialkov, A. B., Gas chromatography-mass spectrometry with supersonic molecular beams. *Journal of Mass Spectrometry* **2008,** *43*, 141-163.
139. Amirav, A.; Keshet, U.; Danon, A., Soft Cold EI - Approaching molecular ion only with electron ionization. *Rapid Communications in Mass Spectrometry* **2015,** *29*, 1954-1960.
140. Fialkov, A. B.; Amirav, A., Cluster chemical ionization for improved confidence level in sample identification by gas chromatography/mass spectrometry. *Rapid Communications in Mass Spectrometry* **2003,** *17*, 1326-1338.
141. Stark, K. A. S.; Alvino, J. F.; Kirkbride, K. P.; Sumby, C. J.; Metha, G. F.; Lenehan, C. E.; Fitzgerald, M.; Wall, C.; Mitchell, M.; Prior, C., Crystal Structure, Sensitiveness and Theoretical Explosive Performance of Xylitol Pentanitrate (XPN). *Propellants Explos. Pyrotech.* **2019**.
142. Blum, S. W.; Quinn, J. B.; Howe, B. B.; Hefner, M. A.; Winbury, M. M., Pharmacologic and biochemical evaluation of organic nitrates: attempted correlation of activities. *J. Pharmacol. Exp. Ther.* **1971,** *176*, 684-691.
143. Kamlet, M. J.; Jacobs, S. J., Chemistry of Detonations. I. A Simple Method for Calculating Detonation Properties of C–H–N–O Explosives. *The Journal of Chemical Physics* **1968,** *48*, 23-35.
144. Zhang, J.; Xiao, H., Computational studies on the infrared vibrational spectra, thermodynamic properties, detonation properties, and pyrolysis mechanism of octanitrocubane. *The Journal of Chemical Physics* **2002,** *116*, 10674-10683.
145. Yan, Q.-L.; Künzel, M.; Zeman, S.; Svoboda, R.; Bartošková, M., The effect of molecular structure on thermal stability, decomposition kinetics and reaction models of nitric esters. *Thermochimica Acta* **2013,** *566*, 137-148.
146. Montgomery, J. A.; Frisch, M. J.; Ochterski, J. W.; Petersson, G. A., A complete basis set model chemistry. VII. Use of the minimum population localization method. *The Journal of Chemical Physics* **2000,** *112*, 6532-6542.
147. *Cheetah 7.0*, Energetics Materials Center: Lawrence Livermore National Laboratory.
148. *CrysAlisPro, CrysAlis171.NET,*, Version 1.171.34.44; Oxford Diffraction Ltd: Oxfordshire, U.K, 2010.
149. Barbour, L. J., X-Seed — A Software Tool for Supramolecular Crystallography. 2001; Vol. 1, pp 189-191.

150. Sheldrick, G., SHELXL-2014. *University of Göttingen, Göttingen, Germany* **2014**.
151. Sheldrick, G. M., Phase annealing in SHELX-90: direct methods for larger structures. *Acta Crystallogr. Sect. A: Found. Crystallogr.* **1990,** *46*, 467-473.
152. Energetic Materials Testing and Assessment Policy Committee. Manual of Tests. United Kindom Ministry of Defence: U.K., 2002.
153. Smith, M. E.; Wall, C.; Fitzgerald, M., Characterisation of the Major Synthetic Products of the Reactions Between Butanone and Hydrogen Peroxide. *Propellants Explos. Pyrotech.* **2012,** *37*, 282-287.
154. Becke, A. D., Density‐functional thermochemistry. III. The role of exact exchange. *The Journal of Chemical Physics* **1993,** *98*, 5648-5652.
155. Stephens, P.; Devlin, F.; Chabalowski, C.; Frisch, M., AB-INITIO CALCULATION OF VIBRATIONAL ABSORPTION AND CIRCULAR-DICHROISM SPECTRA USING DENSITY-FUNCTIONAL FORCE-FIELDS. *J. Phys. Chem.* **1994,** *98*, 11623-11627.
156. Dunning, T. H., Gaussian basis sets for use in correlated molecular calculations. I. The atoms boron through neon and hydrogen. *The Journal of Chemical Physics* **1989,** *90*, 1007-1023.
157. M. J. Frisch, G. W. T., H. B. Schlegel, G. E. Scuseria, M. A. Robb, J. R. Cheeseman, J. A. Montgomery Jr, T. Vreven, K. N. Kudin, J. C. Burant, J. M. Millam, S. S. Iyengar, J. Tomasi, V. Barone, B. Mennucci, M. Cossi, G. Scalmani, N. Rega, G. A. Petersson, H. Nakatsuji, M. Hada, M. Ehara, K. Toyota, R. Fukuda, J. Hasegawa, M. Ishida, T. Nakajima, Y. Honda, O. Kitao, H. Nakai, M. Klene, X. Li, J. E. Knox, H. P. Hratchian, J. B. Cross, V. Bakken, C. Adamo, J. Jaramillo, R. Gomperts, R. E. Stratmann, O. Yazyev, A. J. Austin, R. Cammi, C. Pomelli, J. W. Ochterski, P. Y. Ayala, K. Morokuma, G. A. Voth, P. Salvador, J. J. Dannenberg, V. G. Zakrzewski, S. Dapprich, A. D. Daniels, M. C. Strain, O. Farkas, D. K. Malick, A. D. Rabuck, K. Raghavachari, J. B. Foresman, J. V. Ortiz, Q. Cui, A. G. Baboul, S. Clifford, J. Cioslowski, B. B. Stefanov, G. Lui, A. Liashenko, P. Piskorz, I. Komaromi, R. L. Martin, D. J. Fox, T. Keith, M. A. Al-Laham, C. Y. Peng, A. Nanayakkara, M. Challacombe, P. M. W. Will, B. Johnson, W. Chen, M. W. Wong, C. Gonzalez, J. A. Pople, *Gaussian 03; Gaussian, Inc*, Wallingford CT, 2004.
158. Politzer, P.; Murray, J. S.; Edward Grice, M.; Desalvo, M.; Miller, E., Calculation of heats of sublimation and solid phase heats of formation. *Mol. Phys.* **1997,** *91*, 923-928.
159. Curtiss, L. A.; Raghavachari, K.; Redfern, P. C.; Pople, J. A., Assessment of Gaussian-2 and density functional theories for the computation of enthalpies of formation. *J. Chem. Phys.* **1997,** *106*.
160. Byrd, E. F. C.; Rice, B. M., Improved prediction of heats of formation of energetic materials using quantum mechanical calculations. *The journal of physical chemistry. A* **2006,** *110*, 1005-1013.
161. Rice, B. M.; Pai, S. V.; Hare, J., Predicting heats of formation of energetic materials using quantum mechanical calculations. *Combust. Flame* **1999,** *118*, 445-458.
162. Westwell, M. S.; Searle, M. S.; Wales, D. J.; Williams, D. H., Empirical correlations between thermodynamic properties and intermolecular forces. *J. Am. Chem. Soc.* **1995,** *117*, X-5015.
163. Zhurova, E. A.; Stash, A. I.; Tsirelson, V. G.; Zhurov, V. V.; Bartashevich, E. V.; Potemkin, V. A.; Pinkerton, A. A., Atoms-in-molecules study of intra- and intermolecular bonding in the pentaerythritol tetranitrate crystal. *J. Am. Chem. Soc.* **2006,** *128*, 14728-14734.
164. Fitzgerald, M.; Gardiner, M. G.; Armitt, D.; Dicinoski, G. W.; Wall, C., Confirmation of the molecular structure of tetramethylene diperoxide dicarbamide (TMDD) and its sensitiveness properties. *Journal of Physical Chemistry A* **2015,** *119*, 905-910.
165. Bulian, C.; Lee, H. In *Determination of Lead Azide Arrhenius Kinetics Constants*, 49th AIAA Aerospace Sciences Meeting including the New Horizons Forum and Aerospace Exposition, 2011; p 270.
166. Unreported study conducted on ETN at the Defence Science and Technology Group. Edinburgh, Australia.
167. Mathew, S.; Krishnan, K.; Ninan, K. N., A DSC Study on the Effect of RDX and HMX on the Thermal Decomposition of Phase Stabilized Ammonium Nitrate. *Propellants Explos. Pyrotech.* **1998,** *23*, 150-154.

168. Thompson, L.; Konst, A.; Lee, H. S. In *Preliminary investigation of SPLA/RD-1333 lead azide thermal decomposition kinetics*, 48th AIAA Aerospace Sciences Meeting Including the New Horizons Forum and Aerospace Exposition, 2010.
169. Miller, G. R.; Garroway, A. N., A Review of the Crystal Structures of Common Explosives. Part I: RDX, HMX, TNT, PETN, and Tetryl. Naval Research Lab Washington, D. C., Ed. 2001.
170. Kaye, S. M.; Herman, H. L., Encyclopedia of Explosives and Related Items. Volume 9. US Army Research and Development Command: Dover, New Jersey, 1980.
171. Kaye, S. M., Encyclopedia of Explosives and Related Items. Volume 8. US Army Research and Development Command: Dover, New Jersey, 1978.
172. John, S., Examination of the Proximate Principles of Some of the Lichens. Part II. *Philosophical transactions of the Royal Society of London* **1849,** *139*, 393-401.
173. Erythritol tetranitrate. https://www.thevespiary.org/rhodium/Rhodium/www.roguesci.org/archive/index.php/t-2712-p-2.html (accessed 5th July).
174. ETN / PETN (2 / 5) Melt Composition by Mr. Anonymous. http://www.sciencemadness.org/talk/viewthread.php?tid=890 (accessed 5th July).
175. ETN question. http://www.sciencemadness.org/talk/viewthread.php?tid=156852 (accessed 5th July).
176. Melt casting ETN experiments. http://www.sciencemadness.org/talk/viewthread.php?tid=64582 (accessed 5th July).
177. Desensitize ETN? http://www.sciencemadness.org/talk/viewthread.php?tid=77976 (accessed 5th July).
178. Cruse, C. A.; Goodpaster, J. V., Generating highly specific spectra and identifying thermal decomposition products via Gas Chromatography / Vacuum Ultraviolet Spectroscopy (GC/VUV): Application to nitrate ester explosives. *Talanta* **2019,** *195*, 580-586.
179. Cruse, C. A.; Goodpaster, J. V., Optimization of gas chromatography/vacuum ultraviolet (GC/VUV) spectroscopy for explosive compounds and application to post-blast debris. *Forensic Chemistry* **2021,** *26*.
180. McLennan, L.; Brown-Nash, A.; Busby, T.; Canaria, J.; Kominia, A.; Smith, J. L.; Oxley, J. C.; Dubnikov, F.; Kosloff, R.; Zeiri, Y., Characterization of the Hexanitrate Esters of Sugar Alcohols. *Propellants Explos. Pyrotech.* **2021,** *46*, 579-592.
181. Lease, N.; Kay, L. M.; Brown, G. W.; Chavez, D. E.; Leonard, P. W.; Robbins, D.; Manner, V. W., Modifying Nitrate Ester Sensitivity Properties Using Explosive Isomers. *Crystal Growth and Design* **2019,** *19*, 6708-6714.
182. Gribanov, P. S.; Topchiy, M. A.; Fedyanin, I. V.; Asachenko, A. F.; Nechaev, M. S.; Pleshakov, D. V., Reexamination of an Energetic Nitrate Ester SHN. *Propellants Explos. Pyrotech.* **2017,** *42*, 1014-1019.

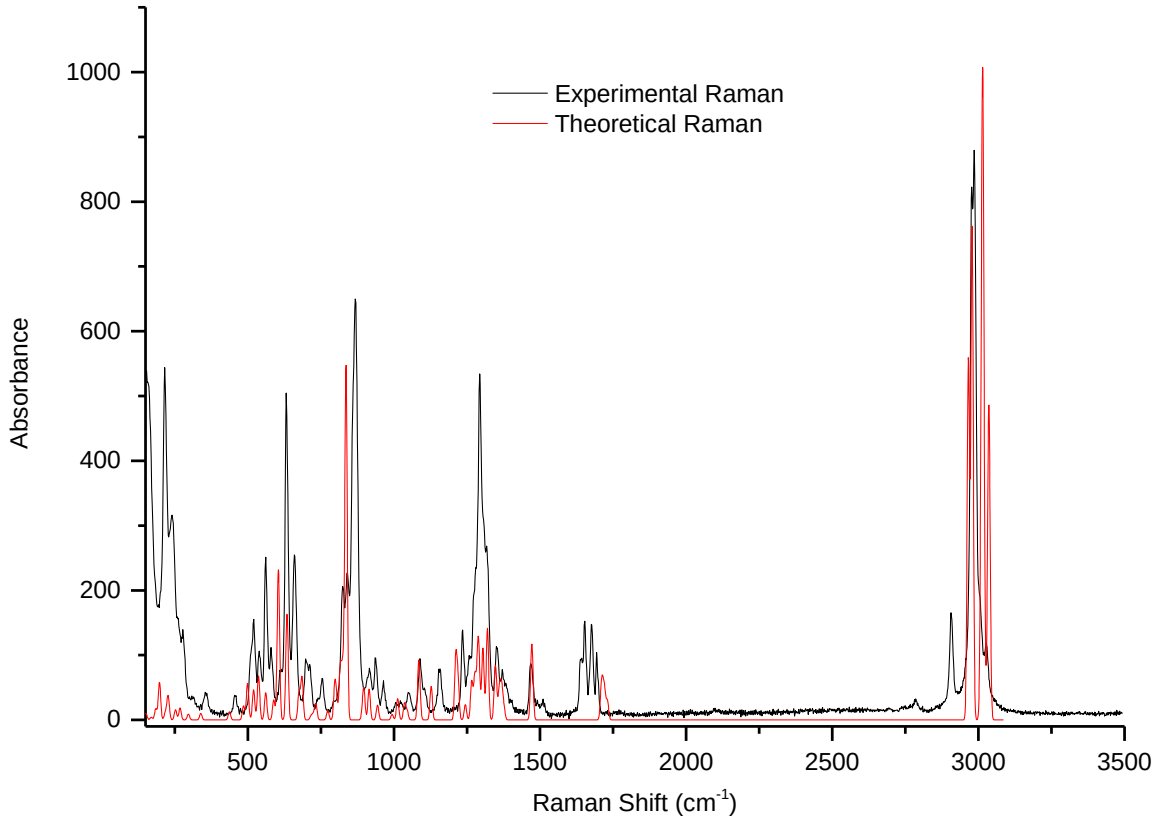

Figure 56: Direct comparison of the experimental Raman spectrum of XPN to the theoretical Raman spectrum of XPN

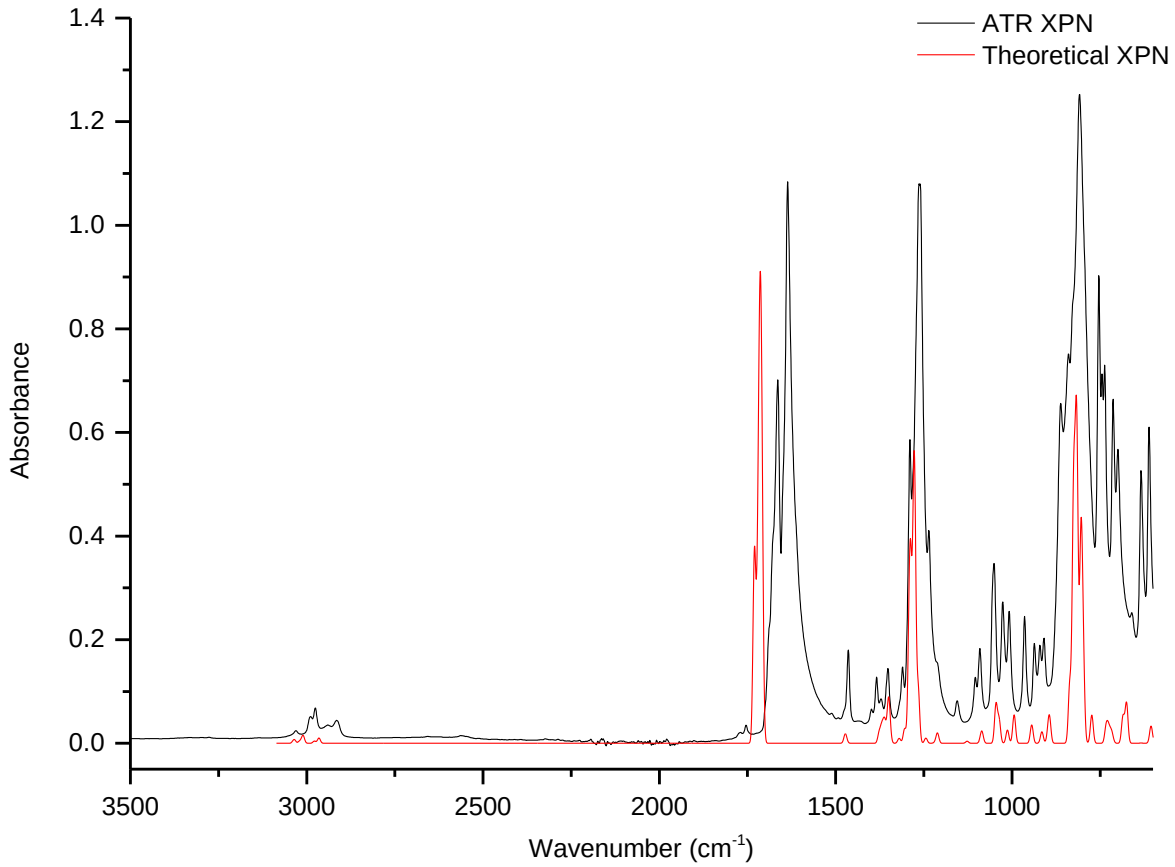

Figure 57: Direct comparison of the experimental ATR IR spectrum of XPN to the theoretical IR spectrum of XPN

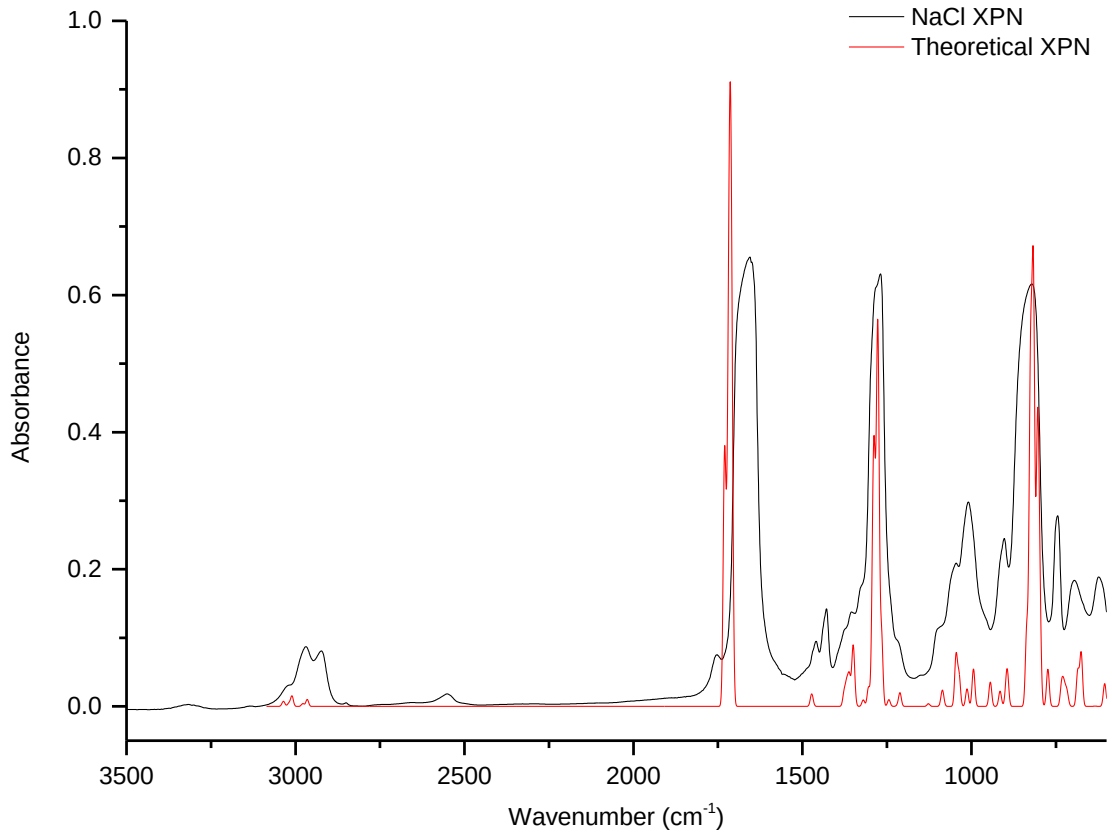

Figure 58: Direct comparison of the experimental NaCl IR spectrum of XPN to the theoretical IR spectrum of XPN

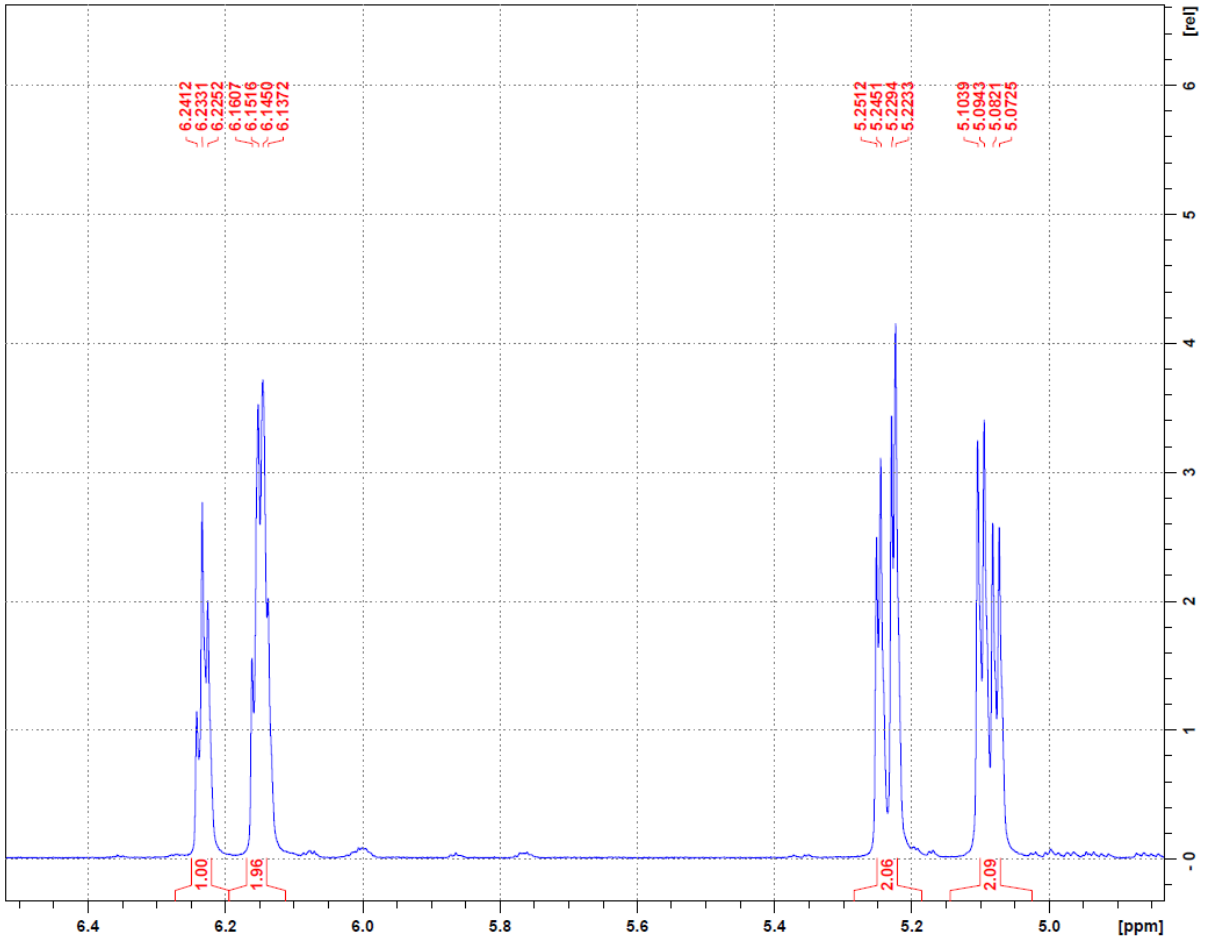

Figure 59: 1H NMR of XPN in (CD3)2CO obtained using a Bruker 600 MHz NMR spectrometer. The signal arising from the 4 (diastereotopic) methylene protons on the terminal carbon atoms was observed as a ABX multiplet centred at δ 5.09 and 5.24 (JAB= 13.0 Hz, JAX = 5.7 Hz, JBX = 3.6 Hz), the signal from the two methine protons on carbon atoms 2 and 4 was observed as a multiplet at 6.15 (2H, m) and the methine proton on C3 gave rise to a triplet at 6.23 (J = 4.8 Hz).

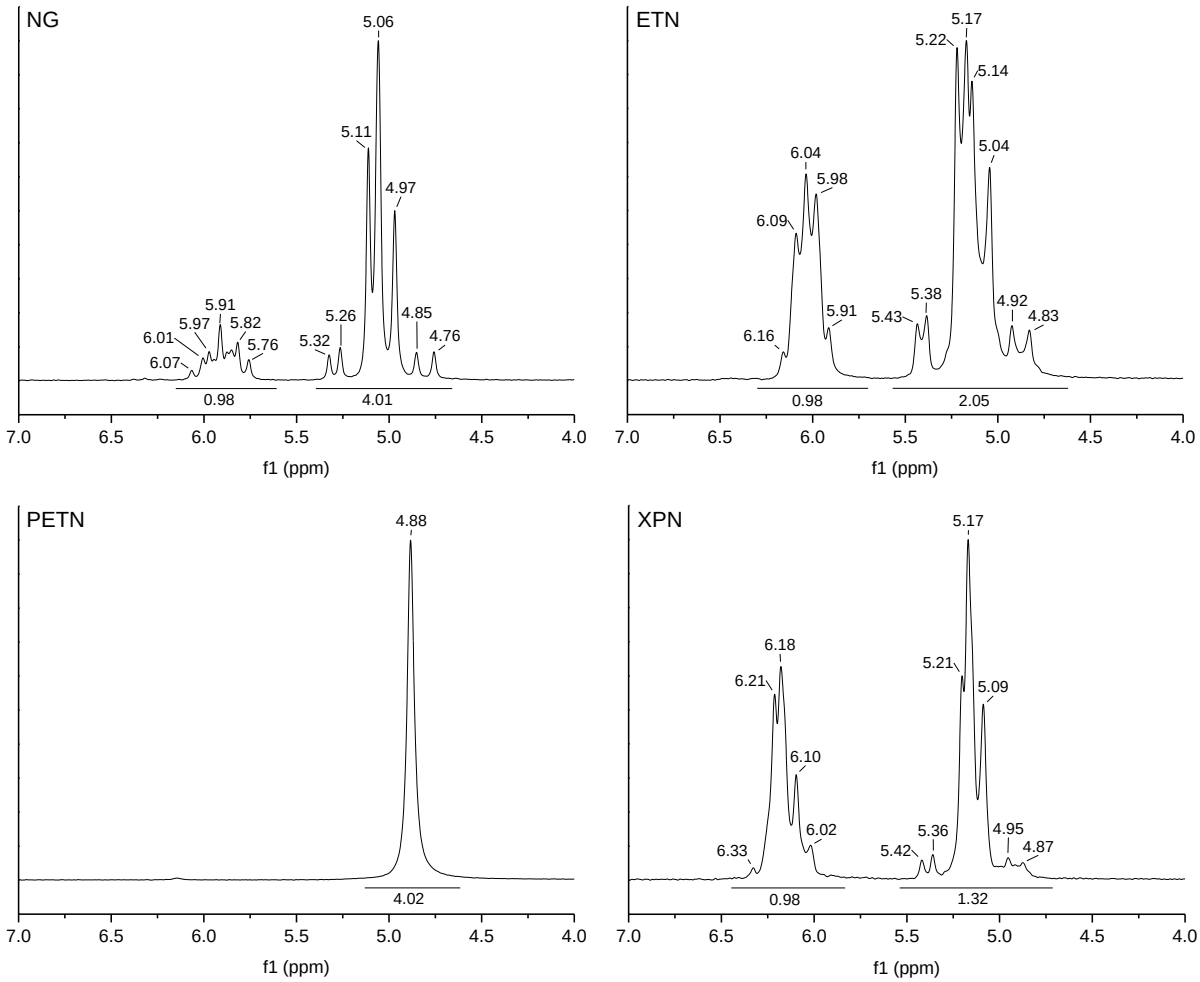

Figure 60: Low field NMR 1H NMR of ETN, NG, XPN and PETN in (CD3)2CO

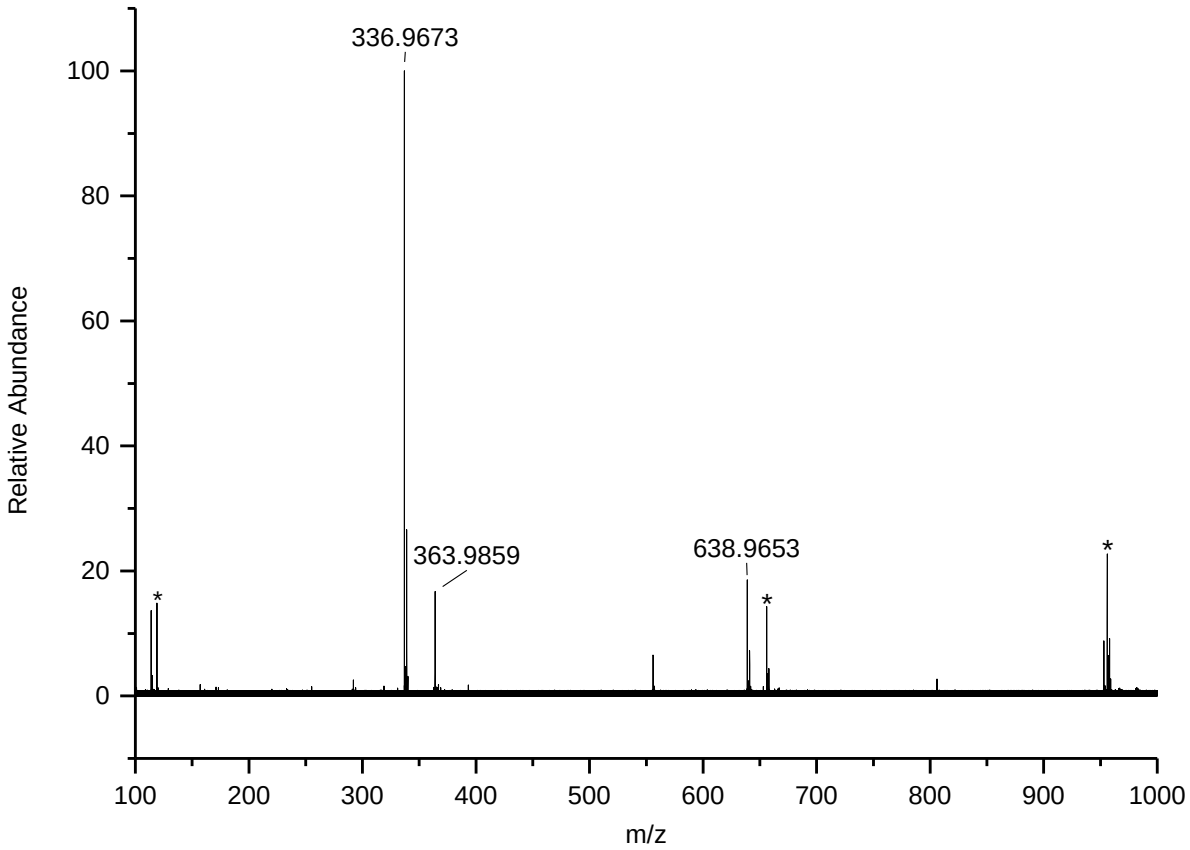

Figure 61: Mass spectrum of ETN obtained using a DSA-TOF MS. The unassigned peaks are either calibration peaks (marked with an asterisk) or background peaks.

Table 12: ETN MS peaks observed in Figure 61 obtained using a DSA-TOF MS.

Mass (m/z)	ppm difference	Ion	Abundance	Formula
638.9653	0.01	$[2M+Cl^{35}]^-/[2M+Cl^{37}]^-$	19	$C_8H_{12}N_8O_{24}Cl$
363.9859	-0.38	$[M+NO_3]^-$	17	$C_4H_6N_5O_{15}$
336.9673/338.9650	-0.67	$[M+Cl^{35}]^-/[M+Cl^{37}]^-$	100	$C_4H_6N_4O_{12}Cl$

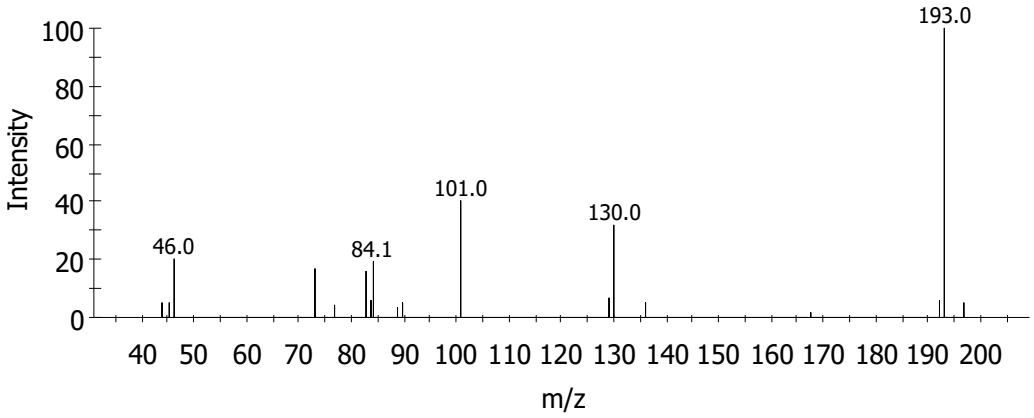

Figure 62: MS/MS data obtained from m/z 193 arising from XPN. Ar collision gas (2.0 mTorr) and 1 V collision induced dissociation energy. Scan range m/z 40 – 200, mass filter m/z 193 with a 0.7 window.

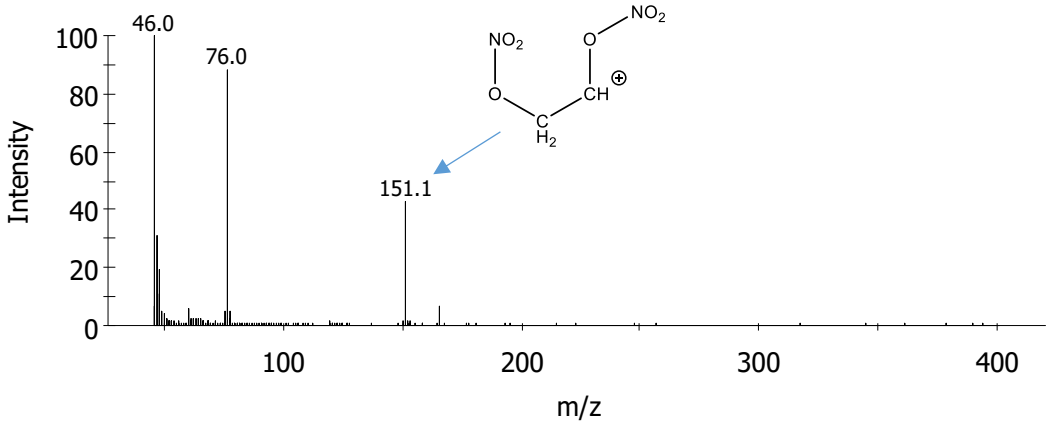

Figure 63: Mass spectrum of NG obtained using GC Cold EI MS. Using the same temperature program as used for the analysis of XPN (retention time approximately 10.55 min), the retention time for NG was approximately 4.62 min.

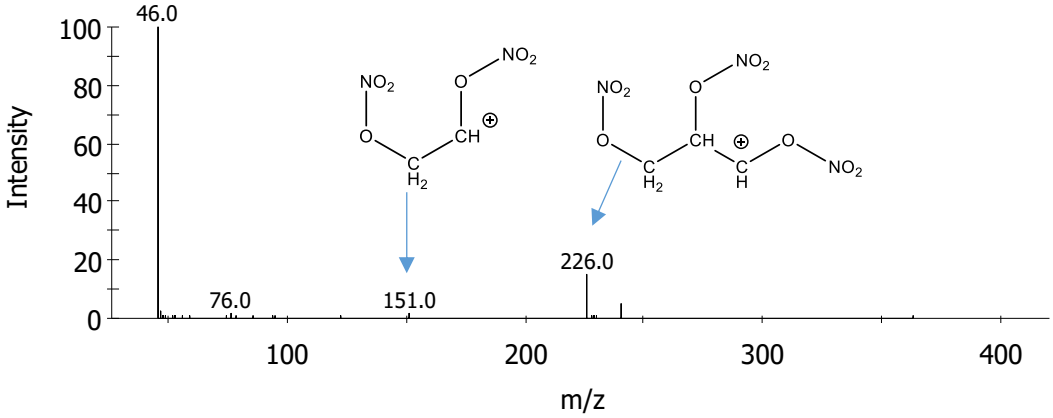

Figure 64: Mass spectrum of ETN obtained using GC Cold EI MS. Using the same temperature program as used for the analysis of XPN, the retention time for ETN was approximately 6.12 min.

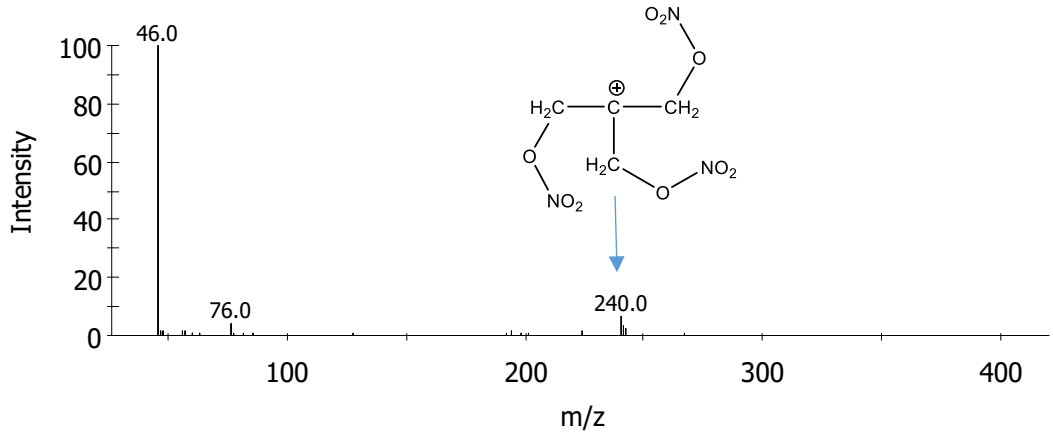

Figure 65: Mass spectrum of PETN obtained using GC Cold EI MS. Using the same temperature program as used for the analysis of XPN, the retention time for PETN was approximately 9.40 min.

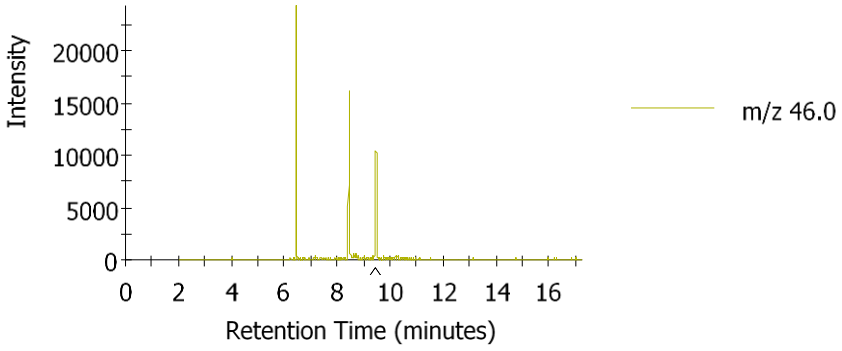

Figure 66: Extracted ion chromatogram (m/z 46) of a mixture of PETN, XPN and ETN

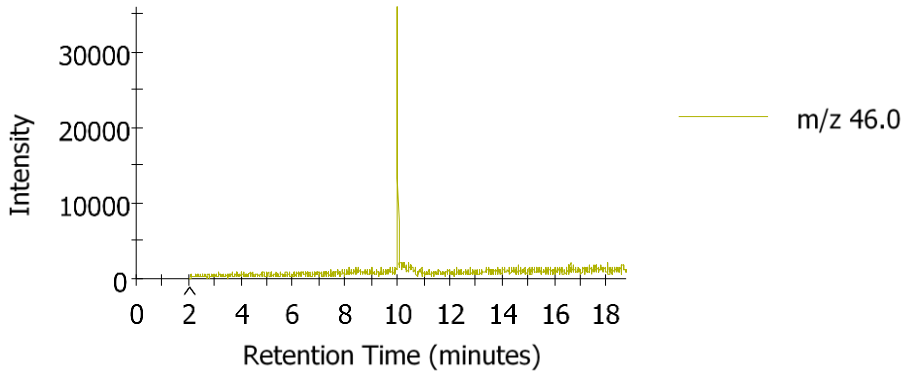

Figure 67: Extracted ion chromatogram (m/z 46) for a solution of XPN

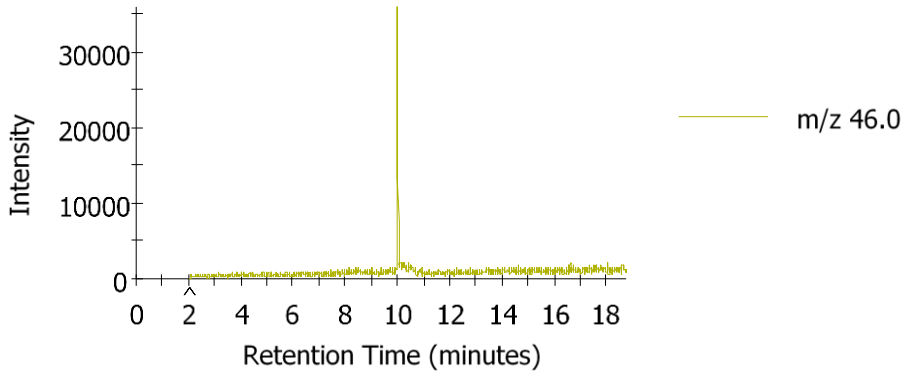

Figure 68: Extracted ion chromatogram (m/z 46 m/z) for a solution of XPN

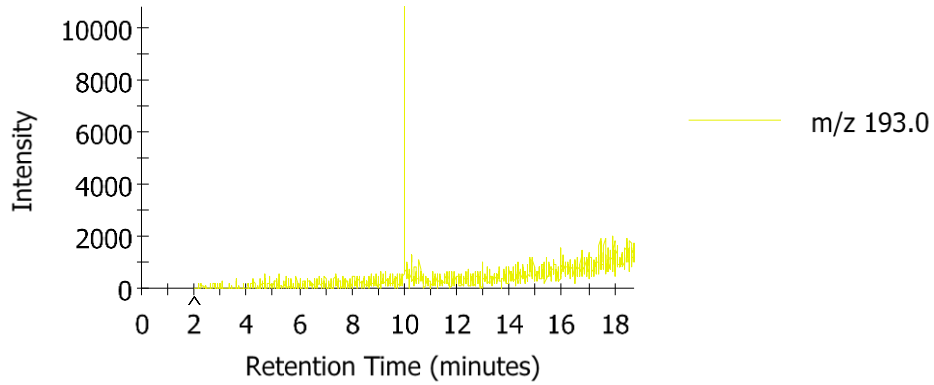

Figure 69: Extracted ion chromatogram (m/z 193) for a solution of XPN